QUANTUM CONTROL OF QUBITS: TIME ORDERING EFFECTS

by

FERDİ ALTINTAŞ

THESIS SUBMITTED TO
THE GRADUATE SCHOOL OF NATURAL AND APPLIED SCIENCES
OF
THE ABANT İZZET BAYSAL UNIVERSITY
IN PARTIAL FULFILLMENT OF THE REQUIREMENTS FOR THE
DEGREE OF
MASTER OF SCIENCE
IN
THE DEPARTMENT OF PHYSICS

JUNE 2010

Approval of the Graduate School of Natural Sciences

Prof. Dr. Nihat Çelebi
Director

I certify that this thesis satisfies all the requirements as a thesis for the degree of Master of Science.

Assoc. Prof. Dr. Nurettin Karagöz
Head of Physics Department

This is to certify that we have read this thesis and that in our opinion it is fully adequate, in scope and quality as a thesis for the degree of Master of Science.

Prof. Dr. Resul Eryiğit
Supervisor

Examining Committee Members

1. Prof. Dr. Resul Eryiğit .....
2. Assoc. Prof. Dr. Cabir Terzioğlu .....
3. Assist. Prof. Dr. Erdal Bekiroğlu .....

ABSTRACT

Quantum Control of Qubits: Time Ordering Effects

Ferdi Altıntaş

Master of Science, Department of Physics

Supervisor: Prof. Dr. Resul Eryiğit

June 2010, 108 pages

In this thesis, I have studied five different problems concerning the qubits and the dynamics of entanglement between the qubits under various conditions. First, the exact analytical dynamics of entanglement between two qubits subject to independent kicks and Gaussian pulses as an external magnetic field lie along z-axes or $x-y$ plane has been investigated. I have showed that "almost-steady" high entanglement can be created between two initially unentangled qubits by using carefully designed kick or pulse sequences.

The dynamics of several quantum correlation measures for a three qubit sytem subject to independent noise in their energy levels has been investigated to understand the life time of quantum correlations for system in contact with an environment. Along these lines, I have compared the dynamics of quantum discord, entanglement and Bell-nonlocalities under the same conditions for three qubits that have stochastic energy levels represented as classical Ornstein-Uhlenbeck noise. I have showed that Bell-nonlocalities as well as bipartite entanglement have life times shorter than the tripartite entanglement, while the quantum discord is immune to sudden death independent of the non-Markovianity of the dynamics and the purity of the initial states. Furthermore, I have concluded

that the non-Markovianity of the dynamics only prolongs the death of quantum correlations, except, quantum discord which does not suffer sudden death.

I have also analyzed the entanglement dynamics of two and three qubits which interact with each other by dipole-dipole interaction. I have assumed each qubit is embedded in its own non-Markovian environment and connected to each other by dipole-dipole interactions through next-nearest, J_1, and next-next-nearest, J_2, couplings. I have showed that the entanglement created by the dipole-dipole interaction is damped to zero by the qubit-environment interactions. Moreover, in the region where $J_2/J_1 < 0$, the full disentanglement time takes longer compared to the region where $J_2/J_1 > 0$.

Keywords: Heisenberg XYZ and XY models; Time Ordering; Kubo-Anderson model; Master equation; Non-Markovian environments.

ÖZET

Qubitlerin Kuantum Kontrolü: Zaman Sıralaması Etkileri

Ferdi Altıntaş

Yüksek Lisans, Fizik Bölümü

Tez Danışmanı: Prof. Dr. Resul Eryiğit

Haziran 2010, 108 sayfa

Bu tezde çeşitli durumlar altında qubitleri ve dolaşıklık dinamiğini içeren 5 farklı problem inceledim. İlk olarak, z-ekseni ve $x-y$ düzleminde dogrultulmuş dış manyetik alan olarak birbirinden bağımsız anlık ve Gaussian sinyallerine maruz kalan iki qubitin analitik dolaşıklık dinamiğini inceledim. Dikkatlice düzenlenmiş ard arda anlık veya Gaussian sinyallerle, başlangıçta dolaşıklığı sıfır olan iki qubitin, "hemen-hemen sabit" yüksek dolaşıklık oluşturabilecegini gösterdim.

Dış ortamla etkileşen bir sistemin kuantum korelasyonlarının ölüm sürelerini anlamak için enerji seviyelerinde birbirinden bagımsız gürültüye maruz kalan üç qubitin değişik kuantum korelasyon ölçümlerini analiz ettim. Bundan yola çıkarak, klasik Ornstein-Uhlenbeck tipi gürültü ile gösterilen rasgele enerji seviyeleri olan 3-qubit için quantum discord, dolaşıklık ve Bell nonlocality dinamiklerini kıyasladım. Quantum discordun anlık ölüme bağışıklığı dinamigin Markovain olmayan özelliği ve ilk durumun saflığından bağımsız iken Bell nonlocality yanısıra iki qubit dolaşıklığın yaşam sürelerinin 3-qubit dolaşıklıktan daha kısa olduğunu gösterdim. Buna ilaveten, anlık ölüme uğramayan quantum discord dışında, Markovian olmayan dinamiğin sadece kuantum korelasyonların ölüm sürelerini uzattığı sonucuna vardım.

Ayrıca birbirleriyle dipole-dipole etkileşimiyle baglı olan iki ve üç qubitlerin dolaşıklık dinamiklerini analiz ettim. Her qubitin kendi Markovain olmayan ortamina batırırldığını ve birbirlerine bir sonraki yakını, J_1, ve sonraki-sonraki enyakın, J_2, komşu çiftleri yoluyla dipole-dipole etkileşimi ile bağlı olduklarını tasarladım. Dipole-dipole etkileşimi ile yaratılmış olan dolaşıklığın, qubit-ortam etkileşiminden dolayı sıfıra sönümlendiğini gösterdim. Ayrıca, $J_2/J_1 < 0$ olduğu bölgelerde tüm edolaşıklığın ölüm zamanının $J_2/J_1 > 0$ olduğu bölgelerde daha uzun sürer.

Anahtar Kelimeler: Heisenberg XYZ and XY modeli; Zaman sıralaması; Kubo-Anderson modeli; Master denklemleri; Markovian olamayan ortamlar.

ACKNOWLEDGEMENTS

I express sincere appreciation to my advisor, Prof. Dr. Resul Eryiğit for his guidance, encouragement and support of this study. I also thank him for his inexhaustible patience, tolerance and trust at me.

I also express sincere appreciation to Assoc. Prof. Dr. Cabir Terzioğlu, Assist. Prof. Dr. Erdal Bekiroğlu, Assist. Prof. Dr. Cihan Parlak for his suggestions and contribitions. My thanks also due to assistants Gürcan Yıldırım and Ali Yılmaz for their help and support during this work.

Thanks to my parents and my wife Sevgi for their love, trust and help. They encouraged me in all phases of my life.

To My Family ...

TABLE OF CONTENTS

LIST OF FIGURES

CHAPTER 1

INTRODUCTION

Quantum entanglement is a nonlocal correlation between two (or more) quantum systems that cannot be accounted for classically. It was first noted and introduced by Einstein, Podolsky and Rosen (EPR) as a paradox in the formalism of the quantum theory [1]. After EPR, quantum mechanics was left in an unsatisfactory position, either it was imcomplete in the sense it failed to account for some elements of physical reality. However, in 1964 Bell introduced Bell inequalities as a refutation of EPR which established a nonlocal nature of quantum mechanics accessible to experimental verifications [2]. Nowadays, entanglement is considered to be not only vital concept but also a prime resource in some fields such as quantum teleportation [3], quantum cryptography [4] and quantum computing [5]. There are some well-defined measures of entanglement, e.g. concurrence [6], negativity [7] and relative entropy [8]. In this thesis, I use concurrence and negativity. For two-qubit case, concurrence is a good measure of entanglement in every sense. It is easily computable and can be used for pure as well as mixed states. However, for higher dimensions or multipartite systems, concurrence is not well-defined whose calculation is based on numerical optimization procedure which does not guarantee exact results [9]. For this case, negativity can be used as a measure of entanglement whose calculation based on partial positive transposes introduced by Peres-Horodecki.

In Chapter II and III, I analyze the control of entanglement between two interacting qubits subject to independently longitudinal and transverse kicks and Gaussian pulses as external magnetic fields. In these chapters, I choose isotropic Heisenberg XYZ model [10] to describe the interaction between qubits. There are also some models such as isotropic or unisotropic Heisenberg XY model [11]

and Dzyaloshinskii-Moriya(DM) model [12] studied in many works to describe qubit-qubit interactions. Also, to study the combined effect of the qubit-qubit interaction and the nonuniformity of the field on entanglement dynamics, I consider the time ordering effect, because the time ordering helps us to understand clearly the time correlation in multiparticle systems as well as to describe analytically the behavior of two-qubit system interacting with a rapidly changing external magnetic fields [13].

However, entanglement is not the only measure of quantum correlations. Quantum discord is a promising canditate to measure all nonclassical correlations hidden in a bipartite systems. It was introduced by Ollivier and Zurek and captures the difference of two natural quantum extensions of the classical mutual information [14]. Although quantum discord is equal to the entanglement for pure states, it includes the quantum correlations which are contained in mixed states that are not entangled. It has a significant application in deterministic quantum computation with one pure qubit [15] and estimation of quantum correlations in the Grover search algorithm [16], in studies of quantum phase transition [17], to define the class of initial system-bath states for which the quantum dynamics is equivalent to a completely positive map [18], and to measure the quantum correlation between relatively accelarated observers [19]. Like quantum discord, violation of Bell-inequalities can be also used as a measure of quantum correlations and in the literature there exists lots of works [20, 21, 22, 23, 24, 25]. It shows the mixed states whose correlation can be reproduced by a local hidden variable model, that is, by classical systems. This indicates that, for mixed states, which are in practice the ones always encountered, a given value of entanglement by itself does not imply their correlations cannot be clasically reproduced with certainity [26].

The models described in Chapter II and III do not include the interaction between the quantum system and its background. However this interaction is inevitable and the background, which is called environment, is often complex

and described by a bath of bosons or fermions, or by classical random fields and theoretically obeys on two assumptions: Markovian (memoryless) and non-Markovian (memory). The Markovian assumption does not mean the past contributions to the current time evolution and the dynamical evolution is governed by a Lindblad master equation [27] . However, the truth every environment is non-Markovian which includes a past contribution to the current time evolution which enters to the master equation by a memory-integral [27, 28]. Due to the inevitable interaction between the qubit and environment, the system undergoes a process called decoherence described by the decay of the off-diagonal elements of the density matrix of the single-qubit in the given basis [29]. Under decoherence process, the entanglement dynamics undergoes a well-known phenomena called entangelement sudden death (ESD) introduced by T. Yu and H. Eberly and defined as the termination of the entanglement in a finite time [30]. In Chapter IV, I investigate the dynamics of quantum correlations of three uncoupled qubits subject to independently zero temperature non-Markovian environments represented as classical Ornstein-Uhlenbeck noises [31]. I investigate how the other quantum correlations, such as quantum discord and Bell-inequalities dehaves under decoherence under the same conditions when entanglement dynamic suffers ESD.

In Chapter IV, I neglect the dipole-dipole interaction between the qubits. However this interaction is inevitable. Thus in Chapter V, I assume two coupled qubits through isotropic Heisenberg XY model embedded independently inside non-Markovian environments represented as classical Ornstein-Uhlenbeck noises. In Chapter VI, I expand the work analyzed in Chapter V for three-qubit system with next-nearest and next-next nearest dipole dipole interactions. In these chapters I analyze the effects of the purity of the initial states, the dipole-dipole interaction between the qubits and the non-Markovianity of the dynamics on bi- and tri-partite entanglements measured by concurrence and negativity, respectively.

CHAPTER 2
ENTANGLEMENT DYNAMICS FOR TWO QUBITS UNDER THE INFLUENCE OF PERIODIC KICS-LONGITUDINAL CASE

2.1 Introduction

In this chapter, I have studied the exact analytical dynamics of two qubits subject to independent longitudinal kicks and Gaussian pulses. Time-ordering effects on the entanglement dynamics are investigated by using concurrence as the entanglement measure. I also explore the effects of pulse width on entanglement dynamics of two qubits initially prepared in a separable state $|\Psi(0)\rangle = |10\rangle$ or maximally entangled state $|\Psi(0)\rangle = (|10\rangle + |01\rangle)/\sqrt{2}$.

The organization of this chapter is as follows. In Sec. 2.2, I introduce the model and show basic formulation for two interacting qubits through Heisenberg XXX model with nonuniform time dependent magnetic fields directed in z-direction. In Sec. 2.3, we discussed the time ordering effects. In Sec. 2.4, I introduce Wootters concurrence as a measure of entanglement. In Sec. 2.4 and 2.5 I explore the efects of sudden kicks and Gaussian pulses on entanglement dynamics of two qubits by chossing a single or multiple pulses or kicks.

2.2 The model and basic formulation

In this chapter, I consider two interacting qubits through Heisenberg XXX model and each qubit is embedded in a time dependent external magnetic fields acting in z-direction. The time dependent Hamiltonian for this system can be

expressed as [10, 32]:

$$\hat{H}(t) = \hat{H}_0 + \hat{H}_{int}(t), \tag{2.1}$$

where

$$\begin{aligned} \hat{H}_0 &= J \sum_{i=x,y,z} \hat{\sigma}_i^1 \hat{\sigma}_i^2, \\ \hat{H}_{int}(t) &= -\hbar \sum_{i=1}^{2} B_z^i(t) \hat{\sigma}_z^i, \end{aligned} \tag{2.2}$$

where $\hat{\sigma}_i^1 = \hat{\sigma}_i \otimes \hat{1}$, $\hat{\sigma_i}^2 = \hat{1} \otimes \hat{\sigma}_i$. Here $\hat{\sigma}_i^{1,2} (i = x, y, z)$ are the usual Pauli spin matrices, J is the exchange interaction coefficient and $B_z^1(t)$ and $B_z^2(t)$ are the time dependent magnetic fields acting on qubit 1 and 2, respectively.

This model includes two simplifying assumptions. First, the time dependence in the interaction Hamiltonian $\hat{H}_{int}(t)$ is contained in a single real function of t. Second, the interaction Hamiltonian does not contain a term proportional to $\hat{H}_0$.

The most general form of an initial pure state of the two-qubit system is $|\Psi(0)\rangle = a_1(0)|00\rangle + a_2(0)|01\rangle + a_3(0)|10\rangle + a_4(0)|11\rangle$, then the probability amplitudes evolve according to

$$i\hbar \frac{d}{dt} \begin{bmatrix} a_1(t) \\ a_2(t) \\ a_3(t) \\ a_4(t) \end{bmatrix} = \begin{bmatrix} J - \hbar B_T(t) & 0 & 0 & 0 \\ 0 & -J + \hbar \Delta B(t) & 2J & 0 \\ 0 & 2J & -J - \hbar \Delta B(t) & 0 \\ 0 & 0 & 0 & J + \hbar B_T(t) \end{bmatrix} \begin{bmatrix} a_1(t) \\ a_2(t) \\ a_3(t) \\ a_4(t) \end{bmatrix}, \tag{2.3}$$

where $\Delta B(t) = B_z^2(t) - B_z^1(t)$, and $B_T(t) = B_z^1(t) + B_z^2(t)$. The solution to

Eq. (2.3) may be written in terms of the time evolution matrix $\hat{U}(t)$ as

$$\begin{bmatrix} a_1(t) \\ a_2(t) \\ a_3(t) \\ a_4(t) \end{bmatrix} = \hat{U}(t) \begin{bmatrix} a_1(0) \\ a_2(0) \\ a_3(0) \\ a_4(0) \end{bmatrix}, \tag{2.4}$$

where an experiment is begun at a time $t = 0$ and completed at $t = T_f$. Since we assume the system is closed, $\sum_{i=1}^{4} P_i(t) = \sum_{i=1}^{4} |a_i(t)|^2 = 1$.

The time evolution operator $\hat{U}(t)$ may be expressed here as

$$\begin{aligned} \hat{U}(t) &= \hat{T} e^{-\frac{i}{\hbar}\int_0^t \hat{H}(t')dt'} = \hat{T} e^{-\frac{i}{\hbar}\int_0^t \left(\hat{H}_0 + \hat{H}_{int}(t')\right)dt'} \\ &= \hat{T} \sum_{n=0}^{\infty} \frac{(-i/\hbar)^n}{n!} \int_0^t \hat{H}(t_n)dt_n ... \int_0^t \hat{H}(t_2)dt_2 \int_0^t \hat{H}(t_1)dt_1 \ . \end{aligned} \tag{2.5}$$

The only non-trivial time dependence in $\hat{U}(t)$ arises from time dependent $\hat{H}(t)$ and time ordering $\hat{T}$. The Dyson time ordering operator $\hat{T}$ [33] specifies that $\hat{H}(t_i)\hat{H}(t_j)$ is properly ordered:

$$\hat{T}\hat{H}(t_i)\hat{H}(t_j) = \hat{H}(t_i)\hat{H}(t_j) + \theta(t_j - t_i)\left[\hat{H}(t_j), \hat{H}(t_i)\right] \ . \tag{2.6}$$

Time ordering imposes a connection between the effects of $\hat{H}(t_i)$ and $\hat{H}(t_j)$ and leads to observable, non-local, time ordering effects when $\left[\hat{H}(t_j), \hat{H}(t_i)\right] \neq 0$.

2.3 Time ordering

Since time ordering effects can be defined as the difference between a result with time ordering and the corresponding result in the limit of no time ordering, it is useful to specify carefully the limit without time ordering. Removing time ordering corresponds to replacing $\hat{T} \to 1$ in Eq. (2.5). This corresponds to the zeroth order term in an eikonal-like, Magnus expansion in commutator terms [34].

2.3.1 Limit of no time ordering

Replacing $\hat{T}$ with 1 in Eq. (2.5), in the Schrödinger picture we have,

$$\begin{aligned}\hat{U}(t) &= \hat{T}e^{-\frac{i}{\hbar}\int_0^t \hat{H}(t')dt'} \rightarrow \sum_{n=0}^{\infty}\frac{(-i/\hbar)^n}{n!}\left[\int_0^t \hat{H}(t')dt'\right]^n \\ &= \sum_{n=0}^{\infty}\frac{(-i/\hbar)^n}{n!}\left[\hat{H}_0 t + \int_0^t \hat{H}_{int}(t')dt'\right]^n = \sum_{n=0}^{\infty}\frac{(-i/\hbar)^n}{n!}\left[\left(\hat{H}_0 + \hat{\bar{H}}_{int}\right)t\right]^n \\ &= e^{-i\hat{\bar{H}}t/\hbar} = \hat{U}^0(t) \quad , \end{aligned} \tag{2.7}$$

where

$$\hat{\bar{H}}_{int}t = \int_0^t \hat{H}_{int}(t')dt',$$

$\hat{\bar{H}} = \hat{H}_0 + \hat{\bar{H}}_{int}$, and $[\hat{H}_0, \hat{\bar{H}}_{int}]$ terms are non-zero. By expanding in powers of $[\hat{H}(t''), \hat{H}(t')]$, it is straightforward to show that to leading order in $\hat{H}_{int}$ and $\hat{H}_0$ the time ordering effect is given by

$$\hat{U}-\hat{U}^0 \simeq -\frac{1}{2\hbar^2}\int_0^t dt'' \int_0^{t''} dt' \left[\hat{H}(t''), \hat{H}(t')\right] = -\frac{1}{2\hbar^2}\left[\hat{H}_0, \hat{H}^0_{int}\right]\int_0^t dt'(t-2t')f(t')\,, \tag{2.8}$$

where $\hat{H}_{int}(t') = \hat{H}^0_{int}f(t')$. This leading term disappears if the pulse centroid $T_k = t/2$ and $f(t')$ is symmetric about T_k. Furthermore, $\hat{U} - \hat{U}^0$ vanishes identically in the special cases of $H_{int}(t') = 0$, $H_{int}(t') = \bar{H}_{int}$, or $B^1_z(t) = B^2_z(t)$ because,

$$[\hat{H}(t''), \hat{H}(t')] = 2i\hbar J\left(\left(B^1_z(t') - B^2_z(t')\right) - \left(B^1_z(t'') - B^2_z(t'')\right)\right)(\hat{\sigma}_y \otimes \hat{\sigma}_x - \hat{\sigma}_x \otimes \hat{\sigma_y}). \tag{2.9}$$

Here we have used the well known identities $(\hat{A}\otimes\hat{B})(\hat{C}\otimes\hat{D}) = \hat{A}\hat{C}\otimes\hat{B}\hat{D}$ and $\hat{\sigma}_i\hat{\sigma}_j = \hat{1}\delta_{ij} + i\epsilon_{ijk}\hat{\sigma}_k$ to calculate the commutation relation in Eq. (2.9).

In general there is no simple analytic form for the exact result $\hat{U}(t)$. For the result without time ordering with $\bar{B}^1_z t = \int_0^t B^1_z(t')dt' = \alpha$, $\bar{B}^2_z t = \int_0^t B^2_z(t')dt' = \beta$

$$
\begin{aligned}
\hat{U}^0(t) &= e^{-\frac{i}{\hbar}(\hat{H}_0 t + \hat{\hat{H}}_{int} t)} \\
&= \begin{bmatrix} y_1 y^* & 0 & 0 & 0 \\ 0 & y(u+iv) & y(-w+iz) & 0 \\ 0 & y(w+iz) & y(u-iv) & 0 \\ 0 & 0 & 0 & y_1^* y^* \end{bmatrix},
\end{aligned} \tag{2.10}
$$

where

$$
\begin{aligned}
y &= e^{\frac{iJt}{\hbar}}, \\
y_1 &= e^{i(\alpha+\beta)}, \\
u &= \cos\left(\frac{\Gamma}{\hbar}\right), \\
v &= \frac{\hbar(\alpha-\beta)}{\Gamma}\sin\left(\frac{\Gamma}{\hbar}\right), \\
w &= 0, \\
z &= -\frac{2Jt}{\Gamma}\sin\left(\frac{\Gamma}{\hbar}\right),
\end{aligned} \tag{2.11}
$$

where $\Gamma = \sqrt{4J^2t^2 + \hbar^2(\alpha-\beta)^2}$. Here we have used the well known method of finding the matrix exponential via eigenvalues and eigenvectors [35].

Similarly, in the intermediate, or interaction, picture, $\hat{U}_I(t) = e^{\frac{i}{\hbar}\hat{H}_0 t}\hat{U}(t)$, and one has

$$
\begin{aligned}
\hat{U}_I(t) &= \hat{T}e^{-\frac{i}{\hbar}\int_0^t \hat{H}^I_{int}(t')dt'} \rightarrow e^{-\frac{i}{\hbar}\int_0^t \hat{H}^I_{int}(t')dt'} \\
&= \sum_{n=0}^{\infty} \frac{(-i/\hbar)^n}{n!}\left[\int_0^t \hat{H}^I_{int}(t')dt'\right]^n = \sum_{n=0}^{\infty}\frac{(-i/\hbar)^n}{n!}\left[\hat{\hat{H}}^I_{int}t\right]^n \\
&= \hat{U}^0_I(t)\,,
\end{aligned} \tag{2.12}
$$

where $\hat{H}^I_{int}(t') = e^{i\hat{H}_0 t'/\hbar}\hat{H}_{int}(t')e^{-i\hat{H}_0 t'/\hbar}$ and $\hat{\hat{H}}^I_{int}t = \int_0^t \hat{H}^I_{int}(t')dt'$. For a sequence of n-positive Gaussian pulses of the form discussed in Section 2.6, it is easy to

show

$$\hat{\tilde{H}}^I_{int}t = -\frac{n}{2}\hbar\Omega(\hat{\sigma}^1_z + \hat{\sigma}^2_z) + \frac{1}{2}\hbar\Delta e^{-\frac{4J^2\tau^2}{\hbar^2}}\left(a(\hat{\sigma}^2_z - \hat{\sigma}^1_z) + b(\hat{\sigma}_x \otimes \hat{\sigma}_y - \hat{\sigma}_y \otimes \hat{\sigma}_x)\right), \tag{2.13}$$

and the propagator $\hat{U}^0_s(t) = e^{-\frac{i}{\hbar}\hat{H}_0 t}\hat{U}^0_I(t)$ is in the form of Eq. (2.10) with elements

$$\begin{aligned}
y &= e^{\frac{iJt}{\hbar}}, \\
y_1 &= e^{in\Omega}, \\
u &= \cos\left(\frac{2Jt}{\hbar}\right)\cos\left(e^{-\frac{4J^2\tau^2}{\hbar^2}}\Delta\kappa\right), \\
v &= \frac{1}{\kappa}\left(a\cos\left(\frac{2Jt}{\hbar}\right) + b\sin\left(\frac{2Jt}{\hbar}\right)\right)\sin\left(e^{-\frac{4J^2\tau^2}{\hbar^2}}\Delta\kappa\right), \\
w &= \frac{1}{\kappa}\left(a\sin\left(\frac{2Jt}{\hbar}\right) - b\cos\left(\frac{2Jt}{\hbar}\right)\right)\sin\left(e^{-\frac{4J^2\tau^2}{\hbar^2}}\Delta\kappa\right), \\
z &= -\sin\left(\frac{2Jt}{\hbar}\right)\cos\left(e^{-\frac{4J^2\tau^2}{\hbar^2}}\Delta\kappa\right),
\end{aligned} \tag{2.14}$$

where $\Delta = (\alpha - \beta), \Omega = (\alpha + \beta)$, and $\kappa = \sqrt{a^2 + b^2}$. Here the propagator is valid for $t - T_n \gg \tau$ and the parameters a and b are determined by the number of pulses as $a = \sum_{i=1}^{n}\cos\left(\frac{4JT_n}{\hbar}\right)$ and $b = \sum_{i=1}^{n}\sin\left(\frac{4JT_n}{\hbar}\right)$.

Another example is a Gaussian pulse-anti pulse sequence, discussed again in Section 2.6. One may show that

$$\hat{\tilde{H}}^I_{int}t = \frac{1}{2}\hbar\Delta e^{-\frac{4J^2\tau^2}{\hbar^2}}\left(a(\hat{\sigma}^2_z - \hat{\sigma}^1_z) + b(\hat{\sigma}_x \otimes \hat{\sigma}_y - \hat{\sigma}_y \otimes \hat{\sigma}_x)\right), \tag{2.15}$$

and the propagator $\hat{U}_s^0(t) = e^{-\frac{i}{\hbar}\hat{H}_0 t}\hat{U}_I^0(t)$ is again in the form of Eq. (2.10) with

$$\begin{aligned}
y &= e^{\frac{iJt}{\hbar}}, \\
y_1 &= 1, \\
u &= \cos\left(\frac{2Jt}{\hbar}\right)\cos\left(e^{-\frac{4J^2\tau^2}{\hbar^2}}\Delta\kappa\right), \\
v &= \frac{1}{\kappa}\left(\cos(\zeta_1) - \cos(\zeta_2)\right)\sin\left(e^{-\frac{4J^2\tau^2}{\hbar^2}}\Delta\kappa\right), \\
w &= \frac{1}{\kappa}\left(\sin(\zeta_1) - \sin(\zeta_2)\right)\sin\left(e^{-\frac{4J^2\tau^2}{\hbar^2}}\Delta\kappa\right), \\
z &= -\sin\left(\frac{2Jt}{\hbar}\right)\cos\left(e^{-\frac{4J^2\tau^2}{\hbar^2}}\Delta\kappa\right),
\end{aligned} \tag{2.16}$$

where $\kappa = 2\left|\sin\left(\frac{2JT_s}{\hbar}\right)\right|, \Delta = (\alpha - \beta), \zeta_i = \frac{2J(t-2T_i)}{\hbar}, T_s = (T_2 - T_1), a = \cos\left(\frac{4JT_1}{\hbar}\right) - \cos\left(\frac{4JT_2}{\hbar}\right)$, and $b = \sin\left(\frac{4JT_1}{\hbar}\right) - \sin\left(\frac{4JT_2}{\hbar}\right)$. Here the propagator is valid for $t - T_2 \gg \tau$ and note if $T_s \to 0$,$\hat{U}_s^0(t) \to e^{-\frac{i}{\hbar}\hat{H}_0 t}$ in the form of (2.26).

2.4 Measure of entanglement

For a pair of qubits, Wootters concurrence [6] can be used as a measure of entanglement. The concurrence function varies from $C = 0$ for separable states to $C = 1$ for maximally entangled states. To calculate the concurrence function one needs to evaluate the matrix

$$\hat{R} = \hat{\rho}(t)(\hat{\sigma}_y \otimes \hat{\sigma}_y)\hat{\rho}^*(t)(\hat{\sigma}_y \otimes \hat{\sigma}_y), \tag{2.17}$$

where $\hat{\rho}(t)$ is the density matrix of the system and $\hat{\rho}^*(t)$ is its complex conjugate. The concurrence is defined as

$$C(\hat{\rho}) = \max\{0, \lambda_1 - \lambda_2 - \lambda_3 - \lambda_4\}, \tag{2.18}$$

where $\lambda_1, \lambda_2, \lambda_3$ and λ_4 are the positive roots of the eigenvalues of $\hat{R}$ in descending order.

Due to discrete symmetry of the total Hamiltonian (2.1), the initial states

$|\Psi(0)\rangle = a_2(0)\,|01\rangle + a_3(0)\,|10\rangle$ and $|\Psi(0)\rangle = a_1(0)\,|00\rangle + a_4(0)\,|11\rangle$ can never get mixed in time. Thus we consider the time evolution of the concurrence of these initial states individually.

The concurrence function for a pure state $|\Psi(t)\rangle = a_2(t)\,|01\rangle + a_3(t)\,|10\rangle$ with density matrix $\hat{\rho}(t) = |\Psi(t)\rangle\,\langle\Psi(t)|$ is given by

$$C(\hat{\rho}) = \max\{0, 2\,|a_2(t)a_3(t)|\}. \tag{2.19}$$

Similarly, for the pure state $|\Psi(t)\rangle = a_1(t)\,|00\rangle + a_4(t)\,|11\rangle$, the concurrence function reads as

$$C(\hat{\rho}) = \max\{0, 2\,|a_1(t)a_4(t)|\}, \tag{2.20}$$

where from Eq. (2.4), the time-dependent coefficients read

$$a_i(t) \;=\; \sum_{j=1}^{4} U_{ij}(t)a_j(0). \tag{2.21}$$

2.5 Entanglement dynamics of kicked qubits

In this part, we examine the entanglement evolution of kicked qubits in the presence of time ordering for the initial pure states $|\Psi(0)\rangle = |10\rangle$(separable) and $|\Psi(0)\rangle = \frac{1}{\sqrt{2}}(|01\rangle + |10\rangle)$(maximally entangled). According to Eq. (2.19) and (2.21), to examine the entanglement evolution one has to present the analytic expressions of the propagators after the kick is active. Thus, we firstly present the analytic expression for the propagator for singly kicked qubits and then discuss the extensions to multiple kicks, using a positive followed by a negative kick and a sequence of two, three and four positive kicks as an example.

2.5.1 Single kick

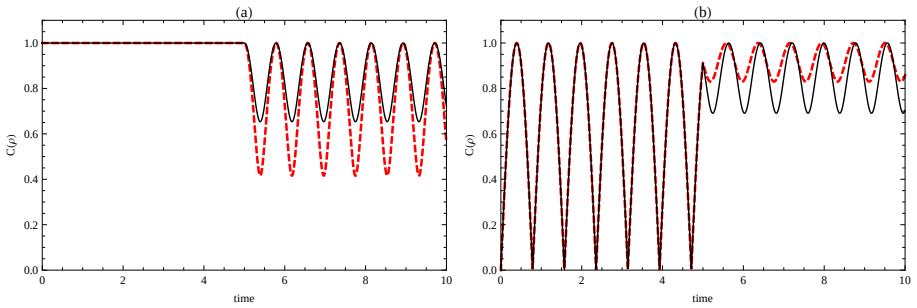

Figure 2.1: Concurrence as a function of time for an ideal positive single kick applied at $T = 5$ for the initial pure states $|\Psi(0)\rangle = \frac{1}{\sqrt{2}}(|01\rangle + |10\rangle)$ (Fig. (a)) and $|\Psi(0)\rangle = |10\rangle$ (Fig. (b)) . The dashed plots correspond to $\alpha = 2\beta$, and the solid plots to $\alpha = 3\beta$. Here we take $\beta = 1, J = 1$ and $\hbar = 1$.

Here we consider two qubits whose states coupled by an interaction field which can be expressed as a sudden "kick" at $t = T$, namely $B_z^1(t) = \alpha\delta(t-T), B_z^2(t) = \beta\delta(t-T)$. For such a kick the integration over time is trivial and the time evolution matrix in Eq. (2.5) becomes

$$\hat{U}^K(t) = e^{-\frac{i}{\hbar}\hat{H}_0(t-T)} e^{-\frac{i}{\hbar}\int_{T-\epsilon}^{T+\epsilon}\hat{H}_{int}(t')dt'} e^{-\frac{i}{\hbar}\hat{H}_0 T}, \tag{2.22}$$

with the same form of (2.10) with

$$\begin{aligned}
y &= e^{\frac{iJt}{\hbar}}, \\
y_1 &= e^{i(\alpha+\beta)}, \\
u &= \cos\left(\frac{2Jt}{\hbar}\right)\cos(\alpha-\beta), \\
v &= \cos\left(\frac{2J(t-2T)}{\hbar}\right)\sin(\alpha-\beta), \\
w &= \sin\left(\frac{2J(t-2T)}{\hbar}\right)\sin(\alpha-\beta), \\
z &= -\sin\left(\frac{2Jt}{\hbar}\right)\cos(\alpha-\beta),
\end{aligned} \tag{2.23}$$

for $t > T$. The propagator for without time ordering is given in Eq. (2.10) and as explained before when $\alpha = \beta$, $\hat{U}^K(t) - \hat{U}^0(t) \to 0$ after the field is active.

2.5.2 A positive followed by a negative kick

The propagator for a sequence of either identical or non-identical pulses can easily be handled by multiplication of several matrices of the form of Eq. (2.22). For example, one may consider a sequence of two kicks of opposite sign at times $t = T_1$ and $t = T_2$, namely, $B_z^1(t) = \alpha\left(\delta(t-T_1) - \delta(t-T_2)\right), B_z^2(t) = \beta\left(\delta(t-T_1) - \delta(t-T_2)\right)$. Following the procedure given in Eq. (2.22), one obtains the time evolution matrix for $t > T_2$,

$$\hat{U}^K(t) = e^{-\frac{i}{\hbar}\hat{H}_0(t-T_2)} e^{-\frac{i}{\hbar}\int_{T_2-\epsilon}^{T_2+\epsilon}\hat{H}_{int}(t')dt'} e^{-\frac{i}{\hbar}\hat{H}_0(T_2-T_1)} e^{-\frac{i}{\hbar}\int_{T_1-\epsilon}^{T_1+\epsilon}\hat{H}_{int}(t')dt'} e^{-\frac{i}{\hbar}\hat{H}_0 T_1}, \quad (2.24)$$

with the same form of (2.10) with

$$\begin{aligned}
y &= e^{\frac{iJt}{\hbar}}, \\
y_1 &= 1, \\
u &= \cos\left(\frac{2Jt}{\hbar}\right)\cos(\Delta)^2 + \cos\left(\frac{2J(t-2T_s)}{\hbar}\right)\sin(\Delta)^2, \\
v &= \left(\cos(\zeta_1) - \cos(\zeta_2)\right)\sin(\Delta)\cos(\Delta), \\
w &= \left(\sin(\zeta_1) - \sin(\zeta_2)\right)\sin(\Delta)\cos(\Delta), \\
z &= -\sin\left(\frac{2Jt}{\hbar}\right)\cos(\Delta)^2 - \sin\left(\frac{2J(t-2T_s)}{\hbar}\right)\sin(\Delta)^2, \qquad (2.25)
\end{aligned}$$

where $\zeta_i = \frac{2J(t-2T_i)}{\hbar}, \Delta = (\alpha - \beta)$, and $T_s = T_2 - T_1$. As $T_s \to 0$ or $\alpha = \beta$, $\hat{U}^K(t)$ reduces to

$$\begin{aligned}
\hat{U}^0(t) &= e^{-\frac{i}{\hbar}\hat{H}_0 t} \\
&= \begin{bmatrix}
e^{-\frac{iJt}{\hbar}} & 0 & 0 & 0 \\
0 & e^{\frac{iJt}{\hbar}}\cos(\frac{2Jt}{\hbar}) & -ie^{\frac{iJt}{\hbar}}\sin(\frac{2Jt}{\hbar}) & 0 \\
0 & -ie^{\frac{iJt}{\hbar}}\sin(\frac{2Jt}{\hbar}) & e^{\frac{iJt}{\hbar}}\cos(\frac{2Jt}{\hbar}) & 0 \\
0 & 0 & 0 & e^{-\frac{iJt}{\hbar}}
\end{bmatrix}, \qquad (2.26)
\end{aligned}$$

because for a positive kick followed by a negative kick $\hat{\bar{H}}_{int}t = 0$.

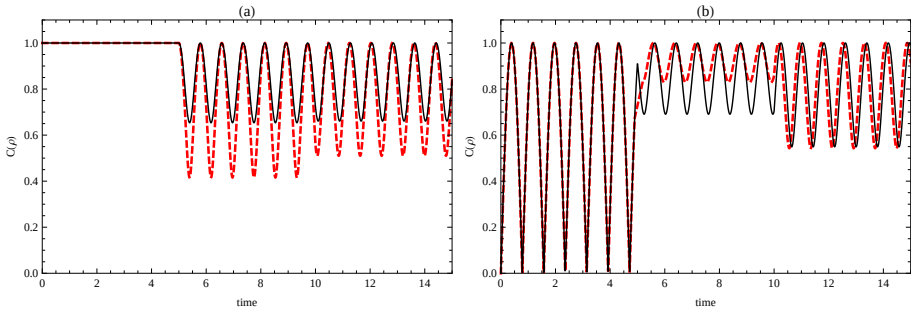

Figure 2.2: Concurrence as a function of time for an ideal positive kick applied at $T_1 = 5$ followed by an ideal negative kick at $T_2 = 10$ for the initial pure states $|\Psi(0)\rangle = \frac{1}{\sqrt{2}}(|01\rangle + |10\rangle)$ (Fig. (a)) , and $|\Psi(0)\rangle = |10\rangle$ (Fig. (b)) . The dashed plots correspond to $\alpha = 2\beta$, and the solid plots to $\alpha = 3\beta$. Here we plot for $t > T_2$ and take $\beta = 1, J = 1$ and $\hbar = 1$.

2.5.3 Two positive kicks

To show the difference between positive and negative kicks applied after the first positive kick on entanglement dynamics of qubits, one may consider a sequence of two positive kicks applied at times $t = T_1$ and $t = T_2$, namely, $B_z^1(t) = \alpha\left(\delta(t-T_1) + \delta(t-T_2)\right), B_z^2(t) = \beta\left(\delta(t-T_1) + \delta(t-T_2)\right)$. Following the procedure given in Eq. (2.22) one obtains the time evolution matrix Eq. (2.24) for $t > T_2$ in the shape of (2.10) with

$$\begin{aligned}
y &= e^{\frac{iJt}{\hbar}}, \\
y_1 &= e^{2i(\alpha+\beta)}, \\
u &= \cos\left(\frac{2Jt}{\hbar}\right)\cos(\Delta)^2 - \cos\left(\frac{2J(t-2T_s)}{\hbar}\right)\sin(\Delta)^2, \\
v &= (\cos(\zeta_1) + \cos(\zeta_2))\sin(\Delta)\cos(\Delta), \\
w &= (\sin(\zeta_1) + \sin(\zeta_2))\sin(\Delta)\cos(\Delta), \\
z &= -\sin\left(\frac{2Jt}{\hbar}\right)\cos(\Delta)^2 + \sin\left(\frac{2J(t-2T_s)}{\hbar}\right)\sin(\Delta)^2,
\end{aligned} \tag{2.27}$$

where $\zeta_i = \frac{2J(t-2T_i)}{\hbar}, \Delta = (\alpha - \beta)$ and $T_s = T_2 - T_1$. Here the propagator for without time ordering can be calculated by replacing $\bar{B}_z^1 t \to 2\alpha$ and $\bar{B}_z^2 t \to 2\beta$ in Eq. (2.10) and note for $\alpha = \beta$, $\hat{U}^K(t) - \hat{U}^0(t)$ vanishes.

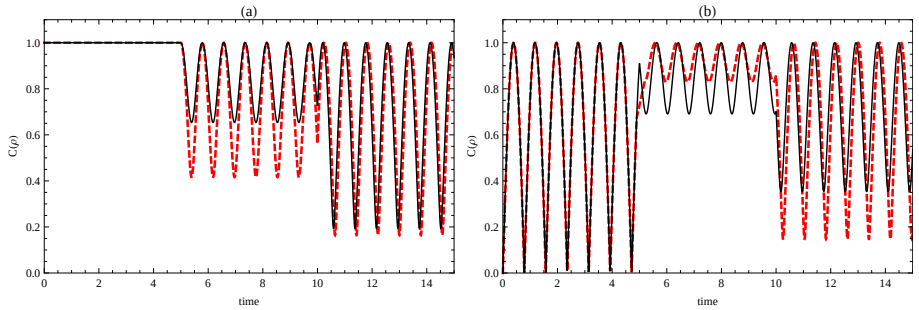

Figure 2.3: Concurrence as a function of time for a sequence of two ideal positive kicks applied at $T_1 = 5$ and $T_2 = 10$ for the initial pure states $|\Psi(0)\rangle = \frac{1}{\sqrt{2}}(|01\rangle + |10\rangle)$ (Fig. (a)) and $|\Psi(0)\rangle = |10\rangle$ (Fig. (b)). The dashed plots correspond to $\alpha = 2\beta$, and the solid plots to $\alpha = 3\beta$. Here we plot for $t > T_2$ and take $\beta = 1, J = 1$ and $\hbar = 1$.

2.5.4 3-4 positive kicks

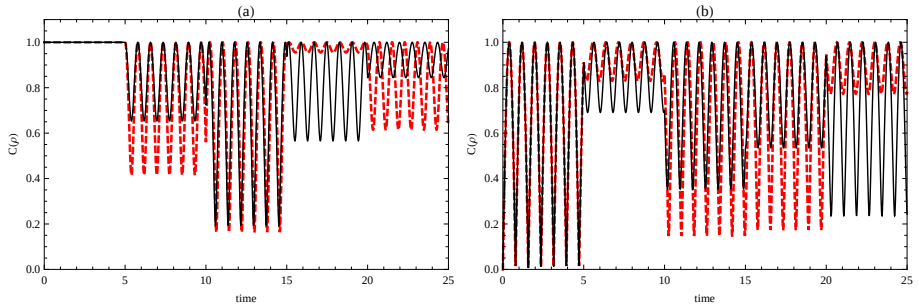

Figure 2.4: Concurrence as a function of time for 4-successive ideal positive kicks for the initial pure states $|\Psi(0)\rangle = \frac{1}{\sqrt{2}}(|01\rangle + |10\rangle)$ (Fig. (a)) and $|\Psi(0)\rangle = |10\rangle$ (Fig. (b)). Here the dashed plots correspond to $\alpha = 2\beta$, and the solid plots to $\alpha = 3\beta$ and we take $\beta = 1, J = 1, \hbar = 1, T_1 = 5, T_2 = 10, T_3 = 15$ and $T_4 = 20$.

Final example is a sequence of n-positive kicks applied at times $t = T_1, t = T_2, ..., t = T_n$, namely $B_z^1(t) = \sum_{i=1}^{n} \alpha\delta(t - T_i), B_z^2(t) = \sum_{i=1}^{n} \beta\delta(t - T_i)$. Following the procedure given in Eq. (2.22), one obtains the time evolution matrix for three positive kicks at times $t > T_3$

$$\begin{aligned} \hat{U}^K(t) &= e^{-\frac{i}{\hbar}\hat{H}_0(t-T_3)} e^{-\frac{i}{\hbar}\int_{T_3-\epsilon}^{T_3+\epsilon}\hat{H}_{int}(t')dt'} e^{-\frac{i}{\hbar}\hat{H}_0(T_3-T_2)} e^{-\frac{i}{\hbar}\int_{T_2-\epsilon}^{T_2+\epsilon}\hat{H}_{int}(t')dt'} \\ &\times e^{-\frac{i}{\hbar}\hat{H}_0(T_2-T_1)} e^{-\frac{i}{\hbar}\int_{T_1-\epsilon}^{T_1+\epsilon}\hat{H}_{int}(t')dt'} e^{-\frac{i}{\hbar}\hat{H}_0 T_1}, \end{aligned} \tag{2.28}$$

with parameters specified in (2.10)

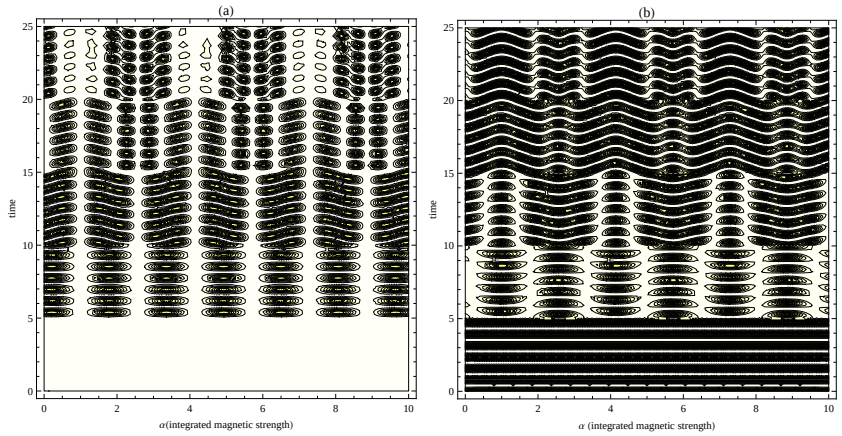

Figure 2.5: The contour plot of concurrence versus time and integrated pulse strength for the initial pure state $|\Psi(0)\rangle = \frac{1}{\sqrt{2}}(|01\rangle + |10\rangle)$ (Fig. (a)) , and for $|\Psi(0)\rangle = |10\rangle$ (Fig. (b)). Here the contour plots include four ideal positive kicks applied at $T_1 = 5, T_2 = 10, T_3 = 15$, and $T_4 = 20$, and we set $J = 1, \beta = 1$ and $\hbar = 1$.

$$
\begin{aligned}
y &= e^{\frac{iJt}{\hbar}}, \\
y_1 &= e^{3i(\alpha+\beta)}, \\
u &= \cos\left(\frac{2Jt}{\hbar}\right)\cos(\Delta)^3 - \sum_{\substack{i,j=1 \\ i<j}}^{3} \cos\left(\frac{2J(t+2(T_i-T_j))}{\hbar}\right)\cos(\Delta)\sin(\Delta)^2, \\
v &= \sum_{i=1}^{3}\cos(\zeta_i)\sin(\Delta)\cos(\Delta)^2 - \cos\left(\frac{2J(t-2(T_1-T_2+T_3))}{\hbar}\right)\sin(\Delta)^3, \\
w &= \sum_{i=1}^{3}\sin(\zeta_i)\sin(\Delta)\cos(\Delta)^2 - \sin\left(\frac{2J(t-2(T_1-T_2+T_3))}{\hbar}\right)\sin(\Delta)^3, \\
z &= -\sin\left(\frac{2Jt}{\hbar}\right)\cos(\Delta)^3 \\
&+ \sum_{\substack{i,j=1 \\ i<j}}^{3}\sin\left(\frac{2J(t+2(T_i-T_j))}{\hbar}\right)\cos(\Delta)\sin(\Delta)^2. \qquad (2.29)
\end{aligned}
$$

Similarly, the the time evolution matrix for four positive kicks for $t > T_4$

$$
\begin{aligned}
\hat{U}^K(t) &= e^{-\frac{i}{\hbar}\hat{H}_0(t-T_4)}e^{-\frac{i}{\hbar}\int_{T_4-\epsilon}^{T_4+\epsilon}\hat{H}_{int}(t')dt'}e^{-\frac{i}{\hbar}\hat{H}_0(T_4-T_3)}e^{-\frac{i}{\hbar}\int_{T_3-\epsilon}^{T_3+\epsilon}\hat{H}_{int}(t')dt'}e^{-\frac{i}{\hbar}\hat{H}_0(T_3-T_2)} \\
&\times e^{-\frac{i}{\hbar}\int_{T_2-\epsilon}^{T_2+\epsilon}\hat{H}_{int}(t')dt'}e^{-\frac{i}{\hbar}\hat{H}_0(T_2-T_1)}e^{-\frac{i}{\hbar}\int_{T_1-\epsilon}^{T_1+\epsilon}\hat{H}_{int}(t')dt'}e^{-\frac{i}{\hbar}\hat{H}_0T_1}, \qquad (2.30)
\end{aligned}
$$

with parameters specified in (2.10)

$$
\begin{aligned}
y &= e^{\frac{iJt}{\hbar}}, \\
y_1 &= e^{4i(\alpha+\beta)}, \\
u &= \cos\left(\frac{2Jt}{\hbar}\right)\cos(\Delta)^4 - \sum_{\substack{i,j=1 \\ i<j}}^{4}\cos\left(\frac{2J(t+2(T_i-T_j))}{\hbar}\right)\cos(\Delta)^2\sin(\Delta)^2 \\
&+ \cos\left(\frac{2J(t+2T_{1234})}{\hbar}\right)\sin(\Delta)^4, \\
v &= \sum_{i=1}^{4}\cos(\zeta_i)\sin(\Delta)\cos(\Delta)^3 - \sum_{\substack{i,j,k=1 \\ i<j<k}}^{4}\cos\left(\frac{2J(t-2(T_i-T_j+T_k))}{\hbar}\right)\cos(\Delta)\sin(\Delta)^3, \\
w &= \sum_{i=1}^{4}\sin(\zeta_i)\sin(\Delta)\cos(\Delta)^3 - \sum_{\substack{i,j,k=1 \\ i<j<k}}^{4}\sin\left(\frac{2J(t-2(T_i-T_j+T_k))}{\hbar}\right)\cos(\Delta)\sin(\Delta)^3, \\
z &= -\sin\left(\frac{2Jt}{\hbar}\right)\cos(\Delta)^4 + \sum_{\substack{i,j=1 \\ i<j}}^{4}\sin\left(\frac{2J(t+2(T_i-T_j))}{\hbar}\right)\cos(\Delta)^2\sin(\Delta)^2 \\
&- \sin\left(\frac{2J(t+2T_{1234})}{\hbar}\right)\sin(\Delta)^4, \qquad (2.31)
\end{aligned}
$$

where $\zeta_i = \frac{2J(t-2T_i)}{\hbar}, \Delta = (\alpha-\beta)$ and $T_{1234} = (T_1 - T_2 + T_3 - T_4)$. Here the propagator for without time ordering can be calculated by replacing $\bar{B}_z^1 t \to n\alpha$ and, $\bar{B}_z^2 t \to n\beta$ in Eq. (2.10) and note for $\alpha = \beta$, $\hat{U}^K(t) - \hat{U}^0(t)$ vanishes.

In this section, we analyze how the successive ideal kicks affect the entanglement evolution of the initially non-entangled state, $|\Psi(0)\rangle = |10\rangle$, and the initially maximal entangled state, $|\Psi(0)\rangle = \frac{1}{\sqrt{2}}(|01\rangle + |10\rangle)$. From Fig. 2.1, 2.2, 2.3 and 2.4, it can be noted that the entanglement dynamics of qubits initially prepared in the in these states can be changed by sudden kicks and each kick can change the amplitude and minimum of the oscillation of the entanglement evolution of each state while it does not have any effect on the frequency of the oscillation. Also, from Fig. 2.2 and 2.3 the positive kick and negative kick applied after the first kick shows different aspects on the entanglement evolution of each state. For example, the amplitude of the entanglement oscillation for each state for

positive kick applied after first kick is greater than the negative one. Moreover, from Fig. 2.4 the initially maximal entangled state can nearly return its initial condition after the third positive kick for $\alpha = 2\beta$. Finally, as shown Fig. 2.5, the entanglement evolution for each state has a periodic pattern and repeats itself in the increase of the integrated magnetic strength and note every kick creates a different oscillating pattern.

2.6 Entanglement dynamics of qubits perturbed by a sequence of gaussian pulses

In this part, we discuss the time evolution of the entanglement caused by a Gaussian pulse of the form $B_z^i(t) = \frac{\alpha_i}{\sqrt{\pi}\tau} e^{-\frac{(t-T_k)^2}{\tau^2}}$, ($\alpha_{1,2} = \alpha, \beta$), centered at T_k with width τ. The time evolution of the concurrence for the initial pure states $|\Psi(0)\rangle = \frac{1}{\sqrt{2}}(|01\rangle + |10\rangle)$ and $|\Psi(0)\rangle = |10\rangle$ are evaluated by numerically integrating the equations in (2.3) and using Eq. (2.19). Here we shall determine how the entanglement depends on the pulse witdh τ by choosing a single pulse, a positive pulse followed by a negative pulse, and multiple pulses centered at $T_1 = 5, T_2 = 10, T_3 = 15$ and $T_4 = 20$. For convenience we shall set $J = 1, \beta = 1$ and $\hbar = 1$. Note in the limit as $\tau \to 0$, the results of entanglement evolution of kicked qubits in the presence of time ordering can be reached that are analyzed in the previous section.

2.6.1 Single Pulse

In Fig. 2.6 we show the results of a calculation for the concurrence for the initial pure states $|\Psi(0)\rangle = \frac{1}{\sqrt{2}}(|01\rangle + |10\rangle)$ and $|\Psi(0)\rangle = |10\rangle$ when strongly perturbed by a single Gaussian pulse centered at $t = T_1$ with width τ. We have obtained our results by numerically integrating the coupled equations,

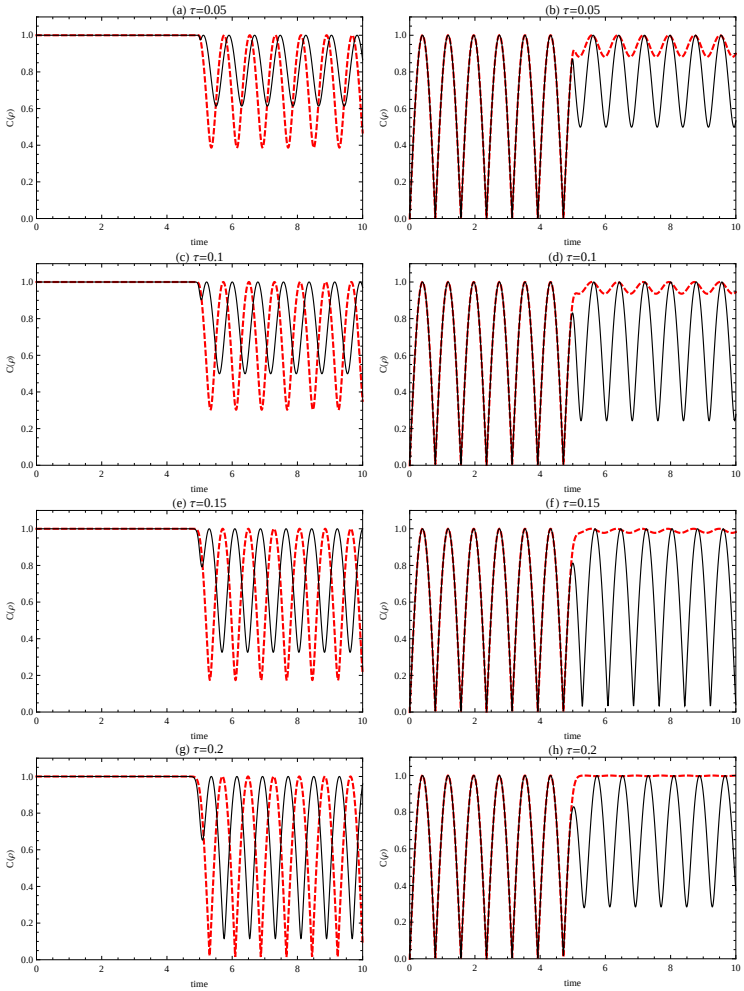

Figure 2.6: Concurrence as a function of time for a single pulse of width τ for the initial pure states $|\Psi(0)\rangle = \frac{1}{\sqrt{2}}(|01\rangle + |10\rangle)$ (Fig. (a), (c), (e) and (g)) and $|\Psi(0)\rangle = |10\rangle$ (Fig. (b), (d), (f) and (h)). The dashed plots correspond to $\alpha = 2\beta$, and the solid plots to $\alpha = 3\beta$.

$$
\begin{aligned}
i\hbar\dot{a}_2(t) &= \left(-J - \frac{\hbar(\alpha-\beta)}{\sqrt{\pi}\tau} e^{-\frac{(t-T_1)^2}{\tau^2}}\right) a_2(t) + 2Ja_3(t) \\
i\hbar\dot{a}_3(t) &= \left(-J + \frac{\hbar(\alpha-\beta)}{\sqrt{\pi}\tau} e^{-\frac{(t-T_1)^2}{\tau^2}}\right) a_3(t) + 2Ja_2(t) \quad . \qquad (2.32)
\end{aligned}
$$

As shown Fig. 2.6, the width of the pulse has a significant effect on the entanglement evolution of qubits. For example, for the pulse width $\tau = 0.2$ and $\alpha = 2\beta$, the minimum of $C(\rho)$ of $|\Psi(0)\rangle = \frac{1}{\sqrt{2}}(|01\rangle + |10\rangle)$ can go to zero awhile the state $|\Psi(0)\rangle = |10\rangle$ can have a constant full entanglement.

A positive followed by a negative pulse

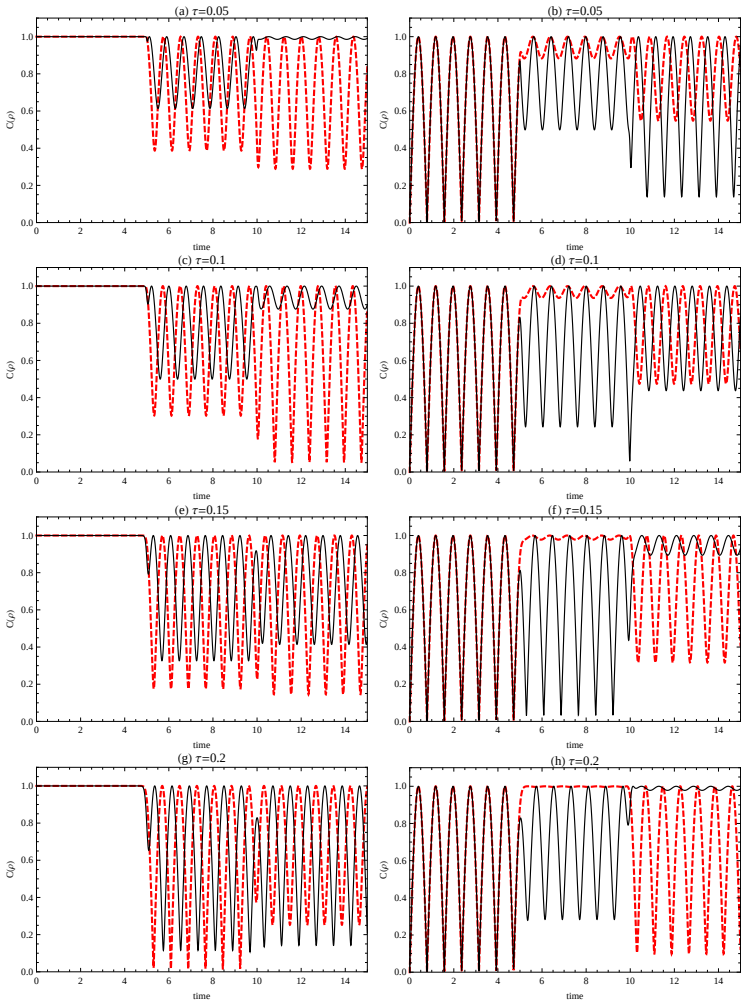

Figure 2.7: Concurrence as a function of time for a positive pulse followed by a negative pulse of width τ for the initial pure states $|\Psi(0)\rangle = \frac{1}{\sqrt{2}}(|01\rangle + |10\rangle)$ (Fig. (a), (c), (e) and (g)) and $|\Psi(0)\rangle = |10\rangle$ (Fig. (b), (d), (f) and (h)). The dashed plots correspond to $\alpha = 2\beta$, and the solid plots to $\alpha = 3\beta$.

In Fig. 2.7 we show the results of a calculation for the concurrence for the initial pure states $|\Psi(0)\rangle = \frac{1}{\sqrt{2}}(|01\rangle + |10\rangle)$ and $|\Psi(0)\rangle = |10\rangle$ when strongly perturbed by a single Gaussian pulse centered at $t = T_1$ followed by a negative Gaussian pulse centered at $t = T_2$ with the same width τ. For this double pulse the coupled equations are

$$
\begin{aligned}
i\hbar\dot{a}_2(t) &= \left(-J - \frac{\hbar(\alpha-\beta)}{\sqrt{\pi}\tau}(e^{-\frac{(t-T_1)^2}{\tau^2}} - e^{-\frac{(t-T_2)^2}{\tau^2}})\right) a_2(t) + 2Ja_3(t) \\
i\hbar\dot{a}_3(t) &= \left(-J + \frac{\hbar(\alpha-\beta)}{\sqrt{\pi}\tau}(e^{-\frac{(t-T_1)^2}{\tau^2}} - e^{-\frac{(t-T_2)^2}{\tau^2}})\right) a_3(t) + 2Ja_2(t) \quad (2.33)
\end{aligned}
$$

2.6.2 A sequence of two positive pulses

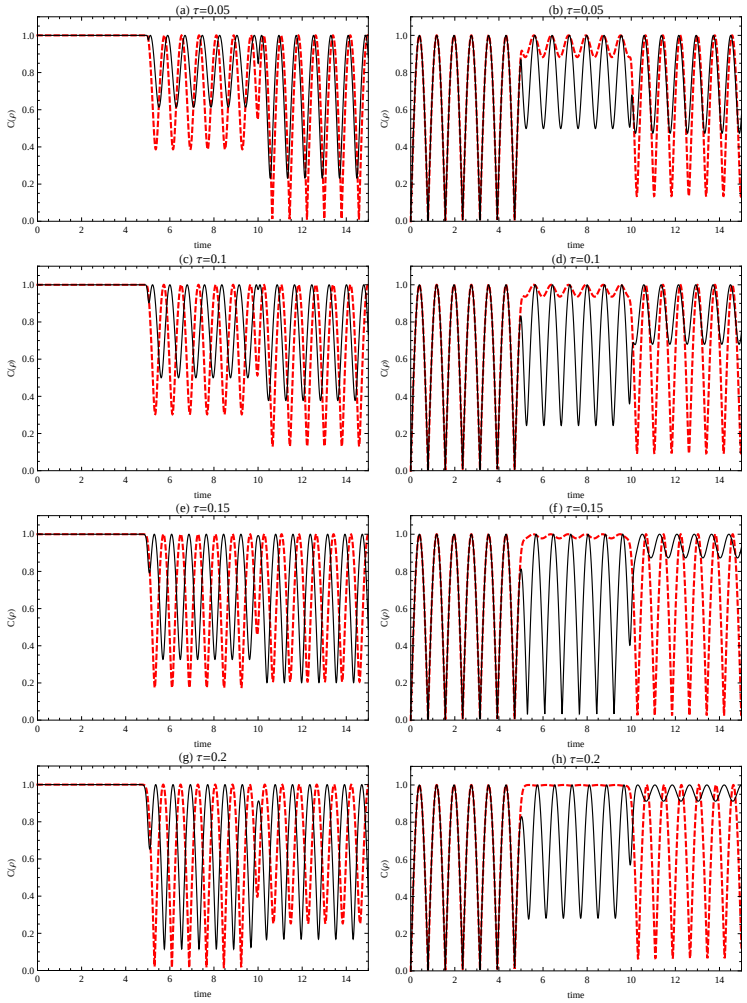

Figure 2.8: Concurrence as a function of time for a sequence of two positive pulses witdh τ for the initial pure states $|\Psi(0)\rangle = \frac{1}{\sqrt{2}}(|01\rangle + |10\rangle)$ (Fig. (a), (c), (e) and (g)) and $|\Psi(0)\rangle = |10\rangle$ (Fig. (b), (d), (f) and (h)). The dashed plots correspond to $\alpha = 2\beta$, and the solid plots to $\alpha = 3\beta$.

In Fig. 2.8 we show the results of a calculation for the concurrence for the initial pure states $|\Psi(0)\rangle = \frac{1}{\sqrt{2}}(|01\rangle + |10\rangle)$ and $|\Psi(0)\rangle = |10\rangle$ when strongly perturbed by a sequence of two positive Gaussian pulses centered at $t = T_1$, and

$t = T_2$ with the same width τ. For this double pulse the coupled equations are

$$\begin{aligned} i\hbar\dot{a}_2(t) &= \left(-J - \frac{\hbar(\alpha-\beta)}{\sqrt{\pi}\tau}(e^{-\frac{(t-T_1)^2}{\tau^2}} + e^{-\frac{(t-T_2)^2}{\tau^2}})\right) a_2(t) + 2Ja_3(t) \\ i\hbar\dot{a}_3(t) &= \left(-J + \frac{\hbar(\alpha-\beta)}{\sqrt{\pi}\tau}(e^{-\frac{(t-T_1)^2}{\tau^2}} + e^{-\frac{(t-T_2)^2}{\tau^2}})\right) a_3(t) + 2Ja_2(t) \end{aligned} \quad (2.34)$$

As shown Fig. 2.7 and 2.8, a positive pulse or a negative pulse applied after the first positive pulse shows different aspects on entanglement dynamics of the qubits. For example, the initial state $|\Psi(0)\rangle = \frac{1}{\sqrt{2}}(|01\rangle + |10\rangle)$ with $\tau = 0.05$ and $\alpha = 3\beta$ can become a maximal entangled again after the negative kick while the minimum of $C(\hat{\rho})$ can go to 0.2 after the positive kick. It is interesting that for the pulse width $\tau = 0.2$, the entanglement dynamics of the qubits nearly shows a similar evolution for the two initial states.

2.6.3 A sequence of four positive pulses

In Fig. 2.9 we show results of a calculation for the concurrence for the initial pure states $|\Psi(0)\rangle = \frac{1}{\sqrt{2}}(|01\rangle + |10\rangle)$ and $|\Psi(0)\rangle = |10\rangle$ when strongly perturbed by a sequence of four positive Gaussian pulses centered at $t = T_1, t = T_2, t = T_3$, and $t = T_4$ with the same width τ. For this sequence of pulses the coupled equations are

$$\begin{aligned} i\hbar\dot{a}_2(t) &= \left(-J - \frac{\hbar(\alpha-\beta)}{\sqrt{\pi}\tau}\sum_{i=1}^{4} e^{-\frac{(t-T_i)^2}{\tau^2}}\right) a_2(t) + 2Ja_3(t) \\ i\hbar\dot{a}_3(t) &= \left(-J + \frac{\hbar(\alpha-\beta)}{\sqrt{\pi}\tau}\sum_{i=1}^{4} e^{-\frac{(t-T_i)^2}{\tau^2}}\right) a_3(t) + 2Ja_2(t) \quad . \end{aligned} \quad (2.35)$$

As noted before for the entanglement evolution caused by ideal sudden kicks, the successive pulses and the magnitude of the integrated magnetic strength only change the amplitude of the oscillation of the entanglement evolution and it has no effect on the frequency of the oscillation. As shown Fig. 2.9, the width of the pulses also has no effect on the frequency of the oscillation whose effect is only on

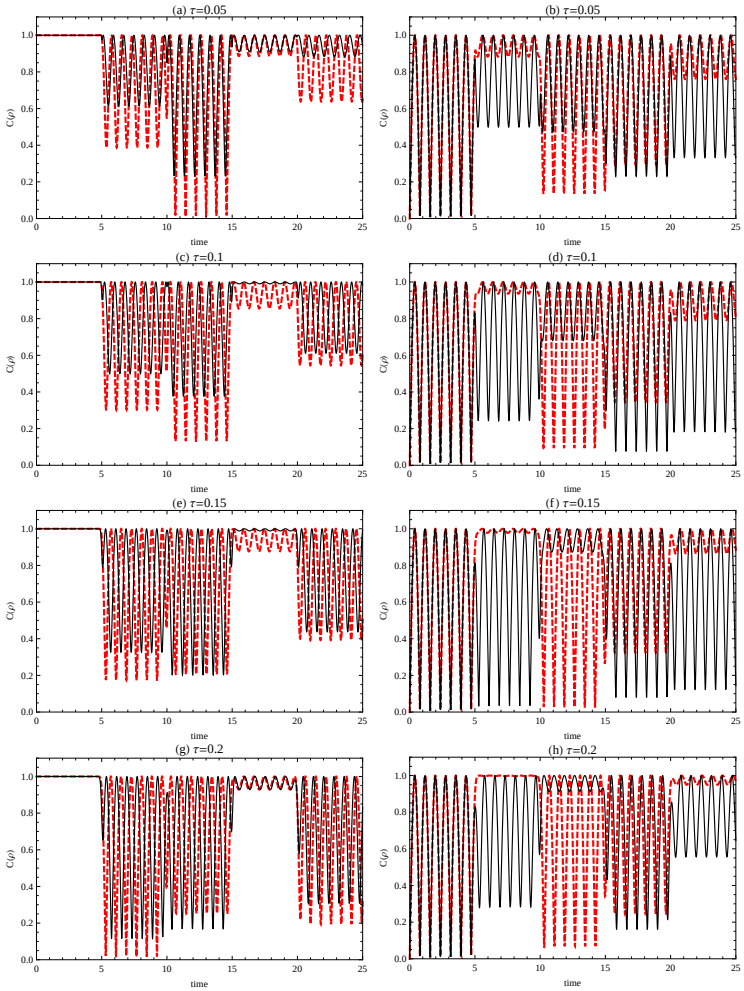

Figure 2.9: Concurrence as a function of time for a sequence of four positive pulses witdh τ for the initial pure states $|\Psi(0)\rangle = \frac{1}{\sqrt{2}}(|01\rangle + |10\rangle)$ (Fig. (a), (c), (e) and (g)) and $|\Psi(0)\rangle = |10\rangle$ (Fig. (b), (d), (f) and (h)). The dashed plots correspond to $\alpha = 2\beta$, and the solid plots to $\alpha = 3\beta$.

the amplitude of it. Also, as shown in Fig. 2.10, the increase of the pulse width breaks down the periodic pattern of the oscillation of the entanglement evolution compared to Fig. 2.5.

There are some interesting features and results of the entanglement dynamics of two coupled qubits under time-dependent magnetic fields. Firstly, the successive pulses (or kicks) and the width of the pulses have a significant and unpredictable effect on the entanglement evolution of the qubits. However, by this control scheme, a non-entangled state can become a fully entangled state, also the mimimum of the entanglement oscillation of the maximally entangled state can go to zero. Secondly, it can be concluded that the frequency of the entanglement

oscillation only depends on the exchange interaction coefficient and independent of all other parameters of the system. Thirdly, it can be easily checked that the initial states $|\Psi(0)\rangle = |11\rangle, |\Psi(0)\rangle = |00\rangle$ and $|\Psi(0)\rangle = \frac{1}{\sqrt{2}}(|11\rangle \pm |00\rangle)$ are robust states in which the entanglement dynamics of qubits prepared in these initial states cannot be changed by the sequence of pulses or kicks. Moreover, the entanglement dynamics of qubits initially prepared in the states $|\Psi(0)\rangle = |01\rangle$ and $|\Psi(0)\rangle = \frac{1}{\sqrt{2}}(|10\rangle - |01\rangle)$ is the same as of $|\Psi(0)\rangle = |10\rangle$ and $|\Psi(0)\rangle = \frac{1}{\sqrt{2}}(|01\rangle + |10\rangle)$, respectively. Finally, the entanglement evolution of qubits prepared in the initial states of $|\Psi(0)\rangle = \frac{1}{\sqrt{2}}(|01\rangle + |10\rangle)$ and and $|\Psi(0)\rangle = |10\rangle$ is controllable by the pulses (or kicks) if and only if $\alpha \neq \beta$, and if $\alpha = \beta$, the entanglement evolution of these states is uneffected by the Gaussian pulses and sudden kicks and the concurrence funciton of $|\Psi(0)\rangle = \frac{1}{\sqrt{2}}(|01\rangle + |10\rangle)$ is equal to 1 and of $|\Psi(0)\rangle = |10\rangle$ is equal to $\left|\sin\left(\frac{4Jt}{\hbar}\right)\right|$.

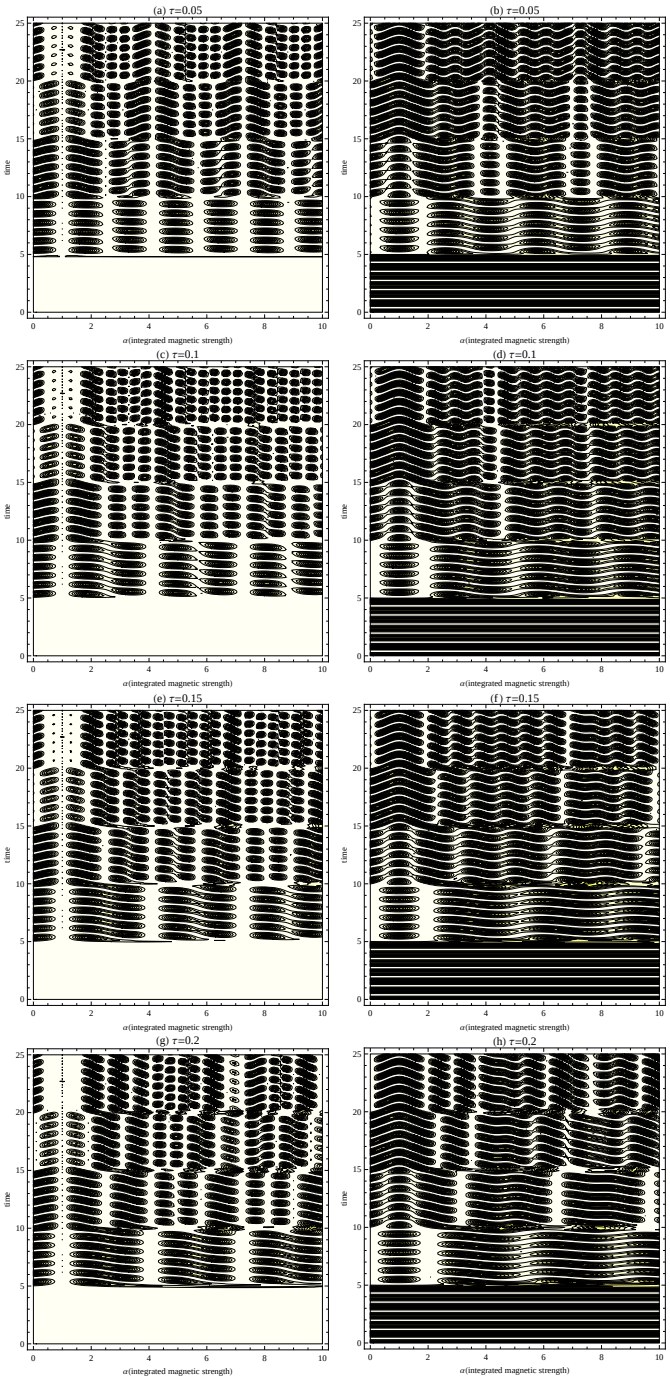

Figure 2.10: The contour plot of concurrence versus time and integrated pulse strength for a sequence of four positive pulses of width τ for the initial pure states $|\Psi(0)\rangle = \frac{1}{\sqrt{2}}(|01\rangle + |10\rangle)$ (Fig. (a), (c), (e) and (g)), and $|\Psi(0)\rangle = |10\rangle$ (Fig. (b), (d), (f) and (h)).

CHAPTER 3
ENTANGLEMENT DYNAMICS FOR TWO QUBITS UNDER THE INFLUENCE OF PERIODIC KICS-TRANSVERSE CASE

3.1 Introduction

In this chapter, I explore the effects of transverse sudden kicks or Gaussian pulses on entanglement dynamics of two-interacting qubits through Heisenberg XXX model. I choose concurrence as a measure of entanglement and by considering initially separable $|\Psi(0)\rangle = |11\rangle$ and maximally entangled $|\Psi(0)\rangle = \frac{1}{\sqrt{2}}(|11\rangle + |00\rangle)$ states the effects of kick or pulse squences on entanglement dynamics are investigated.

The organization of this chapter is as follows. In Sec. 3.2, I introduce the model and show basic formulation for two interacting qubits through Heisenberg XXX model with nonuniform time dependent magnetic fields directed in $x - y$ plane. In Sec. 3.3, I discussed the time ordering effects. In Sec. 3.4, I introduce Wootters concurrence as a measure of entanglement. In Sec. 3.4 and 3.5 I explore the efects of sudden kicks and Gaussian pulses on entanglement dynamics of two qubits by chossing a single or multiple pulses or kicks.

3.2 The model and basic formulation

In this paper, I consider two interacting qubits through Heisenberg XXX model and each qubit is placed in a time-dependent nonuniform magnetic field in $x - y$ plane. The Hamiltonian for this model may be expressed as [11, 56] (we set

$\hbar = 1$):

$$\hat{H}(t) \;=\; \hat{H}_0 + \hat{H}_{int}(t), \tag{3.1}$$

where

$$\begin{aligned} \hat{H}_0 &= J \sum_{i=x,y,z} \hat{\sigma}_i^1 \hat{\sigma}_i^2, \\ \hat{H}_{int}(t) &= \frac{1}{2} \sum_{i=1}^{2} B^i(t)(\cos(\theta)\sigma_x^i + \sin(\theta)\sigma_y^i). \end{aligned} \tag{3.2}$$

Here $\hat{\sigma}_i^{1,2}(i = x, y, z)$ are the usual Pauli spin matrices, $B^1(t)$ and $B^2(t)$ are the external time-dependent magnetic fields on qubit 1 and 2, respectively, J is the exchange interaction coefficient and θ is the angle between magnetic fields and the x-axes (we assume $0 \leq \theta \leq \frac{\pi}{2}$).

In this model, we also consider that the interaction Hamiltonian, $\hat{H}_{int}(t)$, does not contain a term proportional to $\hat{H}_0$ and all of the time dependence in the interaction Hamiltonian is contained in a single real function of t.

The most general form of an initial pure state of the two-qubit system is $|\Psi(0)\rangle \;=\; a_1(0)\,|11\rangle + a_2(0)\,|10\rangle + a_3(0)\,|01\rangle + a_4(0)\,|00\rangle$, then the probability amplitudes evolve according to

$$i\frac{d}{dt}\begin{bmatrix} a_1(t) \\ a_2(t) \\ a_3(t) \\ a_4(t) \end{bmatrix} = \begin{bmatrix} J & \widetilde{B}^2(t) & \widetilde{B}^1(t) & 0 \\ \widetilde{B}^2(t)^* & -J & 2J & \widetilde{B}^1(t) \\ \widetilde{B}^1(t)^* & 2J & -J & \widetilde{B}^2(t) \\ 0 & \widetilde{B}^1(t)^* & \widetilde{B}^2(t)^* & J \end{bmatrix} \begin{bmatrix} a_1(t) \\ a_2(t) \\ a_3(t) \\ a_4(t) \end{bmatrix}, \tag{3.3}$$

where $\widetilde{B}^i(t) = \frac{1}{2}e^{-i\theta}B^i(t)$. The solution to Eq. (3.3) may be written in terms of

the time evolution matrix $\hat{U}(t)$ as

$$\begin{bmatrix} a_1(t) \\ a_2(t) \\ a_3(t) \\ a_4(t) \end{bmatrix} = \hat{U}(t) \begin{bmatrix} a_1(0) \\ a_2(0) \\ a_3(0) \\ a_4(0) \end{bmatrix}, \tag{3.4}$$

where an experiment is begun at a time $t = 0$ and completed at $t = T_f$.

The time evolution operator $\hat{U}(t)$ may be expressed here as

$$\begin{aligned} \hat{U}(t) &= \hat{T} e^{-i \int_0^t \hat{H}(t')dt'} = \hat{T} e^{-i \int_0^t \left(\hat{H}_0 + \hat{H}_{int}(t')\right)dt'} \\ &= \hat{T} \sum_{n=0}^{\infty} \frac{(-i)^n}{n!} \int_0^t \hat{H}(t_n)dt_n ... \int_0^t \hat{H}(t_2)dt_2 \int_0^t \hat{H}(t_1)dt_1 \ . \end{aligned} \tag{3.5}$$

The only non-trivial time dependence in $\hat{U}(t)$ arises from time dependent $\hat{H}(t)$ and time ordering $\hat{T}$. The Dyson time ordering operator $\hat{T}$ [33] specifies that $\hat{H}(t_i)\hat{H}(t_j)$ is properly ordered:

$$\hat{T}\hat{H}(t_i)\hat{H}(t_j) = \hat{H}(t_i)\hat{H}(t_j) + \theta(t_j - t_i)\left[\hat{H}(t_j), \hat{H}(t_i)\right] .$$

Time ordering imposes a connection between the effects of $\hat{H}(t_i)$ and $\hat{H}(t_j)$ and leads to observable, non-local, time ordering effects when $\left[\hat{H}(t_j), \hat{H}(t_i)\right] \neq 0$.

3.3 Time ordering

Since time ordering effects can be defined as the difference between a result with time ordering and the corresponding result in the limit of no time ordering, it is useful to specify carefully the limit without time ordering. Removing time ordering corresponds to replacing $T \to 1$ in Eq. (3.5). This corresponds to the zeroth order term in an eikonal-like, Magnus expansion in commutator terms [34].

3.3.1 Limit of no time ordering

Replacing $\hat{T}$ with 1 in Eq. (3.5), in the Schrödinger picture we have,

$$\begin{aligned}\hat{U}(t) &= \hat{T}e^{-i\int_0^t \hat{H}(t')dt'} \rightarrow \sum_{n=0}^{\infty} \frac{(-i)^n}{n!}\left[\int_0^t \hat{H}(t')dt'\right]^n \\ &= \sum_{n=0}^{\infty} \frac{(-i)^n}{n!}\left[\hat{H}_0 t + \int_0^t \hat{H}_{int}(t')dt'\right]^n = \sum_{n=0}^{\infty} \frac{(-i)^n}{n!}\left[\left(\hat{H}_0 + \hat{\bar{H}}_{int}\right)t\right]^n \\ &= e^{-i\hat{\bar{H}}t} = \hat{U}^0(t) \quad , \end{aligned} \tag{3.6}$$

where

$$\hat{\bar{H}}_{int}t = \int_0^t \hat{H}_{int}(t')dt',$$

$\hat{\bar{H}} = \hat{H}_0 + \hat{\bar{H}}_{int}$, and $[\hat{H}_0, \hat{\bar{H}}_{int}]$ terms are non-zero. By expanding in powers of $[\hat{H}(t''), \hat{H}(t')]$, it is straightforward to show that to leading order in $\hat{H}_{int}$ and $\hat{H}_0$ the time ordering effect is given by

$$\hat{U} - \hat{U}^0 \simeq -\frac{1}{2}\int_0^t dt'' \int_0^{t''} dt' \left[\hat{H}(t''), \hat{H}(t')\right] = -\frac{1}{2}\left[\hat{H}_0, \hat{H}^0_{int}\right]\int_0^t dt'(t - 2t')f(t')\,, \tag{3.7}$$

where $\hat{H}_{int}(t') = \hat{H}^0_{int}f(t')$. This leading term disappears if the pulse centroid $T_k = t/2$ and $f(t')$ is symmetric about T_k. Furthermore, $\hat{U} - \hat{U}^0$ vanishes identically in the special cases of $H_{int}(t') = 0$, $H_{int}(t') = \bar{H}_{int}$, or $B^1_z(t) = B^2_z(t)$ because,

$$[\hat{H}(t''), \hat{H}(t')] = JD\begin{bmatrix} 0 & a & -a & 0 \\ -a^* & 0 & 0 & a \\ a^* & 0 & 0 & -a \\ 0 & -a^* & a^* & 0 \end{bmatrix}, \tag{3.8}$$

where $D = ((B^2(t') - B^1(t')) - (B^2(t'') - B^1(t'')))$ and $a = e^{-i\theta}$.

In general there is no simple analytic form for the exact result $\hat{U}(t)$. For the result without time ordering with $\bar{B}^1_z t = \int_0^t B^1_z(t')dt' = \alpha$, $\bar{B}^2_z t = \int_0^t B^2_z(t')dt' = \beta$, we have

$$\hat{U}^0(t) = e^{-i(\hat{H}_0 t + \hat{\hat{H}}_{int} t)}, \tag{3.9}$$

with elements

$$\begin{aligned}
U_{11} &= \frac{1}{2}\left(e^{-iJt}\cos\left(\frac{\Omega}{2}\right) + e^{iJt}\left(\cos\left(\frac{\Gamma}{2}\right) - \frac{4iJt}{\Gamma}\sin\left(\frac{\Gamma}{2}\right)\right)\right) = U_{44},\\
U_{22} &= \frac{1}{2}\left(e^{-iJt}\cos\left(\frac{\Omega}{2}\right) + e^{iJt}\left(\cos\left(\frac{\Gamma}{2}\right) + \frac{4iJt}{\Gamma}\sin\left(\frac{\Gamma}{2}\right)\right)\right) = U_{33},\\
U_{23} &= \frac{1}{2}\left(e^{-iJt}\cos\left(\frac{\Omega}{2}\right) - e^{iJt}\left(\cos\left(\frac{\Gamma}{2}\right) + \frac{4iJt}{\Gamma}\sin\left(\frac{\Gamma}{2}\right)\right)\right) = U_{32},\\
U_{12} &= \frac{1}{2}ie^{-iJt}e^{-i\theta}\left(e^{2iJt}\frac{\Delta}{\Gamma}\sin\left(\frac{\Gamma}{2}\right) - \sin\left(\frac{\Omega}{2}\right)\right) = U_{34},\\
U_{13} &= -\frac{1}{2}ie^{-iJt}e^{-i\theta}\left(e^{2iJt}\frac{\Delta}{\Gamma}\sin\left(\frac{\Gamma}{2}\right) + \sin\left(\frac{\Omega}{2}\right)\right) = U_{24},\\
U_{21} &= \frac{1}{2}ie^{-iJt}e^{i\theta}\left(e^{2iJt}\frac{\Delta}{\Gamma}\sin\left(\frac{\Gamma}{2}\right) - \sin\left(\frac{\Omega}{2}\right)\right) = U_{43},\\
U_{14} &= \frac{1}{2}e^{-2i\theta}\left(e^{-iJt}\cos\left(\frac{\Omega}{2}\right) - e^{iJt}\left(\cos\left(\frac{\Gamma}{2}\right) - \frac{4iJt}{\Gamma}\sin\left(\frac{\Gamma}{2}\right)\right)\right) = e^{-4i\theta}U_{41},\\
U_{31} &= -\frac{1}{2}ie^{-iJt}e^{i\theta}\left(e^{2iJt}\frac{\Delta}{\Gamma}\sin\left(\frac{\Gamma}{2}\right) + \sin\left(\frac{\Omega}{2}\right)\right) = U_{42},
\end{aligned} \tag{3.10}$$

where $\Gamma = \sqrt{16J^2t^2 + \Delta^2}, \Delta = (\alpha - \beta)$ and $\Omega = (\alpha + \beta)$.

3.4 Measure of entanglement

For any two-qubit case, Wooters concurrence [6] can be used as a measure of entanglement. The concurrence function varies from $C = 0$ for a separable state to $C = 1$ for a maximally entangled state. To calculate the concurrence function one needs to evaluate the matrix

$$\hat{\rho}_{trans}(t) = \hat{\rho}(t)(\hat{\sigma}_y \otimes \hat{\sigma}_y)\hat{\rho}^*(t)(\hat{\sigma}_y \otimes \hat{\sigma}_y), \tag{3.11}$$

where $\hat{\rho}(t)$ is the density matrix of the system and $\hat{\rho}^*(t)$ is its complex conjugate. The concurrence is defined as

$$C(\hat{\rho}) = \max\{0, \lambda_1 - \lambda_2 - \lambda_3 - \lambda_4\}, \tag{3.12}$$

where $\lambda_1, \lambda_2, \lambda_3$ and λ_4 are the positive roots of the eigenvalues of $\hat{\rho}_{trans}(t)$ in descending order. It is straightforward to evaluate the concurrence of a pure state of the form

$$|\Psi(t)\rangle = a_1(t)\,|11\rangle + a_2(t)\,|10\rangle + a_3(t)\,|01\rangle + a_4(t)\,|00\rangle\,, \tag{3.13}$$

where $a_1(t), a_2(t), a_3(t)$ and $a_4(t)$ are the time-dependent complex functions satisfying the condition

$$|a_1(t)|^2 + |a_2(t)|^2 + |a_3(t)|^2 + |a_4(t)|^2 = 1, \tag{3.14}$$

and the density matrix $\hat{\rho}(t) = |\Psi(t)\rangle\,\langle\Psi(t)|$. In this case the concurrence function is given by

$$C(\hat{\rho}) = 2\,|a_1(t)a_4(t) - a_2(t)a_3(t)|\,, \tag{3.15}$$

with time dependent coefficients given by Eq. (3.4):

$$a_i(t) = \sum_{j=1}^{4} U_{ij}(t)a_j(0). \tag{3.16}$$

3.5 Entanglement dynamics of kicked qubits

In this part, we will examine the entanglement evolution of kicked qubits in the presence of time ordering for the initial pure states $|\Psi(0)\rangle = |11\rangle$(separable) and $|\Psi(0)\rangle = \frac{1}{\sqrt{2}}(|11\rangle + |00\rangle)$(maximally entangled). According to Eq. (3.15) and (3.16), to examine the entanglement evolution one has to present the analytic expressions of the propagators after the kick is active. Thus, we firstly present the analytic expression for the propagator for singly kicked qubits and then discuss the extensions to multiple kicks, using a positive followed by a negative kick and

a sequence of two and three positive kicks as an example.

3.5.1 Single kick

Here we consider two qubits whose states are coupled by an external field expressed as a sudden kick at $t = T$. In this case the time dependent magnetic fields on qubit 1 and 2 may be expressed as $B^1(t) = \alpha\delta(t-T)$ and $B^2(t) = \beta\delta(t-T)$, respectively. For such a kick the integration over the time is trivial and the time evolution matrix in Eq. (3.5) becomes for $t > T$

$$\hat{U}^K(t) = e^{-i\hat{H}_0(t-T)} e^{-i\int_{T-\epsilon}^{T+\epsilon} \hat{H}_{int}(t')dt'} e^{-i\hat{H}_0 T}, \tag{3.17}$$

with elements

$$\begin{aligned}
U_{11} &= e^{-iJt}\cos\left(\frac{\alpha}{2}\right)\cos\left(\frac{\beta}{2}\right) = U_{44}, \\
U_{22} &= \frac{1}{2}e^{-iJt}\left(e^{4iJt}\cos\left(\frac{\Delta}{2}\right) + \cos\left(\frac{\Omega}{2}\right)\right) = U_{33}, \\
U_{23} &= -\frac{1}{2}e^{-iJt}\left(e^{4iJt}\cos\left(\frac{\Delta}{2}\right) - \cos\left(\frac{\Omega}{2}\right)\right) = U_{32}, \\
U_{12} &= \frac{1}{2}ie^{-iJt}e^{-i\theta}\left(e^{4iJT}\sin\left(\frac{\Delta}{2}\right) - \sin\left(\frac{\Omega}{2}\right)\right) = e^{-2i\theta}U_{43}, \\
U_{13} &= -\frac{1}{2}ie^{-iJt}e^{-i\theta}\left(e^{4iJT}\sin\left(\frac{\Delta}{2}\right) + \sin\left(\frac{\Omega}{2}\right)\right) = e^{-2i\theta}U_{42}, \\
U_{14} &= -e^{-iJt}e^{-2i\theta}\sin\left(\frac{\alpha}{2}\right)\sin\left(\frac{\beta}{2}\right) = e^{-4i\theta}U_{41}, \\
U_{21} &= -e^{iJ(t-2T)}e^{i\theta}\left(\cos\left(\frac{\beta}{2}\right)\sin\left(\frac{\alpha}{2}\right)\sin(\xi) + i\cos\left(\frac{\alpha}{2}\right)\sin\left(\frac{\beta}{2}\right)\cos(\xi)\right) \\
&= e^{2i\theta}U_{34}, \\
U_{24} &= -\frac{1}{2}ie^{-iJt}e^{-i\theta}\left(e^{2i\xi}\sin\left(\frac{\Delta}{2}\right) + \sin\left(\frac{\Omega}{2}\right)\right) = e^{-2i\theta}U_{31},
\end{aligned} \tag{3.18}$$

where $\Delta = (\alpha-\beta), \Omega = (\alpha+\beta)$ and $\xi = 2J(t-T)$. For this case the propagator without time ordering is given by Eq. (3.9) and as explained before when $\alpha = \beta$, $\hat{U}^K(t) - \hat{U}^0(t) \to 0$ after the kick is active.

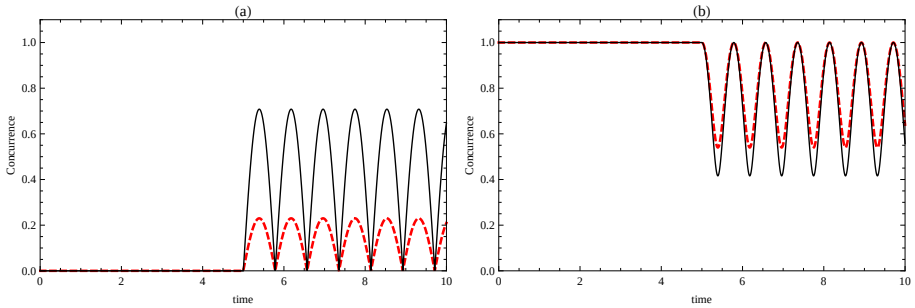

Figure 3.1: Entanglement evolution for a positive single kick applied at $T = 5$ for the initial pure states $|\Psi(0)\rangle = |11\rangle$ (Fig. (a)) and $|\Psi(0)\rangle = \frac{1}{\sqrt{2}}(|11\rangle + |00\rangle)$ (Fig. (a)) with $\beta = J = 1$ and $\theta = \frac{\pi}{2}$. Here the dashed plots correspond to $\alpha = 2\beta$ and the solid plots to $\alpha = 3\beta$.

3.5.2 A positive followed by a negative kick

The second example is the positive kick followed by a negative kick applied at times $t = T_1$ and $t = T_2$. In this case, the time dependent magnetic field on qubits can be expressed as $B^1(t) = \alpha(\delta(t-T_1)-\delta(t-T_2)), B^2(t) = \beta(\delta(t-T_1)-\delta(t-T_2))$. Following the procedure given in Eq. (3.17) one obtains the time evolution matrix for $t > T_2$,

$$\hat{U}^K(t) = e^{-i\hat{H}_0(t-T_2)}e^{-i\int_{T_2-\epsilon}^{T_2+\epsilon}\hat{H}_{int}(t')dt'}e^{-i\hat{H}_0(T_2-T_1)}e^{-i\int_{T_1-\epsilon}^{T_1+\epsilon}\hat{H}_{int}(t')dt'}e^{-i\hat{H}_0T_1}, \quad (3.19)$$

with the elements

$$
\begin{aligned}
U_{11} &= e^{-iJ(t-2T)}\left(\cos(2JT) - i\cos\left(\frac{\Delta}{2}\right)^2\sin(2JT)\right) = U_{44},\\
U_{22} &= \frac{1}{4}e^{-iJ(t+4T)}\left(e^{4iJt} + 2e^{4iJT} + e^{4iJ(t+T)} + e^{4iJt}(e^{4iJT}-1)\cos(\Delta)\right) = U_{33},\\
U_{23} &= \frac{1}{2}e^{-iJt}\left(1 - e^{2iJ(2t-T)}\left(\cos(2JT) + i\cos(\Delta)\sin(2JT)\right)\right) = U_{32},\\
U_{12} &= \frac{1}{2}e^{-iJ(t-6T)}e^{-i\theta}\sin(2JT)\sin(\Delta) = e^{-2i\theta}U_{43},\\
U_{13} &= -\frac{1}{2}e^{-iJ(t-6T)}e^{-i\theta}\sin(2JT)\sin(\Delta) = e^{-2i\theta}U_{42},\\
U_{14} &= -ie^{-iJ(t-2T)}e^{-2i\theta}\sin(2JT)\sin\left(\frac{\Delta}{2}\right)^2 = e^{-4i\theta}U_{41},\\
U_{21} &= -\frac{1}{2}e^{3iJ(t-2T)}e^{i\theta}\sin(2JT)\sin(\Delta) = -U_{31},\\
U_{24} &= \frac{1}{2}e^{3iJ(t-2T)}e^{-i\theta}\sin(2JT)\sin(\Delta) = -U_{34},
\end{aligned}
\tag{3.20}
$$

where $\Delta = (\alpha - \beta)$. Here, for simplicity, we assume periodic kicks applied at $T_1 = T$ and $T_2 = 2T$. Note if $\alpha = \beta$, $\hat{U}^K(t)$ reduces to

$$
\begin{aligned}
\hat{U}^0(t) &= e^{-i\hat{H}_0 t}\\
&= \begin{bmatrix}
e^{-iJt} & 0 & 0 & 0\\
0 & e^{\frac{iJt}{\hbar}}\cos(2Jt) & -ie^{iJt}\sin(2Jt) & 0\\
0 & -ie^{iJt}\sin(2Jt) & e^{iJt}\cos(2Jt) & 0\\
0 & 0 & 0 & e^{-iJt}
\end{bmatrix},
\end{aligned}
\tag{3.21}
$$

because for a positive kick followed by a negative kick $\hat{\hat{H}}_{int}t = 0$.

3.5.3 Two positive kicks

The next example is a sequence of two positive kicks applied at times $t = T_1$ and $t = T_2$, namely, $B^1(t) = \alpha(\delta(t-T_1)+\delta(t-T_2)), B^2(t) = \beta(\delta(t-T_1)+\delta(t-T_2))$. Following the procedure given in Eq. (3.17) one obtains the matrix elements of the time evolution matrix (3.19) for $t > T_2$ as

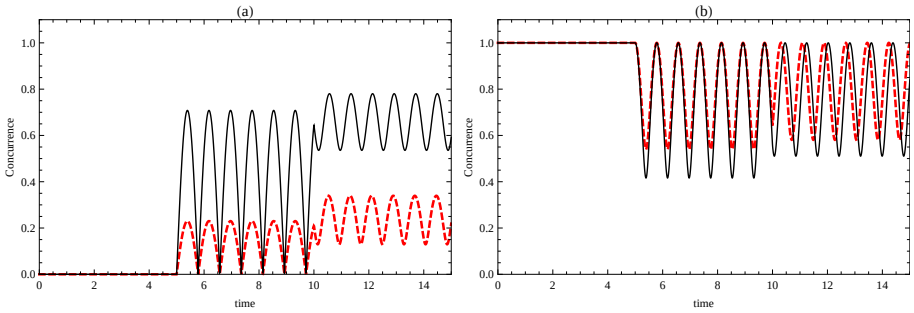

Figure 3.2: Entanglement evolution for a positive kick at $T_1 = 5$ followed by a negative kick at $T_2 = 10$ for the initial pure states $|\Psi(0)\rangle = |11\rangle$ (Fig. (a)) and $|\Psi(0)\rangle = \frac{1}{\sqrt{2}}(|11\rangle + |00\rangle)$ (Fig. (b)) with $\beta = J = 1$ and $\theta = \frac{\pi}{2}$. Here the dashed plots correspond to $\alpha = 2\beta$ and the solid plots to $\alpha = 3\beta$.

$$
\begin{aligned}
U_{11} &= \frac{1}{4}e^{-iJt}\left(1 + e^{4iJT}\left(\cos(\Delta) - 1\right) + \cos(\Delta) + 2\cos(\Omega)\right) = U_{44},\\
U_{22} &= \frac{1}{4}e^{-iJt}\left(e^{4iJt} + e^{4iJ(t-T)}\left(\cos(\Delta) - 1\right) + e^{4iJt}\cos(\Delta) + 2\cos(\Omega)\right) = U_{33},\\
U_{23} &= -\frac{1}{4}e^{-iJt}\left(e^{4iJt} + e^{4iJ(t-T)}\left(\cos(\Delta) - 1\right) + e^{4iJt}\cos(\Delta) - 2\cos(\Omega)\right) = U_{32},\\
U_{12} &= \frac{1}{2}ie^{-iJt}e^{-i\theta}\left(e^{6iJT}\cos(2JT)\sin(\Delta) - \sin(\Omega)\right) = e^{-2i\theta}U_{43},\\
U_{13} &= -\frac{1}{2}ie^{-iJt}e^{-i\theta}\left(e^{6iJT}\cos(2JT)\sin(\Delta) + \sin(\Omega)\right) = e^{-2i\theta}U_{42},\\
U_{14} &= \frac{1}{4}e^{-iJt}e^{-2i\theta}\left(e^{4iJT} - 1 - (1 + e^{4iJT})\cos(\Delta) + 2\cos(\Omega)\right) = e^{-4i\theta}U_{41},\\
U_{21} &= \frac{1}{4}ie^{-iJt}e^{i\theta}\left(e^{4iJ(t-2T)}(1 + e^{4iJT})\sin(\Delta) - 2\sin(\Omega)\right) = e^{2i\theta}U_{34},\\
U_{24} &= -\frac{1}{4}ie^{-iJt}e^{-i\theta}\left(e^{4iJ(t-2T)}(1 + e^{4iJT})\sin(\Delta) + 2\sin(\Omega)\right) = e^{-2i\theta}U_{31}, \quad (3.22)
\end{aligned}
$$

where $\Delta = (\alpha - \beta)$ and $\Omega = (\alpha + \beta)$. Here, for simplicity, we set $T_1 = T, T_2 = 2T$. The propagator for without time ordering can be calculated by replacing $\bar{B}^1 t \to 2\alpha$ and $\bar{B}^2 t \to 2\beta$ in Eq. (3.9) and note for $\alpha = \beta$, $\hat{U}^K(t) - \hat{U}^0(t)$ vanishes.

3.5.4 Three positive kicks

The final example is a sequence of three positive kicks applied at times $t = T_1, t = T_2$, and $t = T_3$ namely, $B^1(t) = \sum_{i=1}^{3} \alpha\delta(t - T_i), B^2(t) = \sum_{i=1}^{3} \beta\delta(t - T_i)$. Following the procedure given in Eq. (3.17) one obtains the time evolution matrix for $t > T_3$,

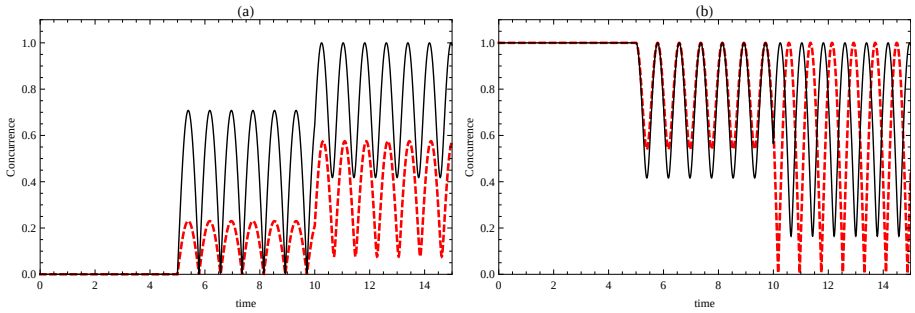

Figure 3.3: Entanglement evolution for a sequence of two positive kicks applied at $T_1 = 5$ and $T_2 = 10$ for the initial pure states $|\Psi(0)\rangle = |11\rangle$ (Fig. (a)) and $|\Psi(0)\rangle = \frac{1}{\sqrt{2}}(|11\rangle + |00\rangle)$ (Fig. (b)) with $\beta = J = 1$ and $\theta = \frac{\pi}{2}$. Here the dashed plots correspond to $\alpha = 2\beta$ and the solid plots to $\alpha = 3\beta$.

$$\begin{aligned} \hat{U}^K(t) &= e^{-i\hat{H}_0(t-T_3)} e^{-i\int_{T_3-\epsilon}^{T_3+\epsilon} \hat{H}_{int}(t')dt'} e^{-i\hat{H}_0(T_3-T_2)} e^{-i\int_{T_2-\epsilon}^{T_2+\epsilon} \hat{H}_{int}(t')dt'} \\ &\times e^{-i\hat{H}_0(T_2-T_1)} e^{-i\int_{T_1-\epsilon}^{T_1+\epsilon} \hat{H}_{int}(t')dt'} e^{-i\hat{H}_0 T_1}, \end{aligned} \tag{3.23}$$

with matrix elements for $T_1 = T, T_2 = 2T, T_3 = 3T$,

$$
\begin{aligned}
U_{11} &= \frac{1}{8}e^{-iJt}\left((3-2e^{4iJT}-e^{8iJT})\cos\left(\frac{\Delta}{2}\right)+(1+e^{4iJT})^2\cos\left(\frac{3\Delta}{2}\right)+4\cos\left(\frac{3\Omega}{2}\right)\right)\\
&= U_{44},\\
U_{22} &= \frac{1}{2}e^{-iJt}\left(\cos\left(\frac{3\Omega}{2}\right)+e^{4iJ(t-T)}\cos\left(\frac{\Delta}{2}\right)((1+\cos(4JT))\cos(\Delta)+i\sin(4JT)-1)\right)\\
&= U_{33},\\
U_{23} &= \frac{1}{2}e^{-iJt}\left(\cos\left(\frac{3\Omega}{2}\right)-e^{4iJ(t-T)}\cos\left(\frac{\Delta}{2}\right)((1+\cos(4JT))\cos(\Delta)+i\sin(4JT)-1)\right)\\
&= U_{32},\\
U_{12} &= \frac{1}{2}ie^{-iJt}e^{-i\theta}\left(e^{8iJT}(\cos(4JT)+2\cos(2JT)^2\cos(\Delta))\sin\left(\frac{\Delta}{2}\right)-\sin\left(\frac{3\Omega}{2}\right)\right)\\
&= e^{-2i\theta}U_{43},\\
U_{13} &= -\frac{1}{2}ie^{-iJt}e^{-i\theta}\left(e^{8iJT}(\cos(4JT)+2\cos(2JT)^2\cos(\Delta))\sin\left(\frac{\Delta}{2}\right)+\sin\left(\frac{3\Omega}{2}\right)\right)\\
&= e^{-2i\theta}U_{42},\\
U_{14} &= \frac{1}{8}e^{-i(Jt+2\theta)}\left((2e^{4iJT}+e^{8iJT}-3)\cos\left(\frac{\Delta}{2}\right)-(1+e^{4iJT})^2\cos\left(\frac{3\Delta}{2}\right)+4\cos\left(\frac{3\Omega}{2}\right)\right)\\
&= e^{-4i\theta}U_{41},\\
U_{21} &= \frac{1}{2}ie^{-iJt}e^{i\theta}\left(e^{4iJ(t-2T)}(\cos(4JT)+2\cos(2JT)^2\cos(\Delta))\sin\left(\frac{\Delta}{2}\right)-\sin\left(\frac{3\Omega}{2}\right)\right)\\
&= e^{2i\theta}U_{34},\\
U_{24} &= -\frac{1}{2}ie^{-iJt}e^{-i\theta}\left(e^{4iJ(t-2T)}(\cos(4JT)+2\cos(2JT)^2\cos(\Delta))\sin\left(\frac{\Delta}{2}\right)+\sin\left(\frac{3\Omega}{2}\right)\right)\\
&= e^{-2i\theta}U_{31}, \qquad (3.24)
\end{aligned}
$$

where $\Delta = (\alpha - \beta)$ and $\Omega = (\alpha + \beta)$. Here the propagator for without time ordering can be calculated by replacing $\bar{B}^1 t \to 3\alpha$ and $\bar{B}^2 t \to 3\beta$ in Eq. (3.9) and note for $\alpha = \beta$, $\hat{U}^K(t) - \hat{U}^0(t)$ vanishes.

3.6 Entanglement dynamics of qubits perturbed by gaussian pulses

In this part, we will examine the entanglement evolution of qubits whose states are strongly perturbed by a Gaussian pulse of the form $B^i(t) = \frac{\alpha_i}{\sqrt{\pi}\tau}e^{-\frac{(t-T_k)^2}{\tau^2}}(\alpha_{1,2} =$

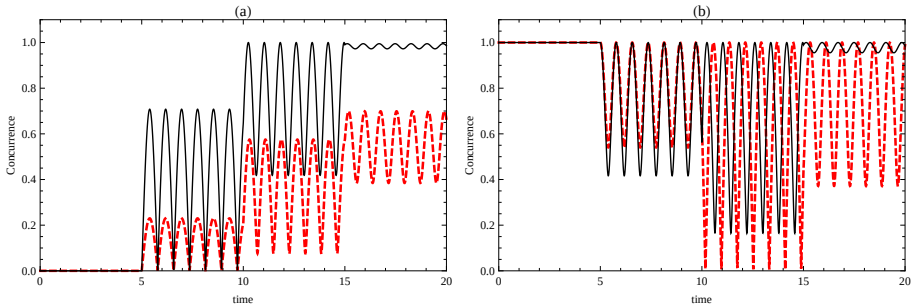

Figure 3.4: Entanglement evolution for a sequence of three positive kicks applied at $T_1 = 5, T_2 = 10$ and $T_3 = 15$ for the initial pure states $|\Psi(0)\rangle = |11\rangle$ (Fig. (a)) and $|\Psi(0)\rangle = \frac{1}{\sqrt{2}}(|11\rangle + |00\rangle)$ (Fig. (a)) with $\beta = J = 1$ and $\theta = \frac{\pi}{2}$. Here the dashed plots correspond to $\alpha = 2\beta$ and the solid plots to $\alpha = 3\beta$.

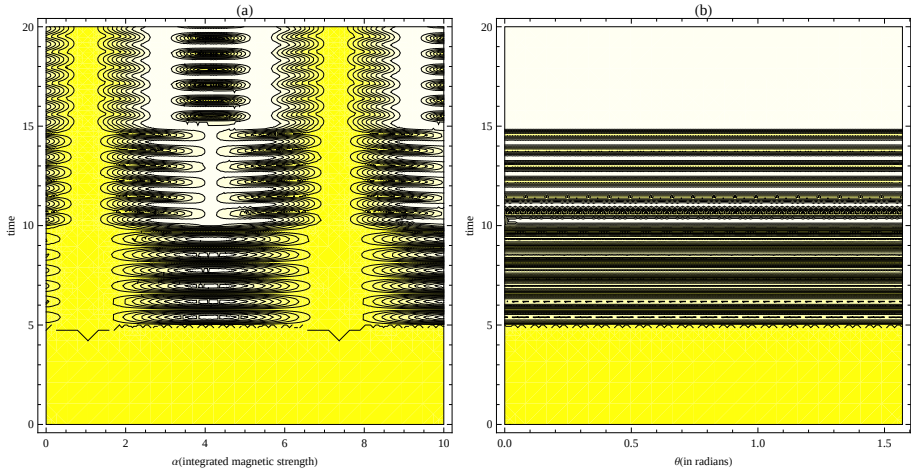

Figure 3.5: Fig. (a) shows the contour plot of concurrence versus time and integrated magnetic strength for the initial state $|\Psi(0)\rangle = |11\rangle$ with $\theta = \frac{\pi}{2}$. Fig. (b) shows the contour plot of concurrence versus time and the angle for the same initial state with $\alpha = 3\beta$. Here the contour plots include three positive kicks applied at $T_1 = 5, T_2 = 10$ and $T_3 = 15$ with $\beta = J = 1$.

$\alpha, \beta)$, centered at T_k with width τ for the initial states $|\Psi(0)\rangle = |11\rangle$ and $|\Psi(0)\rangle = \frac{1}{\sqrt{2}}(|11\rangle + |00\rangle)$. The entanglement evolution of these initial states can be evaluated by using the Eq. (3.15) and numerically integrating the equations in (3.3) which are

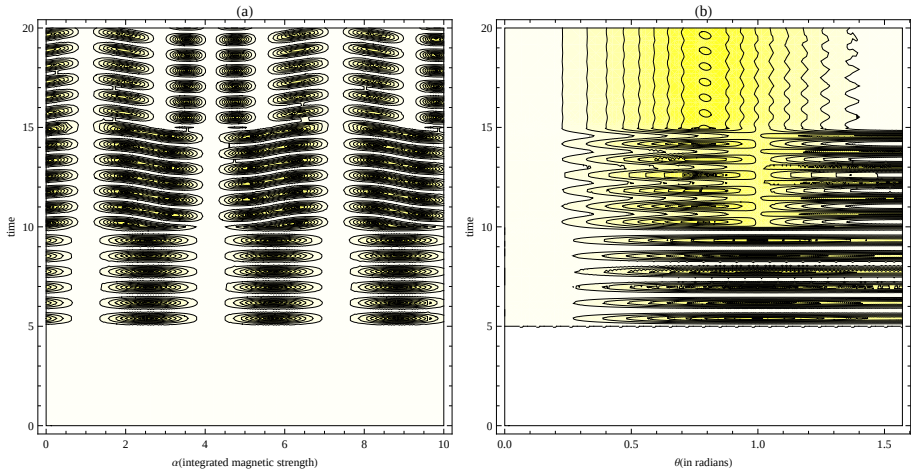

Figure 3.6: Fig. (a) shows the contour plot of concurrence versus time and integrated magnetic strength for the initial state $|\Psi(0)\rangle = \frac{1}{\sqrt{2}}(|11\rangle + |00\rangle)$ with $\theta = \frac{\pi}{2}$. Fig. (b) shows the contour plot of concurrence versus time and the angle for the same initial state with $\alpha = 3\beta$. Here the contour plots include three positive kicks applied at $T_1 = 5, T_2 = 10$ and $T_3 = 15$ with $\beta = J = 1$.

$$
\begin{aligned}
i\dot{a}_1(t) &= Ja_1(t) + \frac{1}{2}e^{-i\theta}B^2(t)a_2(t) + \frac{1}{2}e^{-i\theta}B^1(t)a_3(t), \\
i\dot{a}_2(t) &= \frac{1}{2}e^{i\theta}B^2(t)a_1(t) - Ja_2(t) + 2Ja_3(t) + \frac{1}{2}e^{-i\theta}B^1(t)a_4(t), \\
i\dot{a}_3(t) &= \frac{1}{2}e^{i\theta}B^1(t)a_1(t) + 2Ja_2(t) - Ja_3(t) + \frac{1}{2}e^{-i\theta}B^2(t)a_4(t), \\
i\dot{a}_4(t) &= \frac{1}{2}e^{i\theta}B^1(t)a_2(t) + \frac{1}{2}e^{i\theta}B^2(t)a_3(t) + Ja_4(t). \qquad (3.25)
\end{aligned}
$$

Here we shall determine how the entanglement evolution depends on the pulse width,τ, by choosing a single pulse, a positive pulse followed by a negative pulse and a sequence of two and three positive pulses as an example. Note in the limit as $\tau \to 0$, the results of entanglement evolution of kicked qubits in the presence of time ordering can be reached that are analyzed in the previous section.

3.6.1 Single Pulse

In Fig. 3.7, we show the results of a calculation of the entanglement evolution of qubits for the initial pure states $|\Psi(0)\rangle = \frac{1}{\sqrt{2}}(|11\rangle + |00\rangle)$ and $|\Psi(0)\rangle = |11\rangle$ when strongly perturbed by a single positive Gaussian pulse centered at $t =$

T_1 with width τ. The results can be obtained by numerically integrating the coupled equations in (3.25) with replacing $B^1(t) \to \frac{\alpha}{\sqrt{\pi}\tau} e^{-\frac{(t-T_1)^2}{\tau^2}}$ and $B^2(t) \to \frac{\beta}{\sqrt{\pi}\tau} e^{-\frac{(t-T_1)^2}{\tau^2}}$.

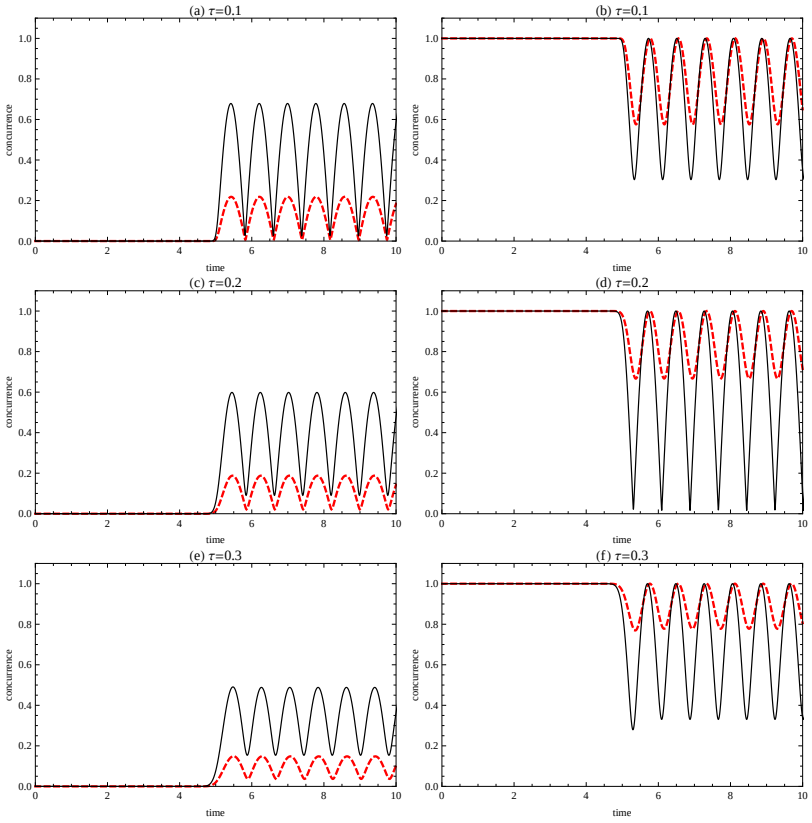

Figure 3.7: Entanglement evolution of qubits perturbed by a single Gaussian pulse centered at $T_1 = 5$ with width τ for the initial pure states $|\Psi(0)\rangle = |11\rangle$ (Fig. (a), (c) and (e)) and $|\Psi(0)\rangle = \frac{1}{\sqrt{2}}(|11\rangle + |00\rangle)$ (Fig. (b), (d) and (f)) with $\beta = J = 1$ and $\theta = \frac{\pi}{2}$.

3.6.2 A positive followed by a negative pulse

In Fig. 3.8, we show the results of a calculation of the entanglement evolution of qubits when strongly perturbed by a single Gaussian pulse centered at $t = T_1$ followed by a negative Gaussian pulse centered at $t = T_2$ with the same width, τ. The results can be obtained by numerically integrating the coupled equatins in (3.25) with replacing $B^1(t) \to \frac{\alpha}{\sqrt{\pi}\tau}(e^{-\frac{(t-T_1)^2}{\tau^2}} - e^{-\frac{(t-T_2)^2}{\tau^2}})$ and $B^2(t) \to \frac{\beta}{\sqrt{\pi}\tau}(e^{-\frac{(t-T_1)^2}{\tau^2}} - e^{-\frac{(t-T_2)^2}{\tau^2}})$.

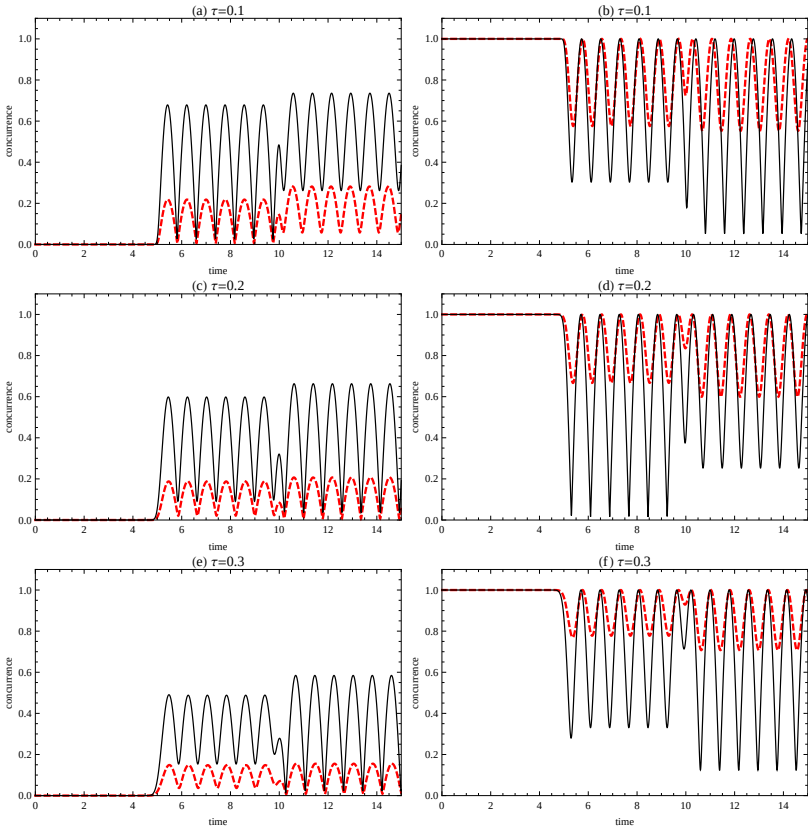

Figure 3.8: Entanglement evolution of qubits perturbed by a positive Gaussian pulse centered at $T_1 = 5$ followed by a negative Gaussian pulse centered at $T_2 = 10$ with the same width τ for the initial pure states $|\Psi(0)\rangle = |11\rangle$ (Fig. (a), (c) and (e)) and $|\Psi(0)\rangle = \frac{1}{\sqrt{2}}(|11\rangle + |00\rangle)$ (Fig. (b), (d) and (f)) with $\beta = J = 1$ and $\theta = \frac{\pi}{2}$.

3.6.3 A sequence of two pulses

Fig. 3.9 shows the calculation of the entanglement evolution of qubits when strongly perturbed by a sequence of two positive Gaussian pulses centered at $t = T_1$ and $t = T_2$ with the same width, τ. The results can be obtained by numerically integrating the coupled equations in (3.25) with replacing $B^1(t) \rightarrow \frac{\alpha}{\sqrt{\pi}\tau}(e^{-\frac{(t-T_1)^2}{\tau^2}} + e^{-\frac{(t-T_2)^2}{\tau^2}})$ and $B^2(t) \rightarrow \frac{\beta}{\sqrt{\pi}\tau}(e^{-\frac{(t-T_1)^2}{\tau^2}} + e^{-\frac{(t-T_2)^2}{\tau^2}})$.

3.6.4 A sequence of three pulses

The last numerical calculation is the entanglement evolution of qubits whose states are coupled to a sequence of three positive Gaussian pulses centered at $t = T_1, t = T_2$ and $t = T_3$ with the same width, τ. The results shown in

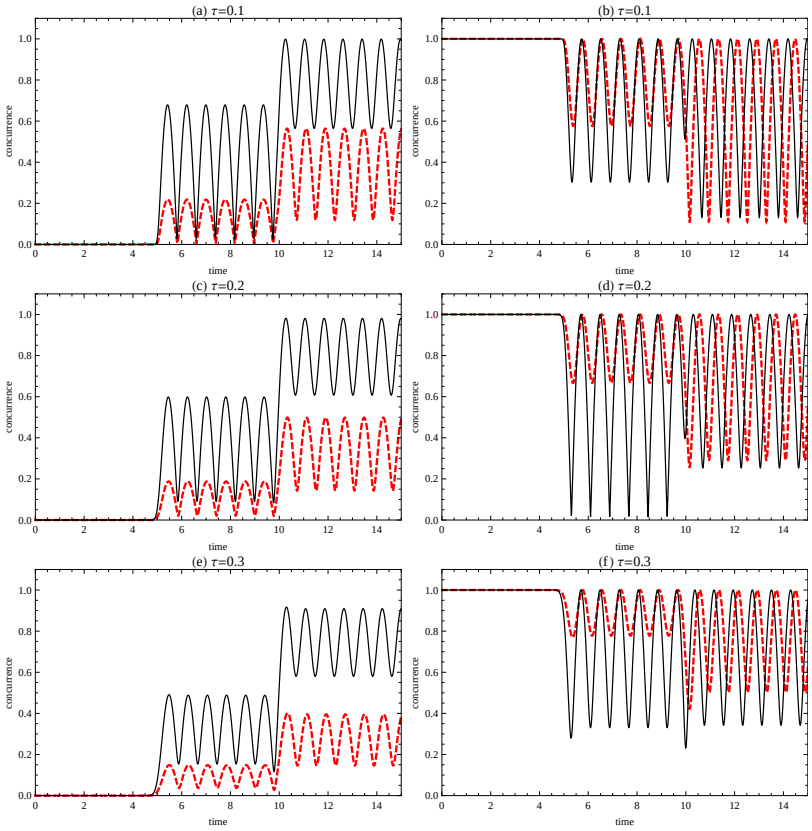

Figure 3.9: Entanglement evolution of qubits perturbed by a sequence of two positive Gaussian pulses centered at $T_1 = 5$ and $T_2 = 10$ with the same width τ for the initial pure states $|\Psi(0)\rangle = |11\rangle$ (Fig. (a), (c) and (e)) and $|\Psi(0)\rangle = \frac{1}{\sqrt{2}}(|11\rangle + |00\rangle)$ (Fig. (b), (d) and (f)) with $\beta = J = 1$ and $\theta = \frac{\pi}{2}$.

Fig. 3.10, 3.11 and 3.12 can be obtained by numerically integrating the coupled equations in (3.25) with replacing $B^1(t) \to \frac{\alpha}{\sqrt{\pi}\tau} \sum_{i=1}^{3} e^{-\frac{(t-T_i)^2}{\tau^2}}$ and $B^2(t) \to \frac{\beta}{\sqrt{\pi}\tau} \sum_{i=1}^{3} e^{-\frac{(t-T_i)^2}{\tau^2}}$.

There are some interesting features of the entanglement dynamics of two coupled qubits under time-dependent magnetic fields in $x-y$ plane. Firstly, the the frequency of the entanglement oscillation caused by Gaussian pulses or sudden kicks only depends on the exchange interation coefficient and independent of the all other parameters of the system. Moreover, the entanglement dynamics of the Bell state $|\Psi(0)\rangle = \frac{1}{\sqrt{2}}(|11\rangle - |00\rangle)$ is the same as of $|\Psi(0)\rangle = \frac{1}{\sqrt{2}}(|11\rangle + |00\rangle)$ if the magnetic fields on qubits applied in x-direction (i.e. $\theta = 0$). Finally, it can be easily checked that the entanglement dynamics of the initial state $|\Psi(0)\rangle = \frac{1}{\sqrt{2}}(|10\rangle + |01\rangle)$ can not be changed under this control scheme, i.e.,

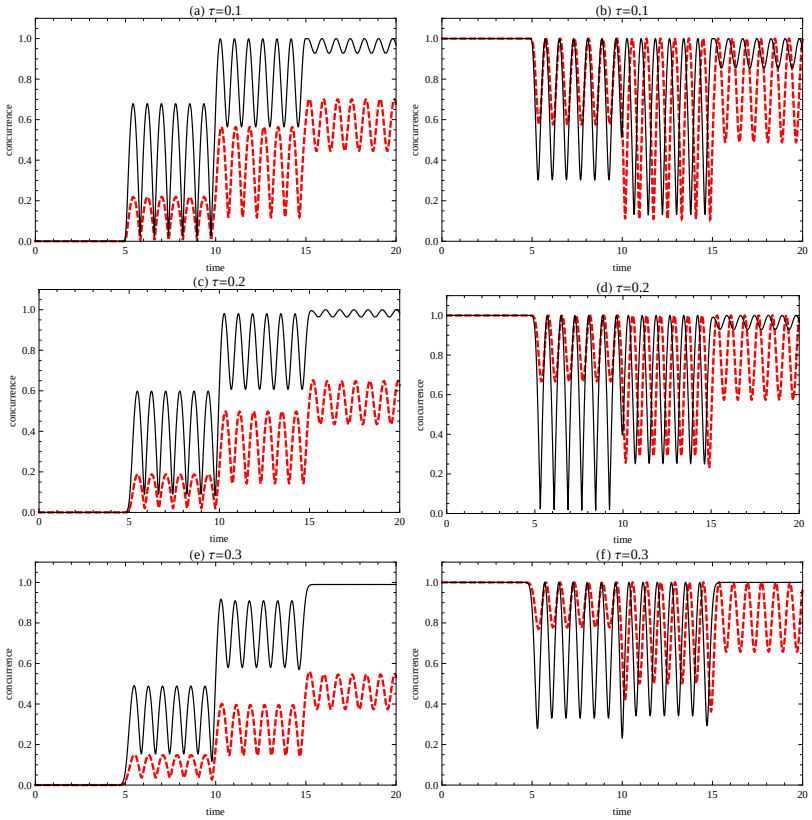

Figure 3.10: Entanglement evolution of qubits perturbed by a sequence of three positive Gaussian pulses centered at $T_1 = 5, T_2 = 10$ and $T_3 = 15$ with the same width τ for the initial pure states $|\Psi(0)\rangle = |11\rangle$ (Fig. (a), (c) and (e)) and $|\Psi(0)\rangle = \frac{1}{\sqrt{2}}(|11\rangle + |00\rangle)$ (Fig. (b), (d) and (f)) with $\beta = J = 1$ and $\theta = \frac{\pi}{2}$.

it is the robust state of this problem.

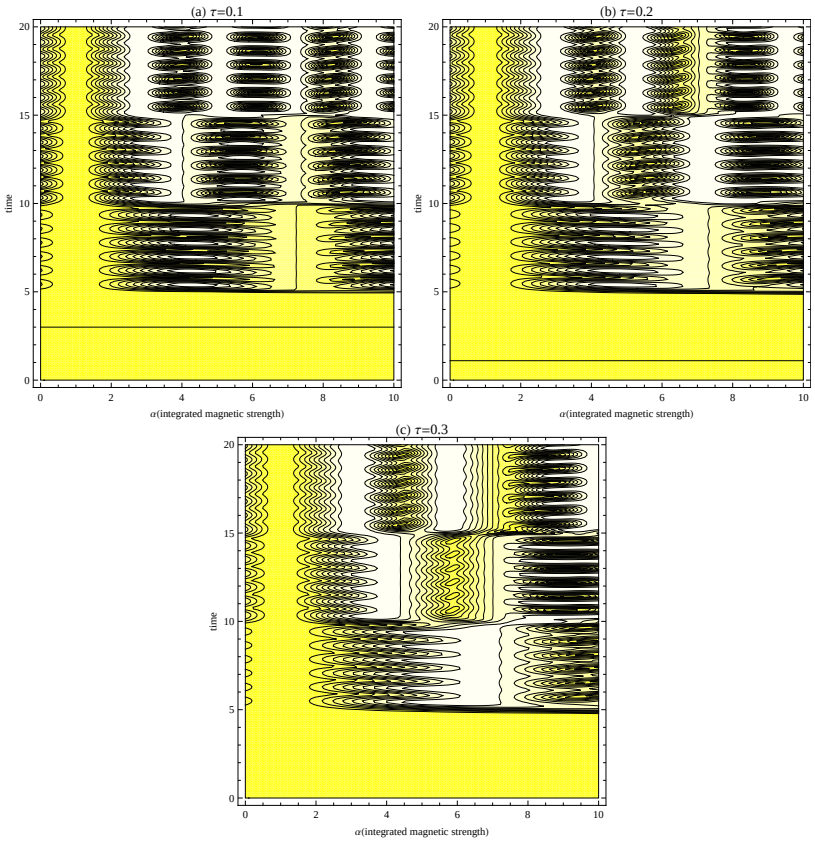

Figure 3.11: The contour plots of concurrence versus time and integrated magnetic strength for the initial state $|\Psi(0)\rangle = |11\rangle$ with $\theta = \frac{\pi}{2}$. Here the contour plots include three positive Gaussian pulses centered at $T_1 = 5, T_2 = 10$ and $T_3 = 15$ with $\beta = J = 1$.

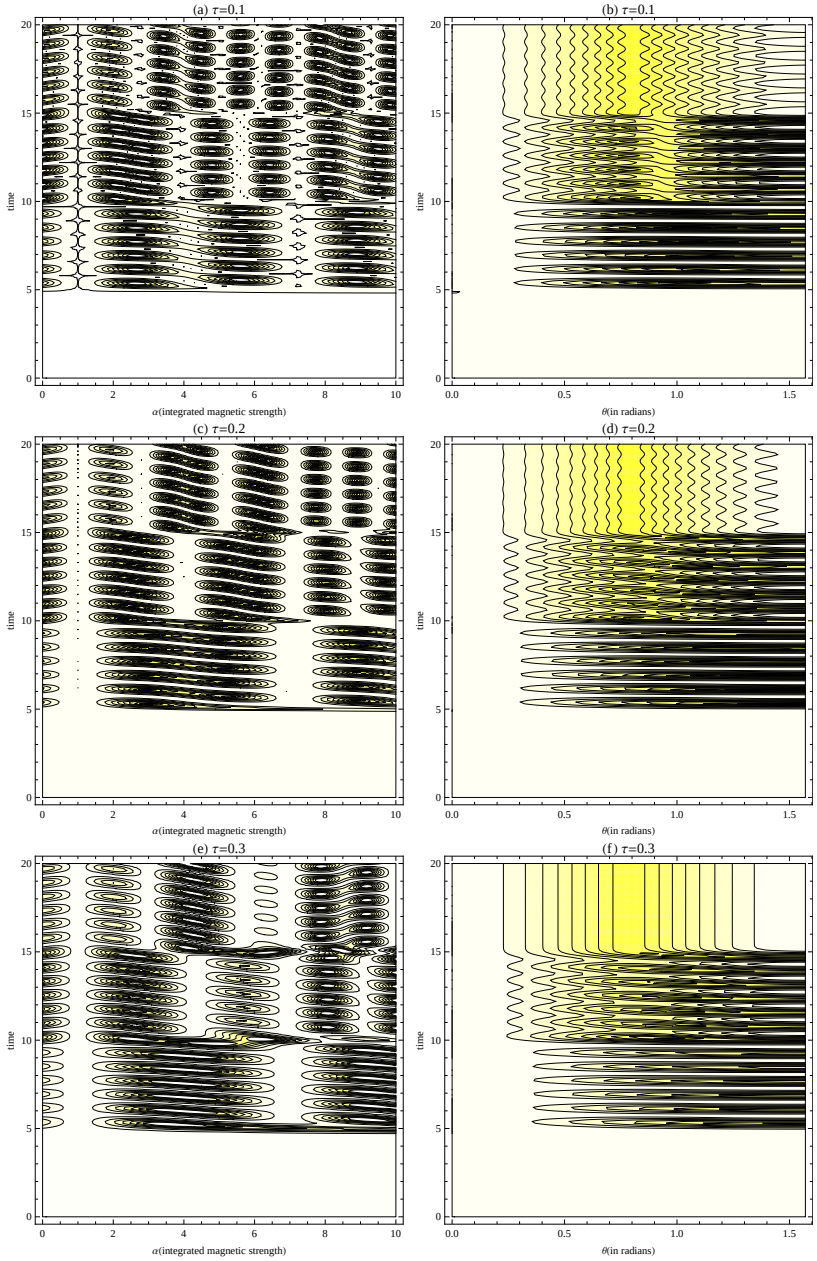

Figure 3.12: (Fig. (a), (c) and (e)) show the contour plot of concurrence versus time and integrated magnetic strength for the initial state $|\Psi(0)\rangle = \frac{1}{\sqrt{2}}(|11\rangle + |00\rangle)$ with $\theta = \frac{\pi}{2}$. Fig. (b), (d) and (f) show the contour plot of concurrence versus time and the angle for the same initial state with $\alpha = 3\beta$. Here the contour plots include three positive Gaussian pulses centered at $T_1 = 5, T_2 = 10$ and $T_3 = 15$ with $\beta = J = 1$.

CHAPTER 4

DYNAMICS OF THE QUANTUM CORRELATIONS IN NON-MARKOVIAN ENVIRONMENTS

4.1 Introduction

In this chapter, I have analyzed the dynamics of Bell nonlocalities as measured by Mermin-Ardehali-Belinksii-Klyshko (MABK) and Svetlichny inequalities, quantum discord and entanglement as measured by concurrence for bipartitions and negativity for tripartite states for a system of three qubits which have energy levels that are stochastic with Ornstein-Uhlenbeck type correlations. The analytic expressions for quantum discord, Bell nonlocalities as well as concurrence and negativity are derived for W- and GHZ-type initial states by exploiting a procedure based on the knowledge of single-qubit dynamics. I consider both Markovian and non-Markovian time evolution and compare and contrast the character of time dependence of quantum correlations.

The organization of this paper is as follows. In Sec. 4.3, I introduce the model and its solution using the procedure analyzed in Sec. 4.2. In Sec. 4.4, I show explicit analytic calculations of quantum discord, concurrence, negativity and Bell nonlocalities for three-qubit system initially prepared in GHZ- and W-type states and explore the effects of non-Markovianity and mixedness on quantum correlations.

4.2 Procedure

I consider a system includes three subsystems $\widetilde{S} = \widetilde{A}, \widetilde{B}, \widetilde{C}$, and each subsystem includes one qubit, $S = A, B, C$, interacting with its local reservoir R_s and there is no other interaction in the whole system. Initially, each qubit and its reservoir

are independent, thus the evolution of the reduced density matrix for qubit S is given by

$$\hat{\rho}^S(t) = Tr_{R_S}\{\hat{U}^{\widetilde{S}}(t)\hat{\rho}^S(0) \otimes \hat{\rho}^{R_S}(0)\hat{U}^{\widetilde{S}\dagger}(t)\}, \tag{4.1}$$

where the trace is taken over the reservoir R_s degrees of freedom and $\hat{U}^{\widetilde{S}}(t)$ is the time evolution operator for the part $\widetilde{S}$. Eq. (4.1) can be expressed in terms of the Kraus operator $\hat{K}^S_{\alpha\beta}(t)$ as

$$\hat{\rho}^S(t) = \sum_{\alpha\beta} \hat{K}^S_{\alpha\beta}(t)\hat{\rho}^S(0)\hat{K}^{S\dagger}_{\alpha\beta}(t). \tag{4.2}$$

Since there is only interaction between single qubit and its corresponding reservoir, the time evolution operator $\hat{U}^T(t)$ of the complete system factorizes as

$$\hat{U}^T(t) = \hat{U}^{\widetilde{A}}(t) \otimes \hat{U}^{\widetilde{B}}(t) \otimes \hat{U}^{\widetilde{C}}(t), \tag{4.3}$$

then the reduced density matrix (4.2) for one qubit can be extended for three qubits as

$$\hat{\rho}^T(t) = \sum_{\alpha_1\beta_1}\sum_{\alpha_2\beta_2}\sum_{\alpha_3\beta_3} \hat{K}^A_{\alpha_1\beta_1}(t)\hat{K}^B_{\alpha_2\beta_2}(t)\hat{K}^C_{\alpha_3\beta_3}(t)\hat{\rho}^T(0)\hat{K}^{C\dagger}_{\alpha_1\beta_1}(t)\hat{K}^{B\dagger}_{\alpha_2\beta_2}(t)\hat{K}^{A\dagger}_{\alpha_3\beta_3}(t). \tag{4.4}$$

Given the basis $\{|1_S\rangle, |2_S\rangle\}$ for qubit S, inserting the identity operator $\hat{I} = \sum_i |i_S\rangle \langle i_S|$, one can get the reduced density matrix elements of the single qubit in the given basis as

$$\left\langle i_S \left| \hat{\rho}^S \right| i'_S \right\rangle = \rho^S_{i_S i'_S}(t) \;\; = \;\; \sum_{l_S l'_S} A^{l_S l'_S}_{i_S i'_S}(t)\rho^S_{l_S l'_S}(0). \tag{4.5}$$

Combining Eqs. (4.2), (4.4) and (4.5), we finally get the reduced density matrix elements of the three-qubit system

$$\begin{aligned} \langle i_1 i_2 i_3 \left| \hat{\rho}(t) \right| i_1' i_2' i_3' \rangle &= \\ \rho_{i_1 i_1', i_2 i_2', i_3 i_3'}(t) &= \sum_{l_1 l_1'} \sum_{l_2 l_2'} \sum_{l_3 l_3'} A_{i_1 i_1'}^{l_1 l_1'}(t) A_{i_2 i_2'}^{l_2 l_2'}(t) A_{i_3 i_3'}^{l_3 l_3'}(t) \rho_{l_1 l_1', l_2 l_2', l_3 l_3'}(0). \end{aligned} \quad (4.6)$$

The procedure given above allows us to obtain the dynamics of three qubits, provided that the dynamics of one qubit is known, by a purely algebraic way and independently from the initial conditions. The procedure for N-qudit system is given in Ref. [51].

We consider the single-qubit density matrix in the form,

$$\hat{\rho}^S(t) = \begin{pmatrix} \rho_{11}^S(t) & \rho_{12}^S(t) \\ \rho_{21}^S(t) & \rho_{22}^S(t) \end{pmatrix}, \quad (4.7)$$

where

$$\begin{aligned} \rho_{11}^S(t) &= u_t^S \rho_{11}^S(0) + v_t^S(t) \rho_{22}^S(0), \\ \rho_{22}^S(t) &= (1 - u_t^S) \rho_{11}^S(0) + (1 - v_t^S) \rho_{22}^S(0), \\ \rho_{12}^S(t) &= \rho_{21}^{S*}(t) = z_t^S \rho_{12}^S(0), \end{aligned} \quad (4.8)$$

where u_t^S, v_t^S and z_t^S are functions of time and determined by the model of chosen.

By considering Eqs. (4.5), (4.6) and (4.8), in the standart basis $|1\rangle \equiv |111\rangle, |2\rangle \equiv |110\rangle, |3\rangle \equiv |101\rangle, |4\rangle \equiv |100\rangle, |5\rangle \equiv |011\rangle, |6\rangle \equiv |010\rangle, |7\rangle \equiv |001\rangle, |8\rangle \equiv |000\rangle$, we can obtain the diagonal elements of the reduced density matrix of three-qubit

system as

$$
\begin{aligned}
\rho_{11}(t) &= u_t^A u_t^B u_t^C \rho_{11}(0) + u_t^A u_t^B v_t^C \rho_{22}(0) + u_t^A v_t^B u_t^C \rho_{33}(0) + u_t^A v_t^B v_t^C \rho_{44}(0) \\
&+ v_t^A u_t^B u_t^C \rho_{55}(0) + v_t^A u_t^B v_t^C \rho_{66}(0) + v_t^A v_t^B u_t^C \rho_{77}(0) + v_t^A v_t^B v_t^C \rho_{88}(0), \\
\rho_{22}(t) &= u_t^A u_t^B (1-u_t^C) \rho_{11}(0) + u_t^A u_t^B (1-v_t^C) \rho_{22}(0) + u_t^A v_t^B (1-u_t^C) \rho_{33}(0) \\
&+ u_t^A v_t^B (1-v_t^C) \rho_{44}(0) + v_t^A u_t^B (1-u_t^C) \rho_{55}(0) + v_t^A u_t^B (1-v_t^C) \rho_{66}(0) \\
&+ v_t^A v_t^B (1-u_t^C) \rho_{77}(0) + v_t^A v_t^B (1-v_t^C) \rho_{88}(0), \\
\rho_{33}(t) &= u_t^A (1-u_t^B) u_t^C \rho_{11}(0) + u_t^A (1-u_t^B) v_t^C \rho_{22}(0) + u_t^A (1-v_t^B) u_t^C \rho_{33}(0) \\
&+ u_t^A (1-v_t^B) v_t^C \rho_{44}(0) + v_t^A (1-u_t^B) u_t^C \rho_{55}(0) + v_t^A (1-u_t^B) v_t^C \rho_{66}(0) \\
&+ v_t^A (1-v_t^B) u_t^C \rho_{77}(0) + v_t^A (1-v_t^B) v_t^C \rho_{88}(0), \\
\rho_{44}(t) &= u_t^A (1-u_t^B)(1-u_t^C) \rho_{11}(0) + u_t^A (1-u_t^B)(1-v_t^C) \rho_{22}(0) \\
&+ u_t^A (1-v_t^B)(1-u_t^C) \rho_{33}(0) + u_t^A (1-v_t^B)(1-v_t^C) \rho_{44}(0) \\
&+ v_t^A (1-u_t^B)(1-u_t^C) \rho_{55}(0) + v_t^A (1-u_t^B)(1-v_t^C) \rho_{66}(0) \\
&+ v_t^A (1-v_t^B)(1-u_t^C) \rho_{77}(0) + v_t^A (1-v_t^B)(1-v_t^C) \rho_{88}(0), \\
\rho_{55}(t) &= (1-u_t^A) u_t^B u_t^C \rho_{11}(0) + (1-u_t^A) u_t^B v_t^C \rho_{22}(0) + (1-u_t^A) v_t^B u_t^C \rho_{33}(0) \\
&+ (1-u_t^A) v_t^B v_t^C \rho_{44}(0) + (1-v_t^A) u_t^B u_t^C \rho_{55}(0) + (1-v_t^A) u_t^B v_t^C \rho_{66}(0) \\
&+ (1-v_t^A) v_t^B u_t^C \rho_{77}(0) + (1-v_t^A) v_t^B v_t^C \rho_{88}(0), \\
\rho_{66}(t) &= (1-u_t^A) u_t^B (1-u_t^C) \rho_{11}(0) + (1-u_t^A) u_t^B (1-v_t^C) \rho_{22}(0) \\
&+ (1-u_t^A) v_t^B (1-u_t^C) \rho_{33}(0) + (1-u_t^A) v_t^B (1-v_t^C) \rho_{44}(0) \\
&+ (1-v_t^A) u_t^B (1-u_t^C) \rho_{55}(0) + (1-v_t^A) u_t^B (1-v_t^C) \rho_{66}(0) \\
&+ (1-v_t^A) v_t^B (1-u_t^C) \rho_{77}(0) + (1-v_t^A) v_t^B (1-v_t^C) \rho_{88}(0), \\
\rho_{77}(t) &= (1-u_t^A)(1-u_t^B) u_t^C \rho_{11}(0) + (1-u_t^A)(1-u_t^B) v_t^C \rho_{22}(0) \\
&+ (1-u_t^A)(1-v_t^B) u_t^C \rho_{33}(0) + (1-u_t^A)(1-v_t^B) v_t^C \rho_{44}(0) \\
&+ (1-v_t^A)(1-u_t^B) u_t^C \rho_{55}(0) + (1-v_t^A)(1-u_t^B) v_t^C \rho_{66}(0) \\
&+ (1-v_t^A)(1-v_t^B) u_t^C \rho_{77}(0) + (1-v_t^A)(1-v_t^B) v_t^C \rho_{88}(0),
\end{aligned}
$$

$$
\begin{aligned}
\rho_{88}(t) &= (1-u_t^A)(1-u_t^B)(1-u_t^C)\rho_{11}(0) + (1-u_t^A)(1-u_t^B)(1-v_t^C)\rho_{22}(0) \\
&+ (1-u_t^A)(1-v_t^B)(1-u_t^C)\rho_{33}(0) + (1-u_t^A)(1-v_t^B)(1-v_t^C)\rho_{44}(0) \\
&+ (1-v_t^A)(1-u_t^B)(1-u_t^C)\rho_{55}(0) + (1-v_t^A)(1-u_t^B)(1-v_t^C)\rho_{66}(0) \\
&+ (1-v_t^A)(1-v_t^B)(1-u_t^C)\rho_{77}(0) + (1-v_t^A)(1-v_t^B)(1-v_t^C)\rho_{88}(0), \qquad (4.9)
\end{aligned}
$$

and the off-diagonal elements as

$$
\begin{aligned}
\rho_{12}(t) &= u_t^A u_t^B z_t^C \rho_{12}(0) + u_t^A v_t^B z_t^C \rho_{34}(0) + v_t^A u_t^B z_t^C \rho_{56}(0) + v_t^A v_t^B z_t^C \rho_{78}(0), \\
\rho_{13}(t) &= u_t^A z_t^B u_t^C \rho_{13}(0) + u_t^A z_t^B v_t^C \rho_{24}(0) + v_t^A z_t^B u_t^C \rho_{57}(0) + v_t^A z_t^B v_t^C \rho_{68}(0), \\
\rho_{14}(t) &= u_t^A z_t^B z_t^C \rho_{14}(0) + v_t^A z_t^B z_t^C \rho_{58}(0), \\
\rho_{15}(t) &= z_t^A u_t^B u_t^C \rho_{15}(0) + z_t^A u_t^B v_t^C \rho_{26}(0) + z_t^A v_t^B u_t^C \rho_{37}(0) + z_t^A v_t^B v_t^C \rho_{48}(0), \\
\rho_{16}(t) &= z_t^A u_t^B z_t^C \rho_{16}(0) + z_t^A v_t^B z_t^C \rho_{38}(0), \\
\rho_{17}(t) &= z_t^A z_t^B u_t^C \rho_{17}(0) + z_t^A z_t^B v_t^C \rho_{28}(0), \\
\rho_{18}(t) &= z_t^A z_t^B z_t^C \rho_{18}(0), \\
\rho_{23}(t) &= u_t^A z_t^B z_t^{C*} \rho_{23}(0) + v_t^A z_t^B z_t^{C*} \rho_{67}(0), \\
\rho_{24}(t) &= u_t^A z_t^B (1-u_t^C)\rho_{13}(0) + u_t^A z_t^B (1-v_t^C)\rho_{24}(0) + v_t^A z_t^B (1-u_t^C)\rho_{57}(0) \\
&+ v_t^A z_t^B (1-v_t^C)\rho_{68}(0), \\
\rho_{25}(t) &= z_t^A u_t^B z_t^{C*} \rho_{25}(0) + z_t^A v_t^B z_t^{C*} \rho_{47}(0), \\
\rho_{26}(t) &= z_t^A u_t^B (1-u_t^C)\rho_{15}(0) + z_t^A u_t^B (1-v_t^C)\rho_{26}(0) + z_t^A v_t^B (1-u_t^C)\rho_{37}(0) \\
&+ z_t^A v_t^B (1-v_t^C)\rho_{48}(0), \\
\rho_{27}(t) &= z_t^A z_t^B z_t^{C*} \rho_{27}(0), \\
\rho_{28}(t) &= z_t^A z_t^B (1-u_t^C)\rho_{17}(0) + z_t^A z_t^B (1-v_t^C)\rho_{28}(0),
\end{aligned}
$$

$$
\begin{aligned}
\rho_{34}(t) &= u_t^A(1-u_t^B)z_t^C\rho_{12}(0) + u_t^A(1-v_t^B)z_t^C\rho_{34}(0) + v_t^A(1-u_t^B)z_t^C\rho_{56}(0) \\
&+ v_t^A(1-v_t^B)z_t^C\rho_{78}(0), \\
\rho_{35}(t) &= z_t^A z_t^{B*} u_t^C \rho_{35}(0) + z_t^A z_t^{B*} v_t^C \rho_{46}(0), \\
\rho_{36}(t) &= z_t^A z_t^{B*} z_t^C \rho_{36}(0), \\
\rho_{37}(t) &= z_t^A(1-u_t^B)u_t^C\rho_{15}(0) + z_t^A(1-u_t^B)v_t^C\rho_{26}(0) + z_t^A(1-v_t^B)u_t^C\rho_{37}(0) \\
&+ z_t^A(1-v_t^B)v_t^C\rho_{48}(0), \\
\rho_{38}(t) &= z_t^A(1-u_t^B)z_t^C\rho_{16}(0) + z_t^A(1-v_t^B)z_t^C\rho_{38}(0), \\
\rho_{45}(t) &= z_t^A z_t^{B*} z_t^{C*} \rho_{45}(0), \\
\rho_{46}(t) &= z_t^A z_t^{B*}(1-u_t^C)\rho_{35}(0) + z_t^A z_t^{B*}(1-v_t^C)\rho_{46}(0), \\
\rho_{47}(t) &= z_t^A(1-u_t^B)z_t^{C*}\rho_{25}(0) + z_t^A(1-v_t^B)z_t^{C*}\rho_{47}(0), \\
\rho_{48}(t) &= z_t^A(1-u_t^B)(1-u_t^C)\rho_{15}(0) + z_t^A(1-u_t^B)(1-v_t^C)\rho_{26}(0) \\
&+ z_t^A(1-v_t^B)(1-u_t^C)\rho_{37}(0) + z_t^A(1-v_t^B)(1-v_t^C)\rho_{48}(0), \\
\rho_{56}(t) &= (1-u_t^A)u_t^B z_t^C\rho_{12}(0) + (1-u_t^A)v_t^B z_t^C\rho_{34}(0) + (1-v_t^A)u_t^B z_t^C\rho_{56}(0) \\
&+ (1-v_t^A)v_t^B z_t^C\rho_{78}(0), \\
\rho_{57}(t) &= (1-u_t^A)z_t^B u_t^C\rho_{13}(0) + (1-u_t^A)z_t^B v_t^C\rho_{24}(0) + (1-v_t^A)z_t^B u_t^C\rho_{57}(0) \\
&+ (1-v_t^A)z_t^B v_t^C\rho_{68}(0), \\
\rho_{58}(t) &= (1-u_t^A)z_t^B z_t^C\rho_{14}(0) + (1-v_t^A)z_t^B z_t^C\rho_{58}(0), \\
\rho_{67}(t) &= (1-u_t^A)z_t^B z_t^{C*}\rho_{23}(0) + (1-v_t^A)z_t^B z_t^{C*}\rho_{67}(0), \\
\rho_{68}(t) &= (1-u_t^A)z_t^B(1-u_t^C)\rho_{13}(0) + (1-u_t^A)z_t^B(1-v_t^C)\rho_{24}(0) \\
&+ (1-v_t^A)z_t^B(1-u_t^C)\rho_{57}(0) + (1-v_t^A)z_t^B(1-v_t^C)\rho_{68}(0), \\
\rho_{78}(t) &= (1-u_t^A)(1-u_t^B)z_t^C\rho_{12}(0) + (1-u_t^A)(1-v_t^B)z_t^C\rho_{34}(0) \\
&+ (1-v_t^A)(1-u_t^B)z_t^C\rho_{56}(0) + (1-v_t^A)(1-v_t^B)z_t^C\rho_{78}(0). \qquad (4.10)
\end{aligned}
$$

4.3 The Model and its Solution

The model we consider in this paper is three uncoupled qubits interacting with its noisy environments independently which cause frequency fluctuations in their energy levels that are random. The Hamiltonian for this model is given by [31] (we set $\hbar = 1$):

$$\hat{H}(t) = \frac{\Omega_A(t)}{2}\hat{\sigma}_z^A + \frac{\Omega_B(t)}{2}\hat{\sigma}_z^B + \frac{\Omega_C(t)}{2}\hat{\sigma}_z^C, \tag{4.11}$$

where $\hat{\sigma}_z$ is the usual Pauli spin matrix in z-direction, $\Omega_{A,B,C}(t)$ are the independent fluctuations of the transition frequencies obeying on non-Markovian approximation with mean value properties

$$M\{\Omega_i(t)\} = 0, \tag{4.12}$$

$$\begin{aligned} M\{\Omega_i(t)\Omega_i(s)\} &= \alpha(t-s) \\ &= \frac{\Gamma_i\gamma}{2}e^{-\gamma|t-s|}, i = A, B, C, \end{aligned} \tag{4.13}$$

where $M\{...\}$ stands for the statistical mean over the noises $\Omega_A(t)$, $\Omega_B(t)$ and $\Omega_C(t)$. Here $\Gamma_i (i = A, B, C)$ are the damping rates due to coupling to the environments, γ is the noise bandwidth which determines the environment's finite correlation time of the noise ($\tau_c = \gamma^{-1}$) and $\alpha(t-s)$ is the reservoir correlation function. For simplicity, we will take the noise properties to be the same for A, B and C (e.g., $\Gamma_A = \Gamma_B = \Gamma_C \equiv \Gamma$), although independent. And note in the limit $\gamma \to \infty (\tau_c \to 0)$, Ornstein-Uhlenbeck noise reduces to the well-known Markov case:

$$\alpha(t-s) = \Gamma\delta(t-s). \tag{4.14}$$

For the total system described by the Hamiltonian (4.11), the stochastic Schrödinger equation is given by

$$i\frac{d}{dt}\left|\Psi(t)\right\rangle = \hat{H}(t)\left|\Psi(t)\right\rangle, \tag{4.15}$$

with solution

$$\left|\Psi(t)\right\rangle = \hat{U}(t,\Omega_A,\Omega_B,\Omega_C)\left|\Psi(0)\right\rangle, \tag{4.16}$$

where the stochastic propagator $\hat{U}(t,\Omega_A,\Omega_B,\Omega_C)$ is given by

$$\hat{U}(t,\Omega_A,\Omega_B,\Omega_C) = e^{-\frac{i}{2}\int_0^t(\Omega_A(s)\hat{\sigma}_z^A+\Omega_B(s)\hat{\sigma}_z^B+\Omega_C(s)\hat{\sigma}_z^C)ds}. \tag{4.17}$$

The reduced density matrix for spins A, B and C is then obtained from the statistical mean

$$\hat{\rho}(t) = M\{\left|\Psi(t)\right\rangle\left\langle\Psi(t)\right|\}. \tag{4.18}$$

Since we assume independent reservoirs and the only interaction between qubit and its reservoir, we can apply the procedure given in 4.2. Using the stochastic Schrödinger equation (4.15) and reduced density matrix (4.18), the single qubit master equation for the reduced density matrix can be derived [27, 28, 52] :

$$\frac{d}{dt}\hat{\rho}(t) = -\frac{G(t)}{2}(\hat{\rho}(t) - \hat{\sigma}_z\hat{\rho}(t)\hat{\sigma}_z), \tag{4.19}$$

where

$$G(t) = \int_0^t \alpha(t-s)ds = \frac{\Gamma}{2}(1-e^{-\gamma t}). \tag{4.20}$$

Here $G(t)$ is a time-dependent coefficient which includes the memory information of the environmental noises.

Since we assume the noise properties to be the same for the qubits, the parameters given in (4.8) are:

$$\begin{aligned} u_t^A &= u_t^B = u_t^C = 1, \\ v_t^A &= v_t^B = v_t^C = 0, \\ z_t^A &= z_t^B = z_t^C = e^{-f(t)}, \end{aligned} \tag{4.21}$$

where

$$\begin{aligned} f(t) &= \int_0^t G(s)ds \\ &= \frac{\Gamma}{2}\left(t + \frac{1}{\gamma}(e^{-\gamma t} - 1)\right). \end{aligned} \tag{4.22}$$

Using (4.9), (4.10) and (4.21), the matrix elements of the reduced density matrix for three-qubit can be determined:

$$\begin{aligned} \rho_{ii}(t) &= \rho_{ii}(0), \qquad \{i = 1, 2, \ldots, 8\}, \\ \rho_{ij}(t) &= \rho_{ij}(0)e^{-f(t)}, \quad \{ij = 12, 13, 15, 24, 26, 34, 37, 48, 56, 57, 68, 78\}, \\ \rho_{ij}(t) &= \rho_{ij}(0)e^{-2f(t)}, \quad \{ij = 14, 16, 17, 23, 25, 28, 35, 38, 46, 47, 58, 67\}, \\ \rho_{ij}(t) &= \rho_{ij}(0)e^{-3f(t)}, \quad \{ij = 18, 27, 36, 45\}. \end{aligned} \tag{4.23}$$

4.4 Correlation Measurements

Quantum Entanglement: For a pair of qubits, the concurrence as a measure of entanglement is well-defined. It is introduced by Wootters [53] and defined as

$$C = \max\{0, \sqrt{\lambda_1} - \sqrt{\lambda_2} - \sqrt{\lambda_3} - \sqrt{\lambda_4}\}, \tag{4.24}$$

where the quantities $\lambda_i (i = 1, 2, 3, 4)$ are the eigenvalues of the matrix

$$\hat{R} = \hat{\rho}_{AB}(\hat{\sigma}_y^A \otimes \hat{\sigma}_y^B)\hat{\rho}_{AB}^*(\hat{\sigma}_y^A \otimes \hat{\sigma}_y^B), \tag{4.25}$$

in descending order and $\hat{\rho}_{AB}^{*}$ is the conjugate of $\hat{\rho}_{AB}$. For the density matrix with X-form [31],

$$\hat{\rho}_{AB} = \begin{bmatrix} a & 0 & 0 & w \\ 0 & b & z & 0 \\ 0 & z & c & 0 \\ w & 0 & 0 & d \end{bmatrix}, \tag{4.26}$$

the concurrence function (4.24) has a simple analytic form:

$$C = 2\max\{0, z - \sqrt{ad}, w - \sqrt{bc}\}. \tag{4.27}$$

On the other hand, for three-qubit case concurrence is not well-defined. For this case, negativity can be used as a measure of entanglement [7] because of its good calculational properties based on the trace norm of the partial transposes $\hat{\rho}_{ABC}^{T_A}$ of the tripartite state $\hat{\rho}_{ABC}$ [54]. For the state with density matrix $\hat{\rho}_{ABC}$, the negativity reads

$$N = \frac{||\hat{\rho}_{ABC}^{T_A}||_1 - 1}{2}, \tag{4.28}$$

with its definition N is the absolute value of the sum of the negative eigenvalues of $\hat{\rho}_{ABC}^{T_A}$.

Quantum Discord: For two-qubit systems, quantum discord as a measure of quantum correlation was introduced by Ollivier and Zurek [14]. It is defined as the difference between two expressions of mutual information: total and classical correlations, namely,

$$D = I(\hat{\rho}_{AB}) - J(\hat{\rho}_{AB}). \tag{4.29}$$

Here $I(\hat{\rho}_{AB})$ is the total correlation between two subsystems defined as

$$I(\hat{\rho}_{AB}) = S(\hat{\rho}_A) + S(\hat{\rho}_B) - S(\hat{\rho}_{AB}), \tag{4.30}$$

where $S(\hat{\rho}) = -Tr(\hat{\rho}\log_2\hat{\rho})$ is the von Neumann entropy and $\hat{\rho}_A(\hat{\rho}_B)$ is the reduced density matrix of $\hat{\rho}_{AB}$ by tracing out B(A) [54]. The other quantity $J(\hat{\rho}_{AB})$ is the classical correlation between A and B as the maximum information one can get from A by measuring B. It is defined as

$$J(\hat{\rho}_{AB}) = \max_{\{\hat{\Pi}_i\}}\{S(\hat{\rho}_A) - \sum_i p_i S(\hat{\rho}_{A|_i})\}, \tag{4.31}$$

where $\hat{\rho}_{A|_i} = \frac{Tr_B(\hat{\Pi}_i\hat{\rho}_{AB}\hat{\Pi}_i)}{Tr_{AB}(\hat{\Pi}_i\hat{\rho}_{AB}\hat{\Pi}_i)}$ and $\hat{\Pi}_i$ is a set of projectors [37] used to measure subsystem B, corresponding to the outcome i with probability $p_i = Tr_{AB}(\hat{\Pi}_i\hat{\rho}_{AB}\hat{\Pi}_i)$.

In general, it is hard to calculate the analytic expression of the quantum discord. However, if the reduced density matrix of two qubits has X-form as Eq. (4.26) with $b = c$, the quantum discord has a simple analytic form [37]:

$$D = \min\{D_1, D_2\}, \tag{4.32}$$

where

$$\begin{aligned} D_1 &= S(\hat{\rho}_A) - S(\hat{\rho}_{AB}) - a\log_2\left(\frac{a}{a+b}\right) - b\log_2\left(\frac{b}{a+b}\right) \\ &- d\log_2\left(\frac{d}{b+d}\right) - b\log_2\left(\frac{b}{d+b}\right), \\ D_2 &= S(\hat{\rho}_A) - S(\hat{\rho}_{AB}) - \frac{1}{2}(1+\kappa)\log_2\left(\frac{1}{2}(1+\kappa)\right) \\ &- \frac{1}{2}(1-\kappa)\log_2\left(\frac{1}{2}(1-\kappa)\right), \end{aligned} \tag{4.33}$$

where $\kappa = \sqrt{(a-d)^2 + 4|z+w|^2}$.

Bell-Nonlocality: For three-qubit case, violation of Bell-nonlocality can be used as a measure of quantum correlations. From this point, we choose two

kinds of non-locality measures. The first one is introduced by Mermin-Ardehali-Belinksii-Klyshako (MABK) [20, 21, 47, 48, 49]. It is easily computable for three-qubit case and violated whenever $\left|\left\langle \hat{B}\right\rangle_{\rho}\right| = \left|Tr(\hat{B}\hat{\rho}(t))\right| > 1$ where MABK operator is given by

$$\hat{B} = \frac{1}{2}\left(\hat{M}_A\hat{M}_B\hat{M}'_C + \hat{M}_A\hat{M}'_B\hat{M}_C + \hat{M}'_A\hat{M}_B\hat{M}_C - \hat{M}'_A\hat{M}'_B\hat{M}'_C\right). \tag{4.34}$$

The second ineqaulity is put forward by Svetlichny [20, 21, 50] and denotes genuine tripartite Bell non-locality if $\left|\left\langle \hat{S}\right\rangle_{\rho}\right| = \left|Tr(\hat{S}\hat{\rho}(t))\right| > 4$ where the Svetlichny operator is

$$\begin{aligned}\hat{S} &= \hat{M}_A\hat{M}_B\hat{M}_C + \hat{M}_A\hat{M}_B\hat{M}'_C + \hat{M}_A\hat{M}'_B\hat{M}_C + \hat{M}'_A\hat{M}_B\hat{M}_C \\ &- \hat{M}'_A\hat{M}'_B\hat{M}'_C - \hat{M}'_A\hat{M}'_B\hat{M}_C - \hat{M}'_A\hat{M}_B\hat{M}'_C - \hat{M}_A\hat{M}'_B\hat{M}'_C.\end{aligned} \tag{4.35}$$

The primed and unprimed terms in Eqs. (4.34) and (4.35) are called measurement operators and denote two different directions in which the corresponding party measures; the measurement operators corresponding to measurements on qubit K (here K=A,B,C), where the second corresponds to a measurement performed along a direction differing by θ relative that performed on the first qubit, are

$$\begin{pmatrix} \hat{M}_K \\ \hat{M}'_K \end{pmatrix} = \begin{pmatrix} \cos\theta_K & -\sin\theta_K \\ \sin\theta_K & \cos\theta_K \end{pmatrix} \begin{pmatrix} \hat{M}_A \\ \hat{M}'_A \end{pmatrix}, \tag{4.36}$$

where θ_K (K=A,B) are the rotation angles.

To demonstrate the finite-time loss of Bell non-locality in both Markovian and non-Markovian environments, we shall assume two different (non-)locality regimes satisfying:

$$\begin{aligned}(i) \quad & \left|\left\langle \hat{B}\right\rangle_{\rho}\right| > 1, \quad \left|\left\langle \hat{S}\right\rangle_{\rho}\right| > 4, \\ (ii) \quad & \left|\left\langle \hat{B}\right\rangle_{\rho}\right| \leq 1, \quad \left|\left\langle \hat{S}\right\rangle_{\rho}\right| \leq 4,\end{aligned}$$

where the regime (i) shows that the state $\hat{\rho}(t)$ is genuinely tripartite Bell nonlocal. Also we choose the rotation angles in which $\left|\left\langle \hat{B}\right\rangle_{\rho}\right|$ and $\left|\left\langle \hat{S}\right\rangle_{\rho}\right|$ have maximum values at $t = 0$.

In the following, we are interested in some explicit three-qubit initial states called GHZ- and W-type states. As is known GHZ-state cannot transformed into W-state by local operations and classical communication [55]. This means they bear imcompatible multipartite correlations. From this point of view, one may expect that the two initial states might have some differences in their correlation dynamics due to effect of external noise.

4.4.1 GHZ-type states

In this section, we explore the effects of noises on the following three qubit GHZ-type states,

$$\hat{\rho}(0) = \frac{1-r}{8}\hat{I}_8 + r\left|GHZ\right\rangle\left\langle GHZ\right|, \tag{4.37}$$

where $\left|GHZ\right\rangle = \frac{1}{\sqrt{2}}\left(\left|111\right\rangle + \left|000\right\rangle\right)$ is the GHZ-state and r is the purity which ranges from 0 to 1. For this initial state one can define the measurement operators as $\hat{M}_A \equiv \hat{\sigma}_y$ and $\hat{M}'_A \equiv \hat{\sigma}_x$ [20], then

$$\begin{aligned}
\hat{M}_A &= \hat{\sigma}_y \otimes \hat{I}_2 \otimes \hat{I}_2, \\
\hat{M}'_A &= \hat{\sigma}_x \otimes \hat{I}_2 \otimes \hat{I}_2, \\
\hat{M}_B &= \hat{I}_2 \otimes [\cos(\theta_B)\hat{\sigma}_y - \sin(\theta_B)\hat{\sigma}_x] \otimes \hat{I}_2, \\
\hat{M}'_B &= \hat{I}_2 \otimes [\sin(\theta_B)\hat{\sigma}_y + \cos(\theta_B)\hat{\sigma}_x] \otimes \hat{I}_2, \\
\hat{M}_C &= \hat{I}_2 \otimes \hat{I}_2 \otimes [\cos(\theta_C)\hat{\sigma}_y - \sin(\theta_C)\hat{\sigma}_x], \\
\hat{M}'_C &= \hat{I}_2 \otimes \hat{I}_2 \otimes [\sin(\theta_C)\hat{\sigma}_y + \cos(\theta_C)\hat{\sigma}_x].
\end{aligned} \tag{4.38}$$

The expectation value of $\hat{B}$ and $\hat{S}$ operators for the GHZ-state under the classical noises can be easily obtained as:

$$\begin{aligned} \left|\left\langle \hat{B} \right\rangle_{\rho}\right| &= 2re^{-3f(t)} \left|\cos(\theta_{BC})\right|, \\ \left|\left\langle \hat{S} \right\rangle_{\rho}\right| &= 4re^{-3f(t)} \left|\cos(\theta_{BC}) - \sin(\theta_{BC})\right|, \end{aligned} \tag{4.39}$$

where $\theta_{BC} = \theta_B + \theta_C$. Also, it can be noted that this state does not retain bi-partite correlations, however, it retains non-zero tri-partite negativity and equals to

$$N = \max\{0, -\frac{1}{8}(1 - r - 4re^{-3f(t)})\}. \tag{4.40}$$

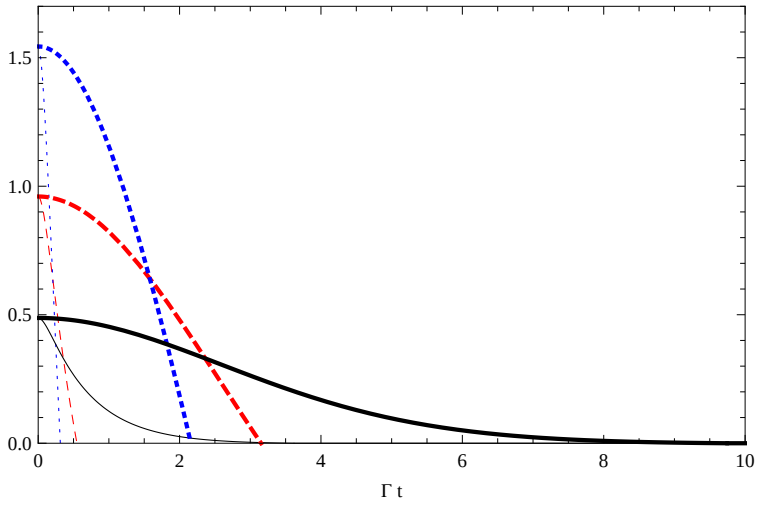

Figure 4.1: The dynamics of N (solid plots), $\left|\left\langle \hat{B} \right\rangle_{\rho}\right| - 1$ (dashed plots) and $\left|\left\langle \hat{S} \right\rangle_{\rho}\right| - 4$ (dotted plots) versus Γt with $r = 0.98$ for GHZ-type initial state. Here the thick plots correspond to non-Markovian regime with $\gamma/\Gamma = 0.1$ and the thin plots to Markovian regime with $\gamma/\Gamma = 10$.

In Fig. 4.1, we plot the dynamics of negativity and Bell-nonlocalities versus Γt for both Markovian ($\gamma/\Gamma = 10$) and non-Markovian ($\gamma/\Gamma = 0.1$) regimes. Also, in Fig. 4.2 we plot the dynamics of them versus Γt and γ/Γ for the qubits initially prepared in GHZ-type state with $r = 0.98$. It can be noted that the dephasing time of negativity is significantly longer than the dephasing time of

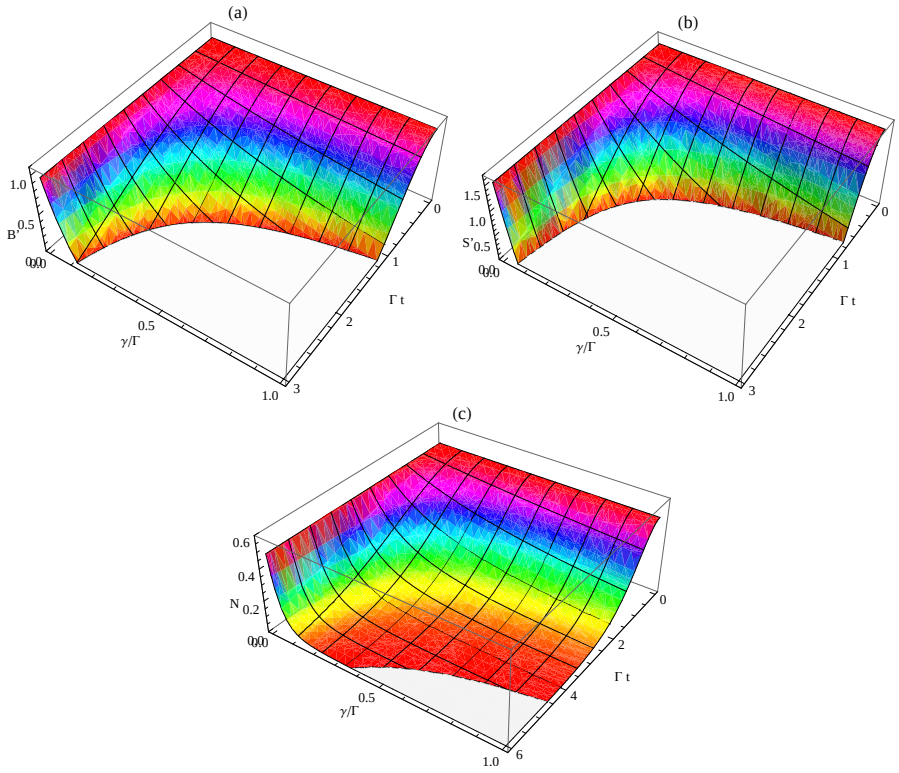

Figure 4.2: The dynamics of $\left|\left\langle \hat{B}\right\rangle_{\rho}\right| - 1$ (Fig. (a)), $\left|\left\langle \hat{S}\right\rangle_{\rho}\right| - 4$ (Fig. (b)) and N (Fig. (c)) versus Γt and γ/Γ with $r = 0.98$ for GHZ-type initial state. (Here B' and S' denote $\left|\left\langle \hat{B}\right\rangle_{\rho}\right| - 1$ and $\left|\left\langle \hat{S}\right\rangle_{\rho}\right| - 4$, respectively).

Bell-nonlocalities for both Markovian and non-Markovian regimes. Also, it can be concluded that non-Markovianity only delays the death, not prevent it.

In non-Markovianity-purity versus entanglement and Bell-nonlocality relation for the GHZ-type initial state (see Fig. 4.3), the non-Markovianity has negligible influence compared to purity on death of entanglement and Bell-nonlocality. On the other hand, is can be noted that purity is the most important parameter for the existance of Bell-nonlocality compared to the entanglement [26].

4.4.2 W-type states

The W-type initial state can be expressed as:

$$\hat{\rho}(0) = \frac{1-r}{8}\hat{I}_8 + r\left|W\right\rangle\left\langle W\right|, \tag{4.41}$$

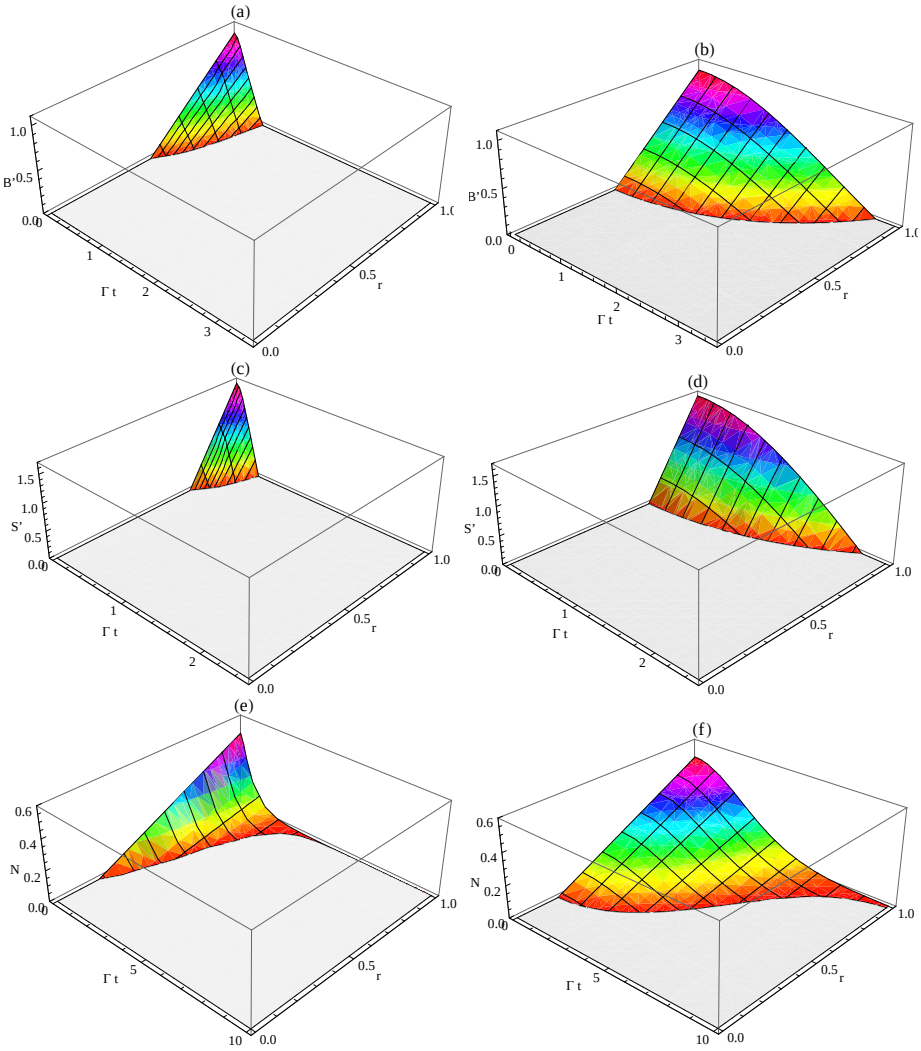

Figure 4.3: The dynamics of $\left|\left\langle \hat{B}\right\rangle_\rho\right| - 1$ (Fig. (a) and (b)), $\left|\left\langle \hat{S}\right\rangle_\rho\right| - 4$ (Fig. (c) and (d)) and N (Fig. (e) and (f)) versus Γt and r for GHZ-type initial state. Fig. (a), (c) and (e) corresponds to Markovian regime with $\gamma/\Gamma = 10$ and Fig. (b), (d) and (f) to non-Markovian regime with $\gamma/\Gamma = 0.1$. (Here B' and S' denote $\left|\left\langle \hat{B}\right\rangle_\rho\right| - 1$ and $\left|\left\langle \hat{S}\right\rangle_\rho\right| - 4$, respectively).

where $|W\rangle = \frac{1}{\sqrt{3}}(|100\rangle + |010\rangle + |001\rangle)$ is the W-state.. For this initial states, the measurement operators are given by [21]

$$\begin{aligned}
\hat{M}_A &= \hat{\sigma}_z \otimes \hat{I}_2 \otimes \hat{I}_2, \\
\hat{M}'_A &= \hat{\sigma}_x \otimes \hat{I}_2 \otimes \hat{I}_2, \\
\hat{M}_B &= \hat{I}_2 \otimes [\cos(\theta_B)\hat{\sigma}_z - \sin(\theta_B)\hat{\sigma}_x] \otimes \hat{I}_2, \\
\hat{M}'_B &= \hat{I}_2 \otimes [\sin(\theta_B)\hat{\sigma}_z + \cos(\theta_B)\hat{\sigma}_x] \otimes \hat{I}_2,
\end{aligned}$$

$$\begin{aligned}\hat{M}_C &= \hat{I}_2 \otimes \hat{I}_2 \otimes [\cos(\theta_C)\hat{\sigma}_z - \sin(\theta_C)\hat{\sigma}_x], \\ \hat{M}'_C &= \hat{I}_2 \otimes \hat{I}_2 \otimes [\sin(\theta_C)\hat{\sigma}_z + \cos(\theta_C)\hat{\sigma}_x]. \end{aligned} \tag{4.42}$$

Then the expectation values of the operators $\hat{B}$ and $\hat{S}$ can be calculated as:

$$\begin{aligned}\left|\left\langle \hat{B} \right\rangle_\rho\right| &= \frac{r}{2}(1 + 2e^{-2f(t)}) \left|\sin(\theta_{BC})\right|, \\ \left|\left\langle \hat{S} \right\rangle_\rho\right| &= r(1 + 2e^{-2f(t)}) \left|(\cos(\theta_{BC}) + \sin(\theta_{BC}))\right|. \end{aligned} \tag{4.43}$$

Unlike GHZ state, W state retains a high degree of bi-partite correlation. Thus, W-type states allow some comparison between tri-partite and bi-partite correlations. The analytic forms of the tri-partite and bi-partite entanglement and quantum discord for this state can be easily calculated as:

$$\begin{aligned} N &= \frac{1}{24}\max\{0, -3 + 3r + 8\sqrt{2}re^{-2f(t)}\}, \\ C &= \frac{1}{6}\max\{0, 4re^{-2f(t)} - \sqrt{3(1-r)(3+r)}\}, \\ D &= \min\{D_1, D_2\}, \end{aligned} \tag{4.44}$$

where

$$\begin{aligned} D_1 &= -\sum_{i=1}^{2} \lambda_i^A \log_2(\lambda_i^A) + \sum_{i=1}^{4} \lambda_i^{AB} \log_2(\lambda_i^{AB}) - a\log_2\left(\frac{a}{a+b}\right) - b\log_2\left(\frac{b}{a+b}\right) \\ &- d\log_2\left(\frac{d}{b+d}\right) - b\log_2\left(\frac{b}{d+b}\right), \\ D_2 &= -\sum_{i=1}^{2} \lambda_i^A \log_2(\lambda_i^A) + \sum_{i=1}^{4} \lambda_i^{AB} \log_2(\lambda_i^{AB}) - \frac{1}{2}(1+\kappa)\log_2\left(\frac{1}{2}(1+\kappa)\right) \\ &- \frac{1}{2}(1-\kappa)\log_2\left(\frac{1}{2}(1-\kappa)\right), \end{aligned} \tag{4.45}$$

where $\lambda_1^A = \frac{3-r}{6}, \lambda_2^A = \frac{3+r}{6}, \lambda_1^{AB} = \frac{1-r}{4}, \lambda_2^{AB} = \frac{3+r}{12}, \lambda_3^{AB} = \frac{1}{12}(3+r-4re^{-2f(t)}), \lambda_4^{AB} = \frac{1}{12}(3+r+4re^{-2f(t)}), a = \frac{1-r}{4}, b = d = \frac{3+r}{12}, z = \frac{r}{3}e^{-2f(t)}$ and $\kappa = \frac{r}{3}\sqrt{1+4e^{-4f(t)}}$.

As shown Fig. 4.4, 4.5 and 4.6, which we analyzed the effects of non-Markovianity on Bell-nonlocalities, two- and three-qubit entanglement and quantum discord

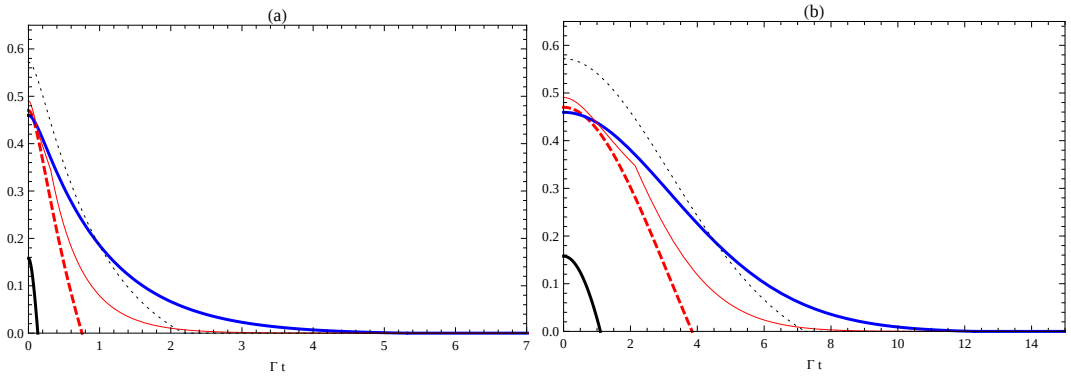

Figure 4.4: (Color online) The dynamics of N (thick blue solid plots), C (thin black dotted plots), D (thin red solid plots), $\left|\left\langle \hat{B} \right\rangle_{\rho}\right| - 1$ (thick dashed red plots) and $\left|\left\langle \hat{S} \right\rangle_{\rho}\right| - 4$ (thick black solid plots) versus Γt with $r = 0.98$ for W-type initial state. Here Fig. (a) corresponds to Markovian regime with $\gamma/\Gamma = 10$ and Fig. (b) to non-Markovain regime with $\gamma/\Gamma = 0.1$.

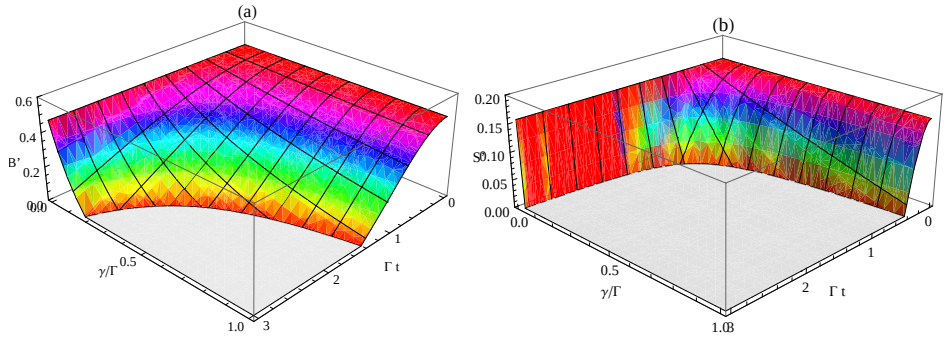

Figure 4.5: The dynamics of $\left|\left\langle \hat{B} \right\rangle_{\rho}\right| - 1$ (Fig. (a)) and $\left|\left\langle \hat{S} \right\rangle_{\rho}\right| - 4$ (Fig. (b)) versus Γt and γ/Γ with $r = 0.98$ for W-type initial state. (Here B' and S' denote $\left|\left\langle \hat{B} \right\rangle_{\rho}\right| - 1$ and $\left|\left\langle \hat{S} \right\rangle_{\rho}\right| - 4$, respectively).

under the same conditions, the tri-partite entanglement has a longer lifetime compared to bi-partite entanglement. This conclusion is independent of Markovianity of the dynamics. Bell-nonlocalities both $\left|\left\langle \hat{B} \right\rangle_{\rho}\right|$ and $\left|\left\langle \hat{S} \right\rangle_{\rho}\right|$ are more fragile compared to all other quantum correlations (entanglement and discord) considered here. Also, quantum discord is found to immune to sudden death independent of the non-Markovianity of the dynamics.

We have analyzed the purity dependence of Bell-nonlocalities as measured by $\left|\left\langle \hat{B} \right\rangle_{\rho}\right|$ and $\left|\left\langle \hat{S} \right\rangle_{\rho}\right|$ for the Markovian and non-Markovian dynamics and present the results in Fig. 4.7 (a)-(d). One can conclude two important findings from

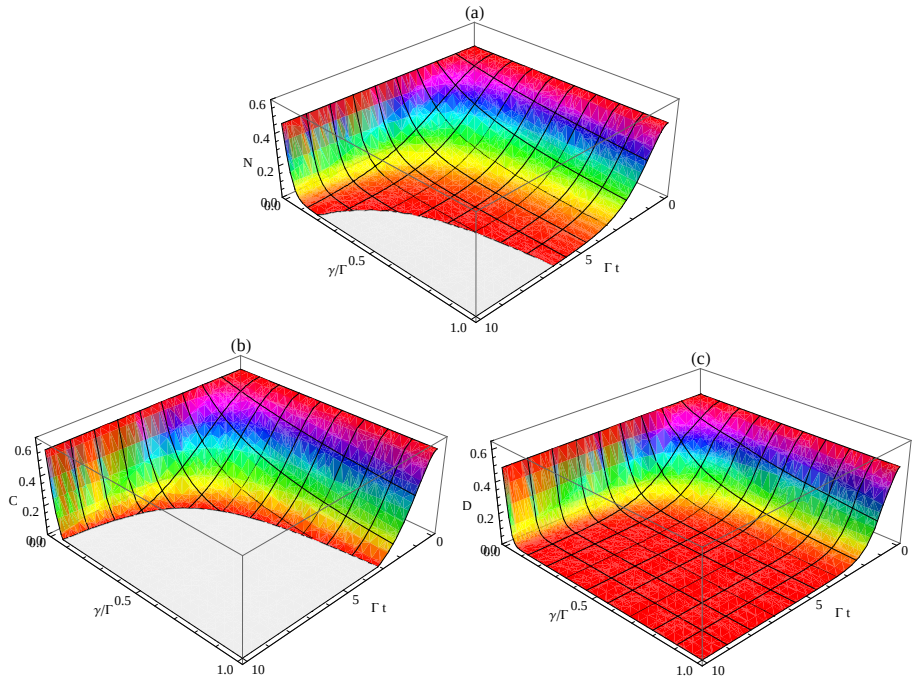

Figure 4.6: The dynamics of N (Fig. (a)), C (Fig. (b)) and D (Fig. (c)) versus Γt and γ/Γ with $r = 0.98$ for W-type initial state.

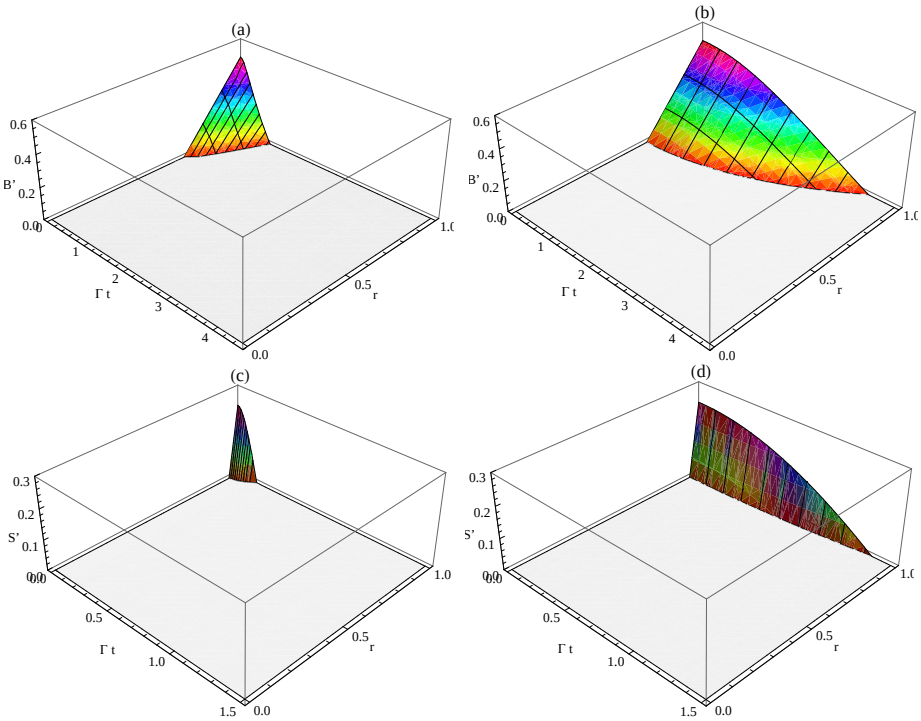

Figure 4.7: The dynamics of $\left|\left\langle \hat{B} \right\rangle_\rho\right| - 1$ (Fig. (a) and (b)) and $\left|\left\langle \hat{S} \right\rangle_\rho\right| - 4$ (Fig. (c) and (d)) versus Γt and r for W-type initial state. Fig. (a) and (c) corresponds to Markovian regime with $\gamma/\Gamma = 10$ and Fig. (b) and (d) to non-Markovian regime with $\gamma/\Gamma = 0.1$. (Here B' and S' denote $\left|\left\langle \hat{B} \right\rangle_\rho\right| - 1$ and $\left|\left\langle \hat{S} \right\rangle_\rho\right| - 4$, respectively).

these figures: i) Both of nonlocalities are highly purity dependent, $\left|\left\langle \hat{B} \right\rangle_{\rho}\right|$ suffers death $r < 0.7$ independent of Markoviatity of the dynamics, while the non-zero $\left|\left\langle \hat{S} \right\rangle_{\rho}\right|$ is limited to a much narrower range of r values ($0.9 < r \leq 1$). ii) As expected, non-Markovian dynamics offer a longer lived nonlocality compared to the Markovian case.

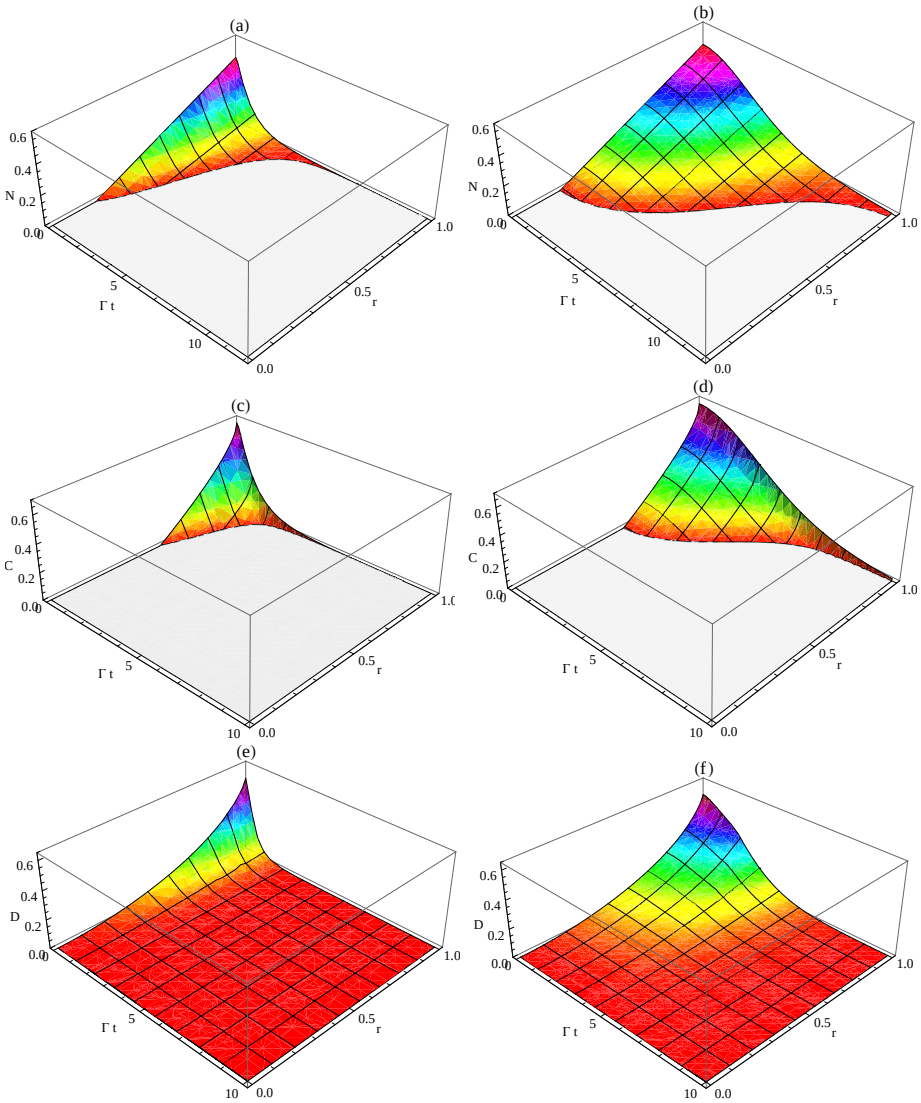

Figure 4.8: The dynamics of N (Fig. (a) and (b)), C (Fig. (c) and (d)) and D (Fig. (e) and (f)) versus Γt and r for W-type initial state. Fig. (a), (c) and (e) corresponds to Markovian regime with $\gamma/\Gamma = 10$ and Fig. (b), (d) and (f) to non-Markovian regime with $\gamma/\Gamma = 0.1$.

Similar to the case of Bell-nonlocalities, we have considered the purity dependence of Markovian and non-Markovian dynamics of tri-partite negativity, bipartite concurrence and quantum discord and display the results in Fig.4.8 (a)-

(f). The most important finding from Fig. 4.8 (a)-(f) is the nonexistence of death for the quantum discord independent of purity and Markovianity of the dynamics, which indicates that although entanglement type quantum correlations die out in finite time, not all types of quantum correlations are lost because of the noisy dynamics. Another important observation concerns the behaviour of Bell-nonlocalities and entanglement measures for the pure initial states ($r = 1$). While there is a sudden death of $\left|\left\langle \hat{B} \right\rangle_{\rho}\right|$ and $\left|\left\langle \hat{S} \right\rangle_{\rho}\right|$ for $r = 1$, there is no ESD in N or C.

CHAPTER 5
ENTANGLEMENT DYNAMICS OF TWO STOCHASTIC QUBITS WITH DIPOLE-DIPOLE INTERACTION

5.1 Introduction

In this chapter, I analyze the exact entanglement dynamics of two stochastic qubits connected to each other by dipole-dipole interaction and each qubit is embedded in its own reservoir which cause stochastic fluctuations in their energy levels represented by Ornstein-Uhlenbeck type correlations. I choose Wootters concurrence as a measure of entanglement and examine the purity, dipole-dipole interaction and non-Markovian effects on entanglement dynamics initially prepared in different states.

The organization of this chapter is as follows. In Sec. 5.2, I introduce our model and exactly solve the reduced density matrix elements for two qubits. In Sec. 5.3, I solve the analytic form of concurrence for an arbitrary X-structured density matrix and report the purity, dipole-dipole interaction as well as non-Markovianity effects on entanglement dynamics.

5.2 The model and its solution

The model we consider in this paper is a two interacting qubits through Heisenberg XX model to be affected separately by separate environments which cause a frequency fluctuations in their energy levels that are random. This model can be reffered as Kubo-Anderson model [58] extended for two qubits. The Hamiltonian

for this model is given by [31, 59] (we set $\hbar = 1$)

$$\hat{H}_{tot}(t) = J(\hat{\sigma}_x^A \hat{\sigma}_x^B + \hat{\sigma}_y^A \hat{\sigma}_y^B) + \frac{\Omega_A(t)}{2}\hat{\sigma}_z^A + \frac{\Omega_B(t)}{2}\hat{\sigma}_z^B, \tag{5.1}$$

where J is coupling strength, $\hat{\sigma}_i^{A,B}(i = x, y, z)$ are the usual Pauli operators and $\Omega_{A,B}(t)$ are the independent frequency fluctuations of the qubits with mean value properties

$$M\{\Omega_i(t)\} = 0, \tag{5.2}$$

$$\begin{aligned} M\{\Omega_i(t)\Omega_i(s)\} &= \alpha(t-s) \\ &= \frac{\Gamma_i \gamma}{2} e^{-\gamma|t-s|}, \quad i = A, B, \end{aligned} \tag{5.3}$$

where $M\{...\}$ stands for the statistical mean over the noises $\Omega_A(t)$ and $\Omega_B(t)$. Here $\Gamma_i(i = A, B)$ are the damping rates due to coupling to the environments, γ is the noise bandwidth which determines the environment's finite correlation time of the noise ($\tau_c = \gamma^{-1}$) and $\alpha(t - s)$ is the reservoir correlation function. For simplicity, we will take the noise properties to be the same for A and B (e.g., $\Gamma_A = \Gamma_B \equiv \Gamma$), although independent. And note in the limit $\gamma \to \infty(\tau_c \to 0)$, Ornstein-Uhlenbeck noise reduces to the well-known Markov case:

$$\alpha(t - s) = \Gamma\delta(t - s). \tag{5.4}$$

For the total system described by the Hamiltonian (5.1), the stochastic Schrödinger equation is given by

$$i\frac{d}{dt}\left|\Psi(t)\right\rangle = \hat{H}_{tot}(t)\left|\Psi(t)\right\rangle, \tag{5.5}$$

with solution

$$|\Psi(t)\rangle = \hat{U}(t, \Omega_A, \Omega_B)\,|\Psi(0)\rangle\,, \tag{5.6}$$

where the stochastic propagator $\hat{U}(t, \Omega_A, \Omega_B)$ is given by

$$\hat{U}(t, \Omega_A, \Omega_B) = e^{-\frac{i}{2}\int_0^t \hat{H}_{tot}(s)ds}. \tag{5.7}$$

The reduced density matrix for spins A and B is then obtained from the statistical mean

$$\hat{\rho}(t) = M\{|\Psi(t)\rangle\,\langle\Psi(t)|\}. \tag{5.8}$$

With the help of the raising and lowering operators, $\hat{\sigma}_{\pm}^{A,B} = (\hat{\sigma}_x^{A,B} \pm i\hat{\sigma}_y^{A,B})/2$, and the stochastic Schrödinger equation (5.5), the master equation for the reduced density matrix can be derived [27, 28, 52]:

$$\frac{d}{dt}\hat{\rho}(t) = -i[\hat{H}, \hat{\rho}(t)] - \frac{G(t)}{2}(2\hat{\rho} - \hat{\sigma}_z^A\hat{\rho}(t)\hat{\sigma}_z^A - \hat{\sigma}_z^B\hat{\rho}(t)\hat{\sigma}_z^B), \tag{5.9}$$

where $\hat{H} = 2J(\hat{\sigma}_+^A\hat{\sigma}_-^B + \hat{\sigma}_-^A\hat{\sigma}_+^B)$ is the interaction Hamiltonian which represents the dipole-dipole interaction [57] between qubits and $G(t) = \int_0^t \alpha(t-s)ds = \frac{\Gamma}{2}(1-e^{-\gamma t})$ is a time-dependent coefficient which includes the memory information of the environmental noises.

The differential equations governing the time evolution of the system in the standart basis $\{|11\rangle\,, |10\rangle\,, |01\rangle\,, |00\rangle\}$ can be easily found as

$$
\begin{aligned}
\dot{\rho}_{ii}(t) &= 0 \quad (i = 1, 4), \\
\dot{\rho}_{22}(t) &= 2iJ(\rho_{23}(t) - \rho^*_{23}(t)), \\
\dot{\rho}_{33}(t) &= -2iJ(\rho_{23}(t) - \rho^*_{23}(t)), \\
\dot{\rho}_{12}(t) &= 2iJ\rho_{13}(t) - G(t)\rho_{12}(t), \\
\dot{\rho}_{13}(t) &= 2iJ\rho_{12}(t) - G(t)\rho_{13}(t), \\
\dot{\rho}_{14}(t) &= -2G(t)\rho_{14}(t), \\
\dot{\rho}_{23}(t) &= 2iJ(\rho_{22}(t) - \rho_{33}(t)) - 2G(t)\rho_{23}(t), \\
\dot{\rho}_{24}(t) &= -2iJ\rho_{34}(t) - G(t)\rho_{24}(t), \\
\dot{\rho}_{34}(t) &= -2iJ\rho_{24}(t) - G(t)\rho_{34}(t),
\end{aligned} \tag{5.10}
$$

where the asterisk in the superscript of ρ^*_{mn} denotes the complex conjugation of ρ_{mn}. Some of these equations can be solved analytically. After a simple calculation, we obtained

$$
\begin{aligned}
\rho_{ii}(t) &= \rho_{ii}(0) \quad (i = 1, 4), \\
\rho_{12}(t) &= (\rho_{12}(0)\cos(2Jt) + i\rho_{13}(0)\sin(2Jt))e^{-f(t)}, \\
\rho_{13}(t) &= (\rho_{13}(0)\cos(2Jt) + i\rho_{12}(0)\sin(2Jt))e^{-f(t)}, \\
\rho_{14}(t) &= \rho_{14}(0)e^{-2f(t)}, \\
\rho_{24}(t) &= (\rho_{24}(0)\cos(2Jt) - i\rho_{34}(0)\sin(2Jt))e^{-f(t)}, \\
\rho_{34}(t) &= (\rho_{34}(0)\cos(2Jt) - i\rho_{24}(0)\sin(2Jt))e^{-f(t)}, \\
\rho_{23}(t) &= \frac{A + B}{2},
\end{aligned} \tag{5.11}
$$

where

$$
\begin{aligned}
f(t) &= \int_0^t G(s)ds \\
&= \frac{\Gamma}{2}\left(t + \frac{1}{\gamma}(e^{-\gamma t} - 1)\right), \\
A &= (\rho_{23}(0) + \rho_{23}^*(0))e^{-2f(t)}, \\
B &= \left(\frac{1}{J^2}\right)^{-\frac{\Gamma+\epsilon}{2\gamma}} \left(\frac{e^{-\gamma t}}{J^2}\right)^{\frac{\Gamma-\epsilon}{2\gamma}} \left(\frac{C+D}{E}\right), \qquad (5.12)
\end{aligned}
$$

where

$$
\begin{aligned}
C &= \left(\frac{1}{J^2}\right)^{\frac{\epsilon}{\gamma}} F_1\left(\kappa_-; 1 - \frac{\epsilon}{\gamma}; -\frac{e^{-\gamma t}\Gamma}{\gamma}\right)(\Gamma(\rho_{23}(0) - \rho_{23}^*(0))((\gamma+\Gamma)(\Gamma - 2\gamma + \epsilon) - 64J^2) \\
&\times F_1\left(\Delta_+; 2 + \frac{\epsilon}{\gamma}; -\frac{\Gamma}{2}\right) + (\gamma^2 + 64J^2 - \Gamma^2)F_1\left(\kappa_+; 1 + \frac{\epsilon}{\gamma}; -\frac{\Gamma}{\gamma}\right)((\rho_{23}(0) - \rho_{23}^*(0)) \\
&\times (\Gamma + \epsilon) + 8iJ(\rho_{22}(0) - \rho_{33}(0)))), \\
D &= \left(\frac{e^{-\gamma t}}{J^2}\right)^{\frac{\epsilon}{\gamma}} F_1\left(\kappa_+; 1 + \frac{\epsilon}{\gamma}; -\frac{e^{-\gamma t}\Gamma}{\gamma}\right)(\Gamma(\rho_{23}(0) - \rho_{23}^*(0))((\gamma+\Gamma)(2\gamma - \Gamma + \epsilon) + 64J^2) \\
&\times F_1\left(\Delta_-; 2 - \frac{\epsilon}{\gamma}; -\frac{\Gamma}{\gamma}\right) + (\gamma^2 + 64J^2 - \Gamma^2)F_1\left(\kappa_-; 1 - \frac{\epsilon}{\gamma}; -\frac{\Gamma}{\gamma}\right)((\rho_{23}(0) - \rho_{23}^*(0)) \\
&\times (\epsilon - \Gamma) - 8iJ(\rho_{22}(0) - \rho_{33}(0)))), \\
E &= \Gamma\left((\gamma+\Gamma)(2\gamma - \Gamma + \epsilon) + 64J^2\right) F_1\left(\Delta_-; 2 - \frac{\epsilon}{\gamma}; -\frac{\Gamma}{\gamma}\right) F_1\left(\kappa_+; 1 + \frac{\epsilon}{\gamma}; -\frac{\Gamma}{\gamma}\right) \\
&+ F_1\left(\kappa_-; 1 - \frac{\epsilon}{\gamma}; -\frac{\Gamma}{\gamma}\right)(2\epsilon(64J^2 + \gamma^2 - \Gamma^2)F_1\left(\kappa_+; 1 + \frac{\epsilon}{\gamma}; -\frac{\Gamma}{\gamma}\right) \\
&+ \Gamma((\gamma+\Gamma)(\Gamma - 2\gamma + \epsilon) - 64J^2)F_1\left(\Delta_+; 2 + \frac{\epsilon}{\gamma}; -\frac{\Gamma}{\gamma}\right)) \qquad (5.13)
\end{aligned}
$$

where $\epsilon = \sqrt{\Gamma^2 - 64J^2}, \kappa_\pm = \frac{2\gamma+\Gamma\pm\epsilon}{2\gamma}, \Delta_\pm = \frac{4\gamma+\Gamma\pm\epsilon}{2\gamma}$ and $F_1(a; b; z)$ is the Kummer confluent hypergeometric function. However $\rho_{22}(t)$ and $\rho_{33}(t)$ have no analytic solutions, they can be solved numerically. Note in the limit as $J \to 0$, the solutions (5.11) reduce to the equations given in Ref. [31] and $\rho_{22}(t)$ and $\rho_{33}(t)$ become time independent and equal to their initial values.

5.3 Entanglement Sudden Death versus Sudden Birth

For any two-qubit case, Wooters concurrence [53] can be used as a measure of entanglement. The concurrence function varies from $C = 0$ for a separable state to $C = 1$ for a maximally entangled state. The concurrence function may be calculated from the density matrix $\hat{\rho}(t)$ for qubits A and B:

$$C(\hat{\rho}) = \max\{0, \sqrt{\lambda_1} - \sqrt{\lambda_2} - \sqrt{\lambda_3} - \sqrt{\lambda_4}\}, \tag{5.14}$$

where the quantities λ_i are the eigenvalues in decreasing order of the matrix

$$\hat{\rho}_{trans}(t) = \hat{\rho}(t)(\hat{\sigma}_y^A \otimes \hat{\sigma}_y^B)\hat{\rho}^*(t)(\hat{\sigma}_y^A \otimes \hat{\sigma}_y^B). \tag{5.15}$$

In the following, we consider entanglement dynamics of qubits with an initial density matrix with the common X-form [60]:

$$\hat{\rho}(0) = \begin{bmatrix} \rho_{11}(0) & 0 & 0 & \rho_{14}(0) \\ 0 & \rho_{22}(0) & \rho_{23}(0) & 0 \\ 0 & \rho_{32}(0) & \rho_{33}(0) & 0 \\ \rho_{41}(0) & 0 & 0 & \rho_{44}(0) \end{bmatrix}, \tag{5.16}$$

which persists its shape in time. Such X-states arise in a wide variety of physical situations and include pure Bell states [61] as well as the well-known Werner mixed states [62].

One can easily show that the concurrence function for the initial mixed state (5.16) is given by

$$C(\rho) = 2\max\{0, |\rho_{23}(t)| - \sqrt{\rho_{11}(0)\rho_{44}(0)}, |\rho_{14}(t)| - \sqrt{\rho_{22}(t)\rho_{33}(t)}\}. \tag{5.17}$$

Case 1: The initially separable and affected by dipole-dipole interaction

In Fig. 5.1, we examine the entanglement evolution of the initial state

$$\hat{\rho}(0) = \begin{bmatrix} \frac{1}{6} & 0 & 0 & 0 \\ 0 & \frac{2}{3} & 0 & 0 \\ 0 & 0 & 0 & 0 \\ 0 & 0 & 0 & \frac{1}{6} \end{bmatrix} . \tag{5.18}$$

It can be noted that this state does not retain any entanglement initially and the entanglement created by dipole-dipole interaction is damped to zero by the environment.

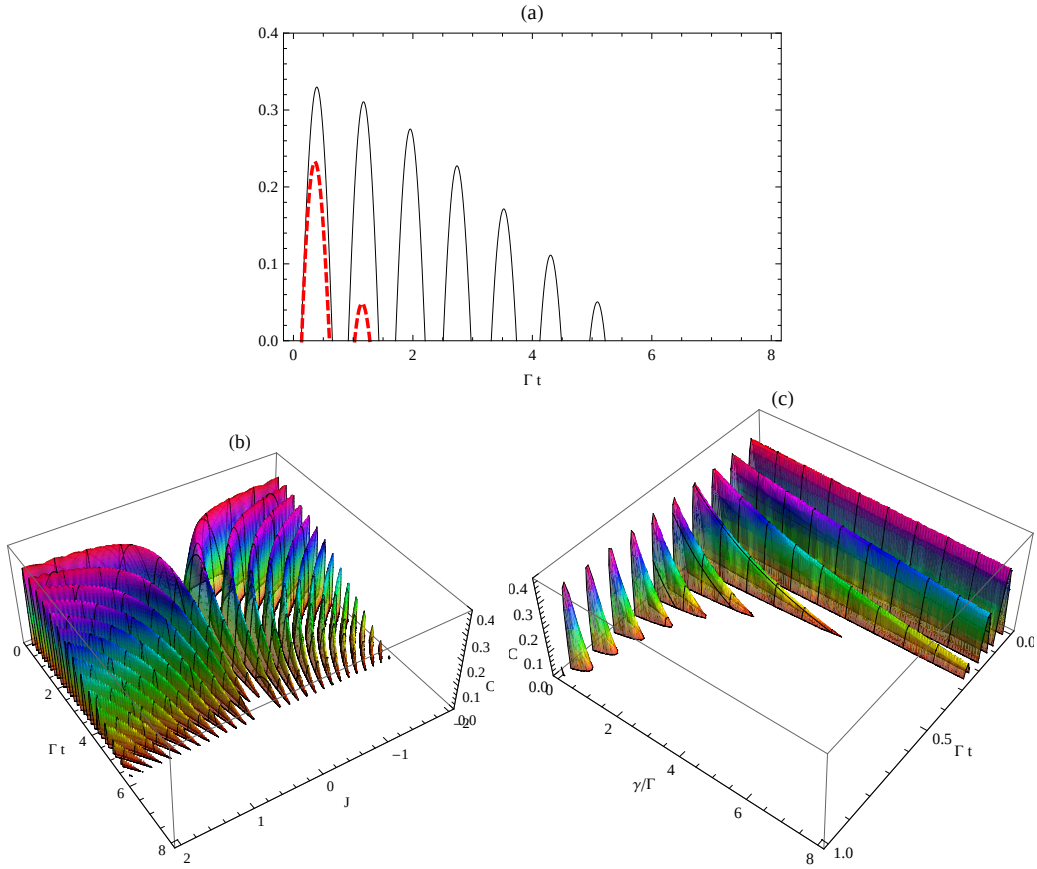

Figure 5.1: C versus Γt with $J = 1$ (Fig.5.1(a)), versus Γt and J with $\gamma/\Gamma = 0.1$ (Fig.5.1(b)) and versus Γt and γ/Γ with $J = 1$ (Fig.5.1(c)). Here the dashed plot corresponds to $\gamma/\Gamma = 10$, while the solid plot to $\gamma/\Gamma = 0.1$.

Case 2: The initially entangled and unaffected by dipole-dipole in-

teraction

The second example is Werner-like initial state in the form

$$\hat{\rho}(0) = \begin{bmatrix} \frac{1-r}{4} & 0 & 0 & 0 \\ 0 & \frac{1+r}{4} & \frac{r}{2} & 0 \\ 0 & \frac{r}{2} & \frac{1+r}{4} & 0 \\ 0 & 0 & 0 & \frac{1-r}{4} \end{bmatrix}, \tag{5.19}$$

where r is the purity of the initial states ranges from 0 to 1. As seen from Fig. 5.2, the dipole-dipole interaction has no effect on the entanglement dynamics of two qubits initially prepared in this state. From Fig. 5.2 (a) and (d), the entanglement dynamics is sensitive to purity and suffers ESD at all times for $r < 0.4$ and independent of the non-Markovianity of the dynamics. Moreover, if $r = 1$, the entanglement dies asymptotically.

Case 3: The initially entangled and affected by dipole-dipole interaction

In Fig. 5.3, we plot the entanglement dynamics of two qubits initially prepared in the state

$$\hat{\rho}(0) = \begin{bmatrix} \frac{1}{6} & 0 & 0 & 0 \\ 0 & \frac{1}{6} & \frac{1}{4} & 0 \\ 0 & \frac{1}{4} & \frac{1}{2} & 0 \\ 0 & 0 & 0 & \frac{1}{6} \end{bmatrix}. \tag{5.20}$$

The important findings from these figures are that in the presence or absence of dipole-dipole interaction, the two qubits retain entanglement at $t = 0$ and damped by the "qubit+environment" interactions to zero. The only effect of the dipole-dipole interaction is to prolong the death time slightly.

The common features of these figures are the non-Markovainity can only prolong the sudden death depending on the magnitude of the ratio γ/Γ inversly, while it cannot prevent it. On the other hand, the dipole-dipole interaction can

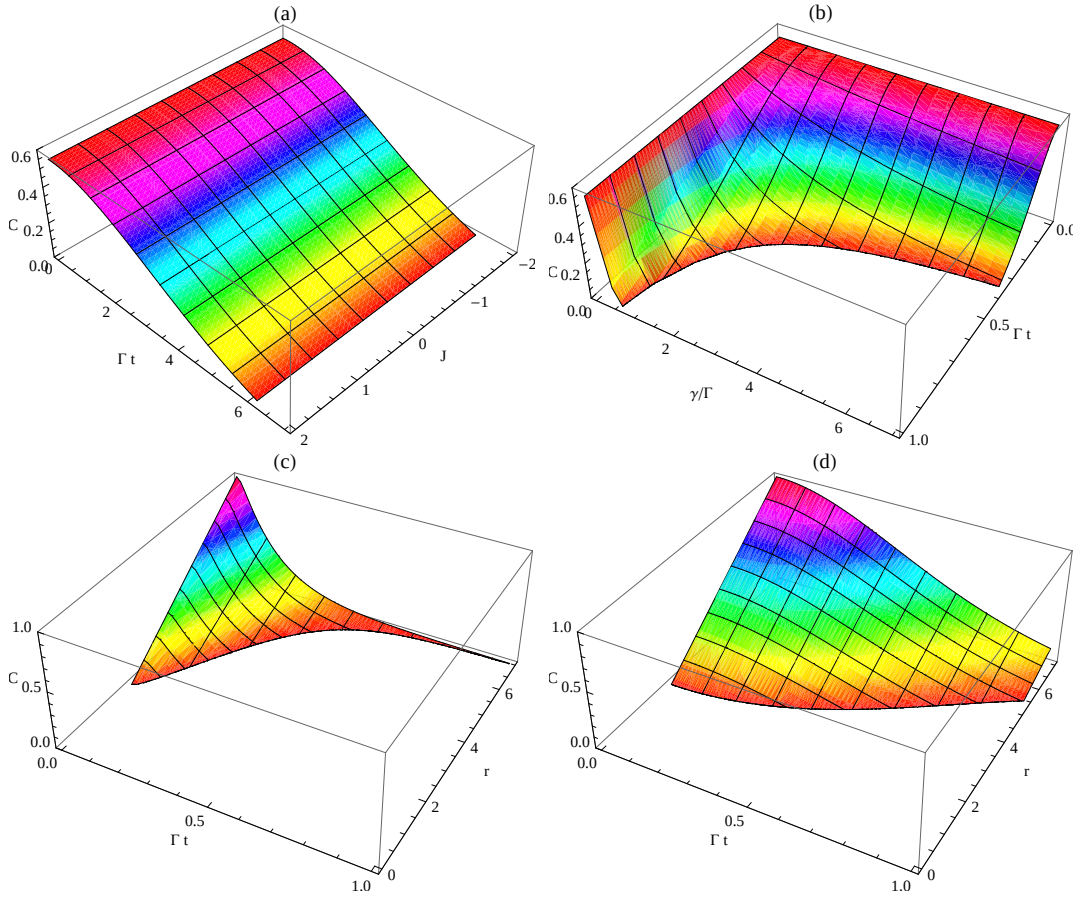

Figure 5.2: C versus Γt and J with $r = 0.7$ and $\gamma/\Gamma = 0.1$ (Fig.5.2(a)), versus Γt and γ/Γ with $r = 0.7$ (Fig.5.2(b)) and versus Γt and r (Fig.5.2(c) with $\gamma/\Gamma = 10$ and Fig.5.2(d) with $\gamma/\Gamma = 0.1$).

slightly prolong the death time but the relation between the J and death time is misterious.

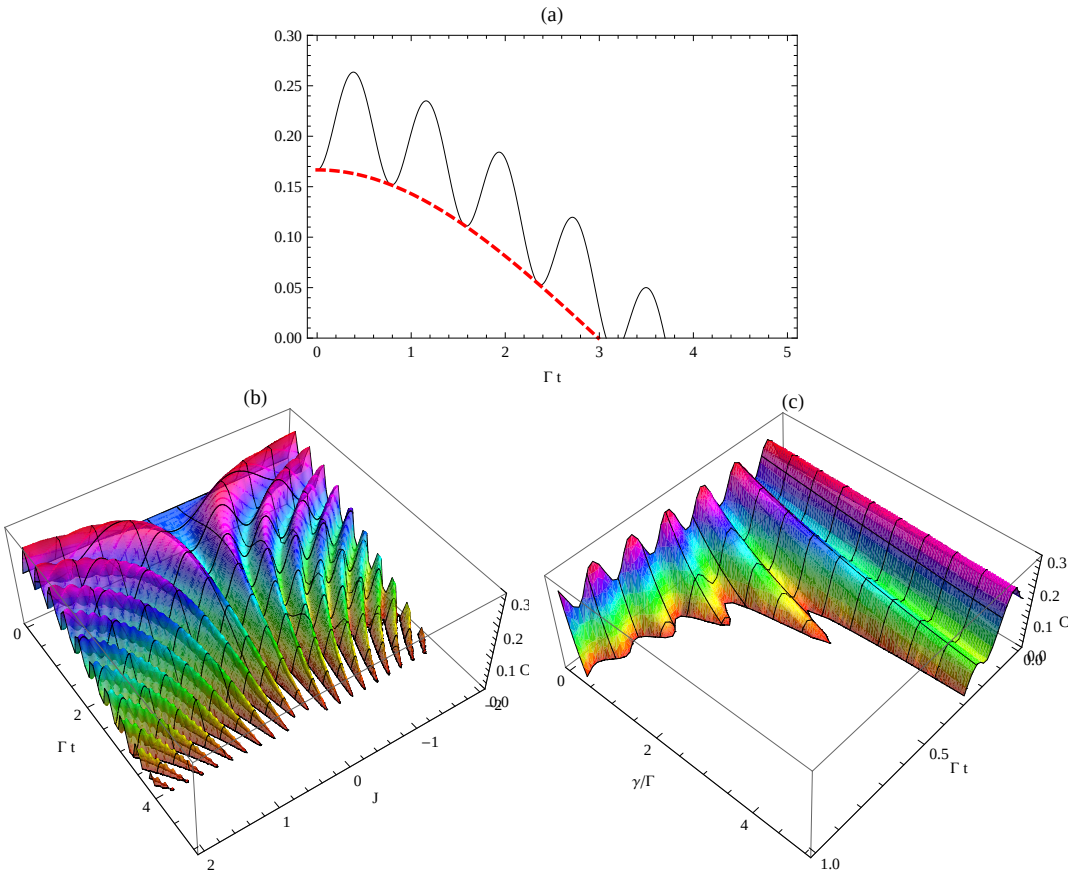

Figure 5.3: C versus Γt with $\gamma/\Gamma = 0.1$ (Fig.5.3(a)), versus Γt and J with $\gamma/\Gamma = 0.1$ (Fig.5.1(b)) and versus Γt and γ/Γ with $J = 1$ (Fig.5.1(c)). Here the dashed plot corresponds to $J = 0$, while the solid plot to $J = 1$.

CHAPTER 6
ENTANGLEMENT DYNAMICS OF THREE STOCHASTIC QUBITS WITH DIPOLE-DIPOLE INTERACTIONS

6.1 Introduction

In this chapter, I consider three-interacting qubits through next nearest and next next nearest couplings and each qubit is embedded in its own reservoir which cause stochastic fluctuations in their energy levels. I analyze the effects of dipole-dipole interaction between qubits, purity of the initial states as well as the non-Markovainity of the dynamics on the entanglement between three qubits measured by negativity and two-qubits measured by concurrence.

The organization of this chapter is as follows. In Sec. 6.2, I introduce our model and solve the differential equations of the reduced density matrix that governs the dynmamics. In Sec. 6.3, I introduce the entanglement measures for both bipartite and tripartite states and analyzed the effects of dipole-dipole interactions, purity and non-Markovianity on the entanglement of the qubits initially prepared in GHZ- and W-type states.

6.2 The model

Our model consits of three interacting qubits coupled to separately by separate environments which cause frequency fluctuations in their energy levels that are random. This model is reffered as Kubo-Anderson model extended for three

interacting qubits. The Hamiltonian for this model can be expressed as [11, 31, 56]

$$\begin{aligned}\hat{H}_{tot}(t) &= J_1(\hat{\sigma}_x^A\hat{\sigma}_x^B + \hat{\sigma}_y^A\hat{\sigma}_y^B + \hat{\sigma}_x^B\hat{\sigma}_x^C + \hat{\sigma}_y^B\hat{\sigma}_y^C) + J_2(\hat{\sigma}_x^A\hat{\sigma}_x^C + \hat{\sigma}_y^A\hat{\sigma}_y^C) \\ &+ \frac{\Omega_A(t)}{2}\hat{\sigma}_z^A + \frac{\Omega_B(t)}{2}\hat{\sigma}_z^B + \frac{\Omega_C(t)}{2}\hat{\sigma}_z^C, \end{aligned} \tag{6.1}$$

where $\hat{\sigma}_i (i = x, y, z)$ are the usual Pauli spin matrices, J_1 and J_2 are the coupling constants between nearest neighbors and next nearest neighbor sites, respectively and $\Omega_i(t)(i = A, B, C)$ are the independent fluctuations of the transition frequencies obeying on non-Markovian approximation with mean value properties,

$$\begin{aligned} M[\Omega_i(t)] &= 0, \\ M[\Omega_i(t)\Omega_i(s)] &= \frac{\Gamma_i\gamma}{2}e^{-\gamma|t-s|}, \quad i = A, B, C, \end{aligned} \tag{6.2}$$

where $M[.]$ denotes the ensemble average over the classical noises. Here, Γ determines the damping rates due to coupling to the environments and γ is the noise bandwith which determines the environment's finite correlation time (that is, $\tau_c = \gamma^{-1}$). For simplicity, we will take all noise properties to be the same for A,B and C, that is, $\Gamma_A = \Gamma_B = \Gamma_C \equiv \Gamma$.

It can be shown that the master equation governing the dynamics of three interacting qubits under the influence of three classical noises can be derived from the corresponding stochastic Schrödinger equation [27, 28, 52],

$$\frac{d\hat{\rho}}{dt} = -i[\hat{H}, \hat{\rho}] - \frac{G(t)}{2}(3\hat{\rho} - \hat{\sigma}_z^A\hat{\rho}\hat{\sigma}_z^A - \hat{\sigma}_z^B\hat{\rho}\hat{\sigma}_z^B - \hat{\sigma}_z^C\hat{\rho}\hat{\sigma}_z^C), \tag{6.3}$$

where $G(t) = \frac{\Gamma}{2}(1 - e^{-\gamma t})$ is the time-dependent coefficient which includes the memory information of the environmental noises, $\hat{H} = 2J_1(\hat{\sigma}_+^A\hat{\sigma}_-^B + \hat{\sigma}_-^A\hat{\sigma}_+^B + \hat{\sigma}_+^B\hat{\sigma}_-^C + \hat{\sigma}_-^B\hat{\sigma}_+^C) + 2J_2(\hat{\sigma}_+^A\hat{\sigma}_-^C + \hat{\sigma}_-^A\hat{\sigma}_+^C)$ is the interaction Hamiltonian which represents the dipole-dipole interaction between nearest neighbor and next nearest neighbor qubits [57] and $\hat{\sigma}_+$ and $\hat{\sigma}_-$ are raising and lowering operators, respectively.

The differential equations governing the time evolution of the system in the

standart basis $\{|1\rangle \equiv |111\rangle, |2\rangle \equiv |110\rangle, |3\rangle \equiv |101\rangle, |4\rangle \equiv |100\rangle, |5\rangle \equiv |011\rangle, |6\rangle \equiv |010\rangle, |7\rangle \equiv |001\rangle, |8\rangle \equiv |000\rangle\}$ can be easily calculated as:

$$
\begin{aligned}
\dot{\rho}_{11} &= 0, \\
\dot{\rho}_{12} &= 2iJ_1\rho_{13} + 2iJ_2\rho_{15} - G(t)\rho_{12}, \\
\dot{\rho}_{13} &= 2iJ_1(\rho_{12} + \rho_{15}) - G(t)\rho_{13}, \\
\dot{\rho}_{14} &= 2iJ_1\rho_{16} + 2iJ_2\rho_{17} - 2G(t)\rho_{14}, \\
\dot{\rho}_{15} &= 2iJ_1\rho_{13} + 2iJ_2\rho_{12} - G(t)\rho_{15}, \\
\dot{\rho}_{16} &= 2iJ_1(\rho_{14} + \rho_{17}) - 2G(t)\rho_{16}, \\
\dot{\rho}_{17} &= 2iJ_1\rho_{16} + 2iJ_2\rho_{14} - 2G(t)\rho_{17}, \\
\dot{\rho}_{18} &= -3G(t)\rho_{18}, \\
\dot{\rho}_{22} &= 2iJ_1(\rho_{23} - \rho_{32}) + 2iJ_2(\rho_{25} - \rho_{52}), \\
\dot{\rho}_{23} &= 2iJ_1(\rho_{22} + \rho_{25} - \rho_{33}) - 2iJ_2\rho_{53} - 2G(t)\rho_{23}, \\
\dot{\rho}_{24} &= 2iJ_1(\rho_{26} - \rho_{34}) + 2iJ_2(\rho_{27} - \rho_{54}) - G(t)\rho_{24}, \\
\dot{\rho}_{25} &= 2iJ_1(\rho_{23} - \rho_{35}) + 2iJ_2(\rho_{22} - \rho_{55}) - 2G(t)\rho_{25}, \\
\dot{\rho}_{26} &= 2iJ_1(\rho_{24} + \rho_{27} - \rho_{36}) - 2iJ_2\rho_{56} - G(t)\rho_{26}, \\
\dot{\rho}_{27} &= 2iJ_1(\rho_{26} - \rho_{37}) + 2iJ_2(\rho_{24} - \rho_{57}) - 3G(t)\rho_{27}, \\
\dot{\rho}_{28} &= -2iJ_1\rho_{38} - 2iJ_2\rho_{58} - 2G(t)\rho_{28}, \\
\dot{\rho}_{33} &= 2iJ_1(\rho_{32} + \rho_{35} - \rho_{23} - \rho_{53}), \\
\dot{\rho}_{34} &= 2iJ_1(\rho_{36} - \rho_{24} - \rho_{54}) + 2iJ_2\rho_{37} - G(t)\rho_{34}, \\
\dot{\rho}_{35} &= 2iJ_1(\rho_{33} - \rho_{25} - \rho_{55}) + 2iJ_2\rho_{32} - 2G(t)\rho_{35}, \\
\dot{\rho}_{36} &= 2iJ_1(\rho_{34} + \rho_{37} - \rho_{26} - \rho_{56}) - 3G(t)\rho_{36}, \\
\dot{\rho}_{37} &= 2iJ_1(\rho_{36} - \rho_{27} - \rho_{57}) + 2iJ_2\rho_{34} - G(t)\rho_{37}, \\
\dot{\rho}_{38} &= -2iJ_1(\rho_{28} + \rho_{58}) - 2G(t)\rho_{38}, \\
\dot{\rho}_{44} &= 2iJ_1(\rho_{46} - \rho_{64}) + 2iJ_2(\rho_{47} - \rho_{74}), \\
\dot{\rho}_{45} &= 2iJ_1(\rho_{43} - \rho_{65}) + 2iJ_2(\rho_{42} - \rho_{75}) - 3G(t)\rho_{45},
\end{aligned}
$$

$$
\begin{aligned}
\dot{\rho}_{46} &= 2iJ_1(\rho_{44}+\rho_{47}-\rho_{66})-2iJ_2\rho_{76}-2G(t)\rho_{46},\\
\dot{\rho}_{47} &= 2iJ_1(\rho_{46}-\rho_{67})+2iJ_2(\rho_{44}-\rho_{77})-2G(t)\rho_{47},\\
\dot{\rho}_{48} &= -2iJ_1\rho_{68}-2iJ_2\rho_{78}-G(t)\rho_{48},\\
\dot{\rho}_{55} &= 2iJ_1(\rho_{53}-\rho_{35})+2iJ_2(\rho_{52}-\rho_{25}),\\
\dot{\rho}_{56} &= 2iJ_1(\rho_{54}+\rho_{57}-\rho_{36})-2iJ_2\rho_{26}-G(t)\rho_{56},\\
\dot{\rho}_{57} &= 2iJ_1(\rho_{56}-\rho_{37})+2iJ_2(\rho_{54}-\rho_{27})-G(t)\rho_{57},\\
\dot{\rho}_{58} &= -2iJ_1\rho_{38}-2iJ_2\rho_{28}-2G(t)\rho_{58},\\
\dot{\rho}_{66} &= 2iJ_1(\rho_{64}+\rho_{67}-\rho_{46}-\rho_{76}),\\
\dot{\rho}_{67} &= 2iJ_1(\rho_{66}-\rho_{47}-\rho_{77})+2iJ_2\rho_{64}-2G(t)\rho_{67},\\
\dot{\rho}_{68} &= -2iJ_1(\rho_{48}+\rho_{78})-G(t)\rho_{68},\\
\dot{\rho}_{77} &= 2iJ_1(\rho_{76}-\rho_{67})+2iJ_2(\rho_{74}-\rho_{47}),\\
\dot{\rho}_{78} &= -2iJ_1\rho_{68}-2iJ_2\rho_{48}-G(t)\rho_{78},\\
\dot{\rho}_{88} &= 0.
\end{aligned}
\tag{6.4}
$$

From these differential equations, it is obvious that the diagonal elements and some of the off-diagonal elements of the three-qubit reduced density matrix elements evolves in time independently:

$$
\hat{\rho}_{ABC} = \begin{bmatrix}
\rho_{11} & 0 & 0 & 0 & 0 & 0 & 0 & \rho_{18} \\
0 & \rho_{22} & \rho_{23} & 0 & \rho_{25} & 0 & 0 & 0 \\
0 & \rho_{32} & \rho_{33} & 0 & \rho_{35} & 0 & 0 & 0 \\
0 & 0 & 0 & \rho_{44} & 0 & \rho_{46} & \rho_{47} & 0 \\
0 & \rho_{52} & \rho_{53} & 0 & \rho_{55} & 0 & 0 & 0 \\
0 & 0 & 0 & \rho_{64} & 0 & \rho_{66} & \rho_{67} & 0 \\
0 & 0 & 0 & \rho_{74} & 0 & \rho_{76} & \rho_{77} & 0 \\
\rho_{81} & 0 & 0 & 0 & 0 & 0 & 0 & \rho_{88}
\end{bmatrix},
\tag{6.5}
$$

which provides us to analyze the entanglement dynamics of three-qubit as well as the two-qubit whose reduced density matrix can be calculated taking partial trace [54] over the third qubit and has an structure of X-form:

$$\hat{\rho}_{12} = \begin{bmatrix} A_{11} & 0 & 0 & 0 \\ 0 & A_{22} & A_{23} & 0 \\ 0 & A_{32} & A_{33} & 0 \\ 0 & 0 & 0 & A_{44} \end{bmatrix}. \tag{6.6}$$

The matrix elements of the reduced matrix of qubits A and B can be obtained by partial tracing over the qubit C and has elements

$$\begin{aligned} A_{11} &= \rho_{11} + \rho_{22}, \quad A_{22} = \rho_{33} + \rho_{44}, \quad A_{33} = \rho_{55} + \rho_{66} \\ A_{44} &= \rho_{77} + \rho_{88}, \quad A_{23} = \rho_{35} + \rho_{46}. \end{aligned} \tag{6.7}$$

Similarly, the matrix elements of the reduced density matrix for qubits A and C are

$$\begin{aligned} A_{11} &= \rho_{11} + \rho_{33}, \quad A_{22} = \rho_{22} + \rho_{44}, \quad A_{33} = \rho_{55} + \rho_{77} \\ A_{44} &= \rho_{66} + \rho_{88}, \quad A_{23} = \rho_{25} + \rho_{47}. \end{aligned} \tag{6.8}$$

6.3 Entanglement sudden death versus sudden birth

For a pair of qubits, the concurrence as a measure of entanglement is well-defined. It is introduced by Wooters [6] and defined as

$$C = \max\{0, \sqrt{\lambda_1} - \sqrt{\lambda_2} - \sqrt{\lambda_3} - \sqrt{\lambda_4}\}, \tag{6.9}$$

where the quantities $\lambda_i (i = 1, 2, 3, 4)$ are the eigenvalues of the matrix

$$\hat{R} = \hat{\rho}_{12}(\hat{\sigma}_y^1 \otimes \hat{\sigma}_y^2)\hat{\rho}_{12}^*(\hat{\sigma}_y^1 \otimes \hat{\sigma}_y^2), \tag{6.10}$$

in descending order and $\hat{\rho}_{12}^{*}$ is the conjugate of $\hat{\rho}_{12}$. For the density matrix (6.6), the concurrence function (6.9) has a simple analytic form:

$$C = 2\max\{0, |A_{23}| - \sqrt{A_{11}A_{44}}\}. \tag{6.11}$$

On the other hand, for three-qubit system, concurrence is not well-defined. For this case negativity [7] can be used as a measure of entanglement whose calculation is based on partial positive transposes [54] introduced by Peres-Horodecki. For the state with density matrix $\hat{\rho}_{ABC}$, the negativity reads

$$N = \frac{\left\|\hat{\rho}_{ABC}^{T_A}\right\|_1 - 1}{2}, \tag{6.12}$$

where $\hat{\rho}_{ABC}^{T_A}$ denotes the partial transpose of $\hat{\rho}_{ABC}$ with respect to the qubit A. From its definition, the negativity (6.12) can also be expressed as

$$N = \sum_{i=1}^{8} \max\{0, -\Lambda_i\}, \tag{6.13}$$

where $\Lambda_i (i = 1, \ldots, 8)$ are the eigenvalues of $\rho_{ABC}^{T_A}$.

In the following, we are interested in some explicit three-qubit initial states called GHZ- and W-type states. As is known GHZ-state cannot transformed into W-state by local operations and classical communication [55]. This means they bear imcompatible multipartite correlations. From this point of view, one may expect that the two initial states might have some differences in their entanglement dynamics.

6.3.1 GHZ-type states

In this section we explore the effects of external noises and dipole-dipole interaction on the following three qubit GHZ-type states,

$$\hat{\rho}_{ABC}(0) = \frac{1-r}{8}\hat{I}_8 + r\,|GHZ\rangle\langle GHZ| \tag{6.14}$$

where $|GHZ\rangle = \frac{1}{\sqrt{2}}(|111\rangle + |000\rangle)$ and r is the purity of the initial states ranges from 0 to 1. These states have no bi-partite entanglement and non-zero negativity.

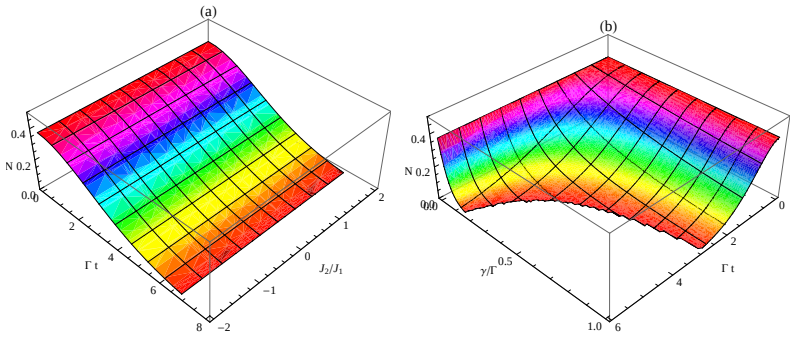

Figure 6.1: Fig. (a) shows the dynamics of negativity versus Γt and J_2/J_1 with $\gamma/\Gamma = 0.1$ and $r = 0.8$. Fig. (b) shows the dynamics of negativity versus γ/Γ and Γt with $r = 0.8$. Here the plots are for GHZ-type initial state.

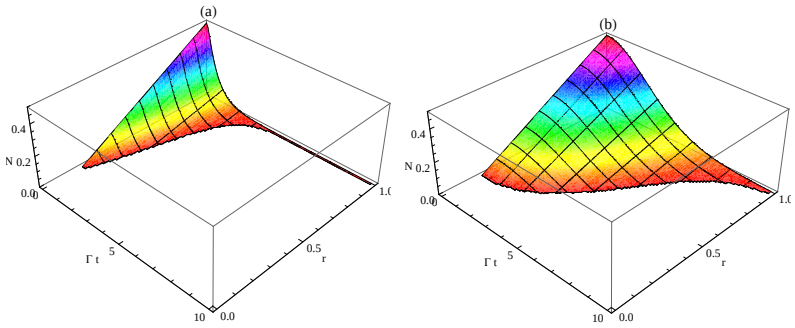

Figure 6.2: The dynamics of negativity versus Γt and r for GHZ-type initial state. Fig. (a) corresponds to Markovian regime with $\gamma/\Gamma = 10$ and Fig. (b) to non-Markovian regime with $\gamma/\Gamma = 0.1$.

In Fig. 6.1 and 6.2, we reported the effects of dipole-dipole interactions, the non-Markovianity and purity on the entanglement dynamics of three qubits initially prepared in GHZ-type states. From Fig. 6.1(a) and 6.1(b), it can be noted that the dipole-dipole interaction has no effect on negativity and the non-Markovianity only prologs the death of entanglement. As seen from Fig. 6.2(a) and 6.2(b), the purity of the initial states has a significant effect on negativity with exponential decay at $r = 1$ and suffers ESD at all times for $r \leq 0.4$ independent of the non-Markovainity of the dynamics.

6.3.2 W-type states

Secondly, we assume W-type initial state expressed as

$$\hat{\rho}_{ABC}(0) = \frac{1-r}{8}\hat{I}_8 + r\,|W\rangle\langle W| \tag{6.15}$$

where $|W\rangle = \frac{1}{\sqrt{3}}(|100\rangle + |010\rangle + |001\rangle)$. Unlike GHZ states the W states retains a high degree of bi-partite entanglement and affected by dipole-dipole interactions.

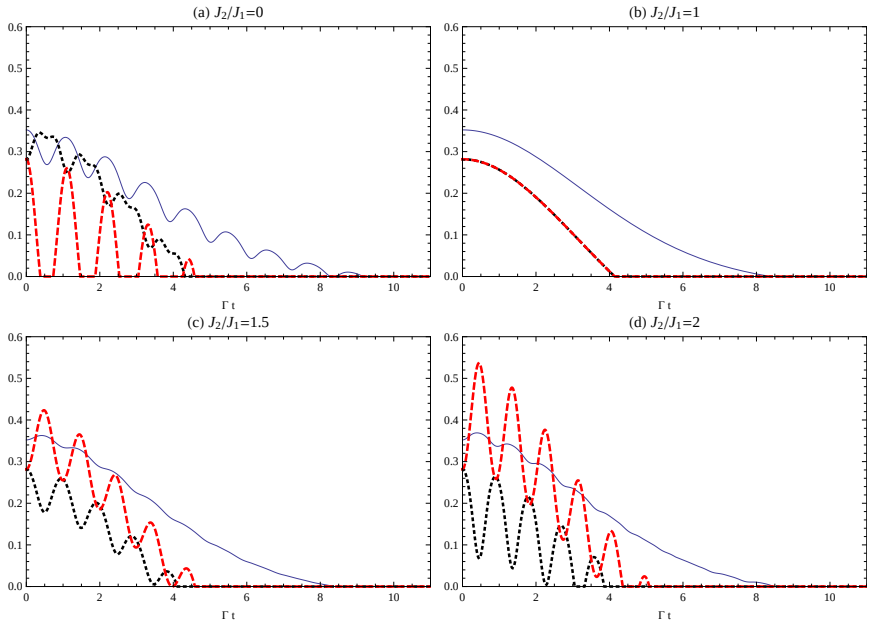

Figure 6.3: The dynamics of N (solid plots), C_{AB} (dotted plots) and C_{AC} (dashed plots) versus Γt with $r = 0.8$ and $\gamma/\Gamma = 0.1$ for W-type initial state. Fig. (a), (b), (c),and (d) correspond to $J_2/J_1 = 0, 1, 1.5$ and 2, respectively.

In Fig. 6.3, 6.4 and 6.5, we analyzed the entanglement dynamics of three and two qubits initially prepared in W-type states. It can be noted that the dipole-dipole interaction has a significant effect on N or C_{AB} with prolonging the deaths for $J_2/J_1 < 0$. Moreover, as seen from Fig. 6.3(b), the two and three qubits are unaffected from the dipole-dipole interactions. As mentioned before, N, C_{AB} and C_{AC} life times take longer in non-Markovain regimes compared to Markovain one. Finally as seen in Fig. 6.6, two qubit entanglement is more sensitive to the purity compared to the three-qubit entanglement, except at $r = 1$ where they do not suffer ESD.

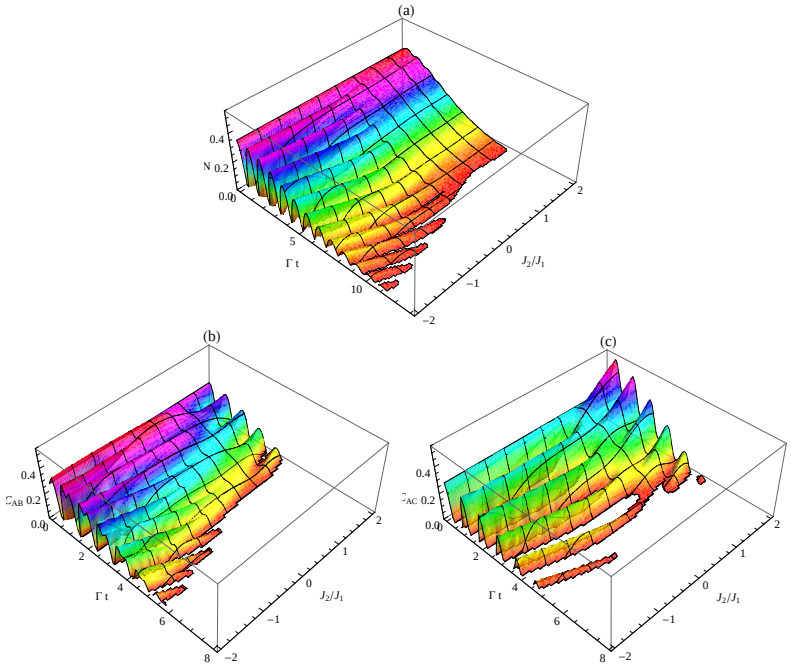

Figure 6.4: The dynamics of N (Fig. (a)), C_{AB} (Fig. (b))and C_{AC} (Fig. (c)) versus Γt and J_2/J_1 for W-type initial state with $\gamma/\Gamma = 0.1$ and $r = 0.8$.

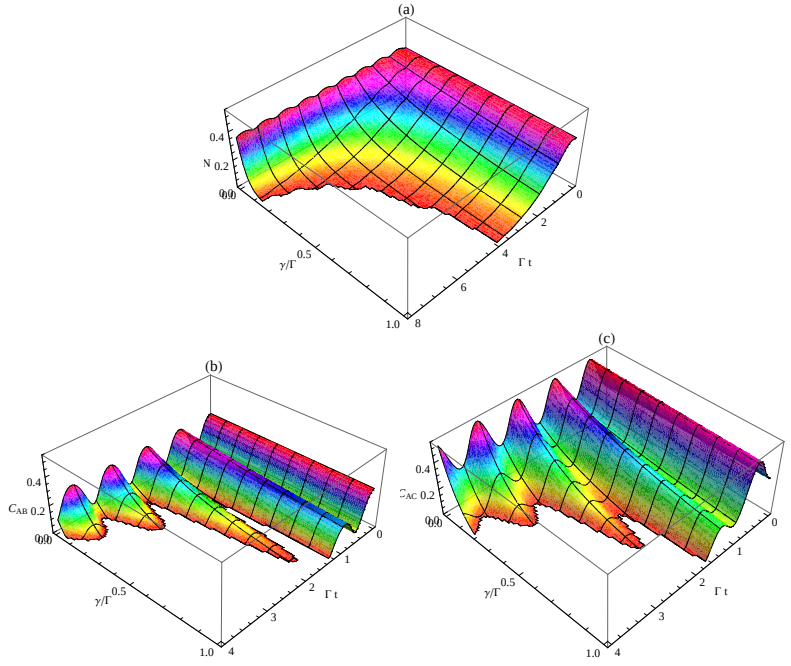

Figure 6.5: The dynamics of N (Fig. (a)), C_{AB} (Fig. (b))and C_{AC} (Fig. (c)) versus Γt and γ/Γ for W-type initial state with $J_2/J_1 = 2$ and $r = 0.8$.

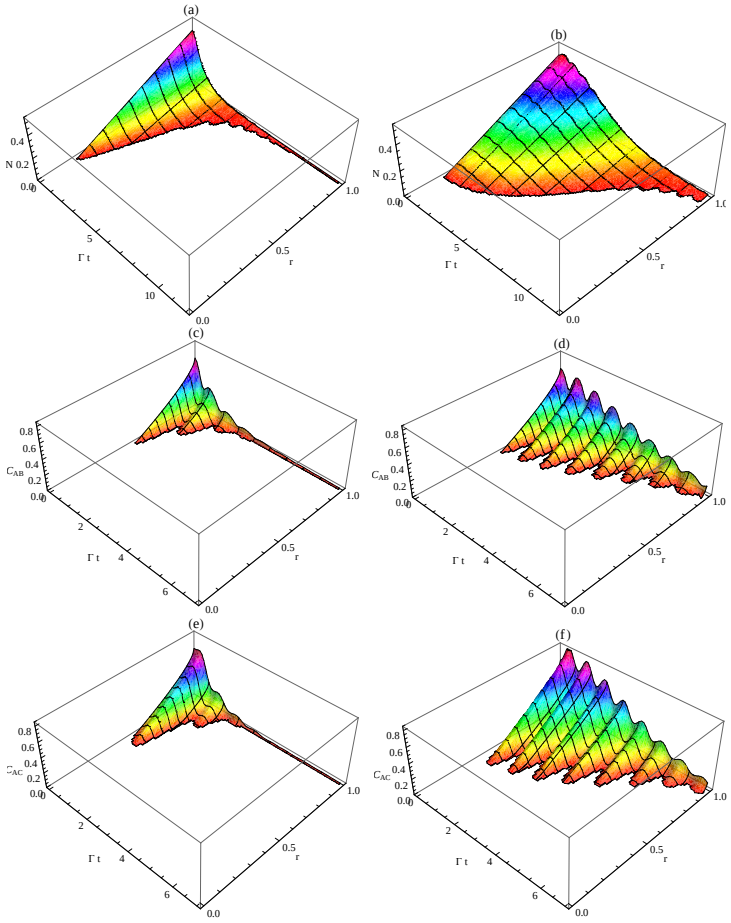

Figure 6.6: The dynamics of N (Fig. (a) and (b)) , C_{AB} (Fig. (c) and (d)) and C_{AC} (Fig. (e) and (f)) versus Γt and r for W-type initial state with $J_2/J_1 = 2$. Fig. (a), (c) and (e) correspond to Markovian regime with $\gamma/\Gamma = 10$ and Fig. (b), (d) and (f) to non-Markovian regime with $\gamma/\Gamma = 0.1$.

CHAPTER 7

CONCLUSION

In Chapter 2, we have studied the exact analytical dynamics of two qubits subject to independent longitudinal kicks and Gaussian pulses. Time-ordering effects on the entanglement dynamics are investigated by using concurrence as the entanglement measure. We have prepared the qubits initially in a separable, $|\Psi(0)\rangle = |10\rangle$, and in a maximally-entangled, $|\Psi(0)\rangle = \frac{1}{\sqrt{2}}(|10\rangle + |01\rangle)$, states and we have most importantly showed that "almost-steady" high entanglement can be created between two initially unentangled qubits by using carefully designed kick or pulse sequences. Furthermore, we have observed that for an initially maximal entangled state, one can create a full entangelement between qubits two or more times by applying pulse sequences.

In Chapter 3, we have explored the effects of transverse sudden kicks or Gaussian pulses on entanglement dynamics of two-interacting qubits through Heisenberg XXX model. We have chosen concurrence as a measure of entanglement and by considering initially separable $|\Psi(0)\rangle = |11\rangle$ and maximally entangled $|\Psi(0)\rangle = \frac{1}{\sqrt{2}}(|11\rangle + |00\rangle)$ states the effects of kick or pulse squences on entanglement dynamics are investigated. We have observed that under this control scheme, one can create a highly full entanglement between two initially separable qubits. Moreover, the minimum of the entanglement oscillation of the initially maximal entangled state can reach to zero. For some cases, for an initially maximal entangled state, the qubits can retain a full entanglement after passing through some pulse or kick sequences.

In Chapter 4, we have analyzed the dynamics of quantum correlations, such as quantum discord, entanglement and Bell nonlocalities for three qubits that have stochastic energy levels. The considered noise have Ornstein-Uhlenbeck type cor-

relations. The dynamics is considered for GHZ- and W-type initial states and the survival times of the quantum correlations are compared. The tripartite entanglement is found to be immune to sudden death for pure GHZ as well as W states, while Bell inequalities cease to be violated for all types of initial states considered in this study. For GHZ-type initial states, there is no bipartite entanglement and quantum discord, while Bell nonlocality and tripartite entanglement as measured by negativity is nonzero for purity greater than approximately 0.4 and 0.2, respectively. Bell inequality is found to be not violated at all purities at much shorter times compared to the sudden death of entanglement. W-type initial states display a richer dynamics, as they contain both bi- and tri-partite entanglement as well as Bell nonlocalities and nonzero quantum discord initially. Quantum discord is observed to be more robust compared to entanglement, because it decays exponentially while the concurrence of the same state suffers sudden death. Also, tripartite entanglement is found to survive longer compared to the bipartite one if the state is mixed; for pure W states, both bi- and tripartite entanglements decrease exponentially with time. We have considered the effects of Markovianity on the dynamics of both types of states and found to the sole effect of non-Markovianity is to prolong the lifetime of quantum correlations compared to the Markovian dynamics. Moreover, it can be noted that once the entanglement and Bell nonlocalities die, rebirth or revival does not occur, also there is no instantaneous dissappearance of the quantum discord at some points, in comparision to the entanglement sudden death in the same range of the parameters of interest [24, 37, 38].

In Chapter 5, we have analyzed the exact entanglement dynamics of two stochastic qubits connected to each other by dipole-dipole interaction. We have assumed each qubit is embedded in its own reservoir which cause stochastic fluctuations in their energy levels represented by Ornstein-Uhlenbeck type correlations. We have chosen Wootters concurrence as a measure of entanglement and examine the purity, dipole-dipole interaction and non-Markovian effects on entanglement

dynamics initially prepared in different states. We have showed that the dipole-dipole interaction can significantly prolong the full disentanglement time, but this does not depend on its magnitude. It seems that the evident effect of J is the increase of the number of ESB with the increasing of J. Further, the entanglement dynamics suffer ESD for $r < 0.25$ independet of the non-Markovianity of the dynamics. On the other hand for $r = 1$, the entanglement dies asymptotically which is independent of the non-Markovianity of the dynamics, too. The sole effect of the non-Markovianity is to prolong the life time of entanglement compared to the Markovian dynamics.

In Chapter 6, we have considered three-interacting qubits through next-nearest and next-next-nearest couplings and each qubit is embedded in its own reservoir which cause stochastic fluctuations in their energy levels. We have analyzed the effects of dipole-dipole interaction between qubits, purity of the initial states as well as the non-Markovainity of the dynamics on the entanglement between three qubits measured by negativity and two-qubits measured by concurrence for GHZ- and W-type initial states. The qubits do not retain bi-partite entanglement and the tri-partite entanglement does not affected by the dipole-dipole interaction if the qubits are initially prepared in GHZ-type states. Most importantly, it can be noted that tri-partite entanglement suffers ESD for $r < 0.2$ at all times and exponential decay for $r = 1$ which are independent of the non-Markovianity of the dynamics for GHZ-type initial states. Unlike GHZ-state, the W-state retains a high degree of bi-partite entanglement and affected from the dipole-dipole interactions. For this initial state, we have observed that the tripartite entanglement has life time longer than the bi-partite entanglement between the qubits A and B as well as A and C in all cases. For the condition $J_2/J_1 = 1$, the tri- and bi-partite entanglements are unaffected from the qubit-qubit interactions. Moreover, when $J_2/J_1 < 0$, the full disentanglement time as well as the number of ESB are larger than the region where $J_2/J_1 > 0$ for all entanglement types. Furthermore, the tripartite entanglement suffers ESD for $r < 0.3$ while C_{AB} and C_{AC} suffer ESD

for $r < 0.3$ and $r < 0.5$, respectively. For the pure state ($r = 1$) all entanglement types between qubits decay exponentially. Finally, we have showed that the non-Markovianity of the dynamics only prolongs the full disenatnglement time, not prevent which is common for GHZ- and W-type initial states.

REFERENCES

[1] A. Einstein, N. Rosen and B. Podolsky, Phys. Rev. **47**, 777 (1935).

[2] J. S. Bell, Physics **1**, 195 (1964).

[3] C. H. Bennett, et al., Phys. Rev. Lett. **69**, 1895 (1993).

[4] A. K. Ekert, Phys. Rev. Lett. **67**, 661 (1991).

[5] P. W. Shor, SIAM J. Comp. **26**, 1484 (1997).

[6] W. K. Wootters, Phys. Rev. Lett., **80**, 2245 (1998).

[7] G. Vidal and R. F. Werner, Phys. Rev. A, **65**, 032314 (2002).

[8] M. S. Abdalla, E. Lashin and G. Sadiek J. Phys. B **41**, 015502 (2008).

[9] F. Mintert, et al., Phys. Rep. **415**, 207 (2005).

[10] D. C. Li and Z. L. Cao, Opt. Comm., **282**, 1226 (2009).

[11] Y. Wang, J. Cao and Y. Wang, Science Direct, Phys. Lett. A **342**, 375 (2005).

[12] J. Souza, F. Lacerda and I. P. Fittipaldi J. Mag. and Mag. Materials **140**, 1501 (1995).

[13] L. Kaplan, et al., Phys. Rev. A, **70**, 063401 (2004).

[14] H. Ollivier and W. H. Zurek, Phys. Rev. Lett., **88**, 017901 (2001).

[15] A. Datta, A. Shaji and C. M. Caves, Phys. Rev. Lett., **100**, 050502 (2008).

[16] J. Cu and H. Fan, arXiv: quant-ph/0904.2703.

[17] M. S. Sarandy, Phys. Rev. A, **80**, 022108 (2009).

[18] A. Shabani and D. A. Lidar, Phys. Rev. Lett., **102**, 100402 (2009).

[19] A. Datta, Phys. Rev. A, **80**, 052304 (2009).

[20] K. Ann and G. Jaeger, Phys. Lett. A, **372**, 6853 (2008).

[21] G. Jaeger and K. Ann, Phys. Lett. A, **372**, 2212 (2008).

[22] Q. Yang, M. Yang and Z. L. Cao, Phys. Lett. A, **372**, 6843 (2008).

[23] L. Qui, A. M. Wang, X. Q. Su and X. S. Ma, Opt. Comm., **281**, 5475 (2008).

[24] B. Bellomo, R. Lo Franco, and G. Compagno, Phys. Rev. A, **78**, 062309 (2008).

[25] A. Miranowicz, Phys. Lett. A, **327**, 272 (2004).

[26] B. Bellomo, R. Lo Franco, and G. Compagno, Advanced Science Letters, **2**, 459 (2009).

[27] W. T Strunz and T. Yu, Phys. Rev. A, **69**, 052115 (2004).

[28] T. Yu, Phys. Rev. A, **69**, 062107 (2004).

[29] E. Jos and H. D. Zeh, Z. Phys. B **59**, 223 (1985).

[30] T. Yu and J. H. Eberly, Phys. Rev. Lett. , **93**, 140404 (2004).

[31] T. Yu and J. H. Eberly, Opt. Comm., **283**, 676 (2010).

[32] G. Sadiek, E. I. Lashin and M. S. Abdalla, Science Direct, **404**, 1719 (2009).

[33] A. L. Godunov and J. H. McGuire, J. Phys. B **34**, 223 (2001).

[34] W. Magnus, Commun. Pure Appl. Math. **7**, 649 (1954).

[35] C. Moler and C. V. Loan, Society for Industrial and Applied Mathematics, Siam Review **45**, 3 (2003).

[36] A. Abliz, H. J. Gao, X. C. Xie, Y. S. Wu and W. M. Liu, Phys. Rev. A **74**, 052105 (2006).

[37] F. F. Fanchini et al., arXiv: quant-ph/0911.1096.

[38] B. Wang, Z. Y Xu, Z. Q. Chen and M. Feng, Phys. Rev. A, **81**, 014101 (2010).

[39] T. Werlang, S. Souza, F. F. Fanchini and C. J. V. Boas, Phys. Rev. A, **80**, 024103 (2009).

[40] R. F. Werner, Phys. Rev. A, **40**, 4277 (1989).

[41] D. P. DiVincenzo, Fort. Phys., **48**, 9 (2000).

[42] C. H. Benneth et al., Phys. Rev. Lett., **70**, 1895 (1993).

[43] N. Gisin et al., Rev. Mod. Phys., **74**, 145 (2002).

[44] M. Ali, A. R. P. Rau and G. Alber, arXiv: quant-ph/1002.3429.

[45] S. Luo, Phys. Rev. A, **77**, 042303 (2008).

[46] N. Li and S. Luo, Phys. Rev. A, **76**, 032327 (2007).

[47] N. D. Mermin, Phys. Rev. Lett., **65**, 1838 (1990).

[48] M. Ardehali, Phys. Rev. A, **46**, 5375 (1992).

[49] A. V. Belinskii and D. N. Klyshko, Sov. Phys. Usp. **36**, 653 (1993).

[50] G. Svetlichny, Phys. Rev. D, **35**, 3066 (1987).

[51] B. Bellomo, R. Lo Franco, and G. Compagno, Phys. Rev. A, **77**, 032342 (2008).

[52] T. Yu, L. Diosi, N. Gisin and W. T Strunz Phys. Rev. A, **60**, 91 (1999).

[53] W. K. Wootters, Phys. Rev. Lett., **80**, 2245 (1998).

[54] D. McMahon, *Quantum Computing Explained*, (Wiley, 2007).

[55] W. Dur, G. Vidal and J. I. Cirac, Phys. Rev. A **62**, 062314 (2000).

[56] Y. Wang, J. Cao and Y. Wang, Phys. Lett. A **342**, 375 (2005).

[57] J. H. Ann, S. J. Wang and H. G. Luo, Physica A **382**, 753 (2007).

[58] R. Kubo, J. Phys. Soc. Jpn. **9** 935 (1954); P. Anderson, J. Phys. Soc. Jpn. **9** 316 (1954).

[59] Y. Wang, J. Cao, Y. Wang, Phys. Lett. A **342** 375 (2005).

[60] T. Yu and J. H. Eberly, Opt. Comm. **264**, 393 (2006).

[61] G. Gao, Opt. Comm. **281**, 876 (2008).

[62] R. Werner, Phys. Rev. A **40** 4277 (1989).